

Annex 59: High Temperature Cooling & Low Temperature Heating in Buildings

Final Report

II. Demand and novel design of indoor terminals in high temperature cooling and low temperature heating system

2016

© Copyright Tsinghua University 2016

All property rights, including copyright, are vested in Tsinghua University, Operating Agent for EBC Annex 59, on behalf of the Contracting Parties of the International Energy Agency Implementing Agreement for a Programme of Research and Development on Energy in Buildings and Communities.

In particular, no part of this publication may be reproduced, stored in a retrieval system or transmitted in any form or by any means, electronic, mechanical, photocopying, recording or otherwise, without the prior written permission of Tsinghua University.

Published by Department of Building Science and Technology, Tsinghua University, 100084 Beijing, P.R. China

Disclaimer Notice: This publication has been compiled with reasonable skill and care. However, neither Tsinghua University nor the Contracting Parties of the International Energy Agency Implementing Agreement for a Programme of Research and Development on Energy in Buildings and Communities make any representation as to the adequacy or accuracy of the information contained herein, or as to its suitability for any particular application, and accept no responsibility or liability arising out of the use of this publication. The information contained herein does not supersede the requirements given in any national codes, regulations or standards, and should not be regarded as a substitute for the need to obtain specific professional advice for any particular application.

Participating countries in EBC:

Australia, Austria, Belgium, Canada, P.R. China, Czech Republic, Denmark, Finland, France, Germany, Ireland, Italy, Japan, Republic of Korea, the Netherlands, New Zealand, Norway, Portugal, Singapore, Spain, Sweden, Switzerland, United Kingdom and the United States of America.

Additional copies of this report may be obtained from:

EBC Executive Committee Support Services Unit (ESSU)
C/o AECOM Ltd
The Colmore Building
Colmore Circus Queensway
Birmingham B4 6AT
United Kingdom
Web: www.iea-ebc.org
Email: essu@iea-ebc.org

Preface

The International Energy Agency

The International Energy Agency (IEA) was established in 1974 within the framework of the Organisation for Economic Co-operation and Development (OECD) to implement an international energy programme. A basic aim of the IEA is to foster international co-operation among the 30 IEA participating countries and to increase energy security through energy research, development and demonstration in the fields of technologies for energy efficiency and renewable energy sources.

The IEA Energy in Buildings and Communities Programme

The IEA co-ordinates international energy research and development (R&D) activities through a comprehensive portfolio of Technology Collaboration Programmes. The mission of the IEA Energy in Buildings and Communities (IEA EBC) Technology Collaboration Programme is to develop and facilitate the integration of technologies and processes for energy efficiency and conservation into healthy, low emission, and sustainable buildings and communities, through innovation and research. (Until March 2013, the IEA EBC Programme was known as the IEA Energy Conservation in Buildings and Community Systems Programme, ECBCS.)

The R&D strategies of the IEA EBC Programme are derived from research drivers, national programmes within IEA countries, and the IEA Future Buildings Forum Think Tank Workshops. These R&D strategies aim to exploit technological opportunities to save energy in the buildings sector, and to remove technical obstacles to market penetration of new energy efficient technologies. The R&D strategies apply to residential, commercial, office buildings and community systems, and will impact the building industry in five areas of focus for R&D activities:

- Integrated planning and building design
- Building energy systems
- Building envelope
- Community scale methods
- Real building energy use

The Executive Committee

Overall control of the IEA EBC Programme is maintained by an Executive Committee, which not only monitors existing projects, but also identifies new strategic areas in which collaborative efforts may be beneficial. As the Programme is based on a contract with the IEA, the projects are legally established as Annexes to the IEA EBC Implementing Agreement. At the present time, the following projects have been initiated by the IEA EBC Executive Committee, with completed projects identified by (*) and joint projects with the IEA Solar Heating and Cooling Technology Collaboration Programme by (☼):

Annex 1:	Load Energy Determination of Buildings (*)
Annex 2:	Ekistics and Advanced Community Energy Systems (*)
Annex 3:	Energy Conservation in Residential Buildings (*)
Annex 4:	Glasgow Commercial Building Monitoring (*)
Annex 5:	Air Infiltration and Ventilation Centre
Annex 6:	Energy Systems and Design of Communities (*)
Annex 7:	Local Government Energy Planning (*)
Annex 8:	Inhabitants Behaviour with Regard to Ventilation (*)
Annex 9:	Minimum Ventilation Rates (*)
Annex 10:	Building HVAC System Simulation (*)
Annex 11:	Energy Auditing (*)
Annex 12:	Windows and Fenestration (*)
Annex 13:	Energy Management in Hospitals (*)
Annex 14:	Condensation and Energy (*)

- Annex 15: Energy Efficiency in Schools (*)
- Annex 16: BEMS 1- User Interfaces and System Integration (*)
- Annex 17: BEMS 2- Evaluation and Emulation Techniques (*)
- Annex 18: Demand Controlled Ventilation Systems (*)
- Annex 19: Low Slope Roof Systems (*)
- Annex 20: Air Flow Patterns within Buildings (*)
- Annex 21: Thermal Modelling (*)
- Annex 22: Energy Efficient Communities (*)
- Annex 23: Multi Zone Air Flow Modelling (COMIS) (*)
- Annex 24: Heat, Air and Moisture Transfer in Envelopes (*)
- Annex 25: Real time HVAC Simulation (*)
- Annex 26: Energy Efficient Ventilation of Large Enclosures (*)
- Annex 27: Evaluation and Demonstration of Domestic Ventilation Systems (*)
- Annex 28: Low Energy Cooling Systems (*)
- Annex 29: ☀ Daylight in Buildings (*)
- Annex 30: Bringing Simulation to Application (*)
- Annex 31: Energy-Related Environmental Impact of Buildings (*)
- Annex 32: Integral Building Envelope Performance Assessment (*)
- Annex 33: Advanced Local Energy Planning (*)
- Annex 34: Computer-Aided Evaluation of HVAC System Performance (*)
- Annex 35: Design of Energy Efficient Hybrid Ventilation (HYBVENT) (*)
- Annex 36: Retrofitting of Educational Buildings (*)
- Annex 37: Low Exergy Systems for Heating and Cooling of Buildings (LowEx) (*)
- Annex 38: ☀ Solar Sustainable Housing (*)
- Annex 39: High Performance Insulation Systems (*)
- Annex 40: Building Commissioning to Improve Energy Performance (*)
- Annex 41: Whole Building Heat, Air and Moisture Response (MOIST-ENG) (*)
- Annex 42: The Simulation of Building-Integrated Fuel Cell and Other Cogeneration Systems (FC+COGEN-SIM) (*)
- Annex 43: ☀ Testing and Validation of Building Energy Simulation Tools (*)
- Annex 44: Integrating Environmentally Responsive Elements in Buildings (*)
- Annex 45: Energy Efficient Electric Lighting for Buildings (*)
- Annex 46: Holistic Assessment Tool-kit on Energy Efficient Retrofit Measures for Government Buildings (EnERGo) (*)
- Annex 47: Cost-Effective Commissioning for Existing and Low Energy Buildings (*)
- Annex 48: Heat Pumping and Reversible Air Conditioning (*)
- Annex 49: Low Exergy Systems for High Performance Buildings and Communities (*)
- Annex 50: Prefabricated Systems for Low Energy Renovation of Residential Buildings (*)
- Annex 51: Energy Efficient Communities (*)
- Annex 52: ☀ Towards Net Zero Energy Solar Buildings (*)
- Annex 53: Total Energy Use in Buildings: Analysis and Evaluation Methods (*)
- Annex 54: Integration of Micro-Generation and Related Energy Technologies in Buildings (*)
- Annex 55: Reliability of Energy Efficient Building Retrofitting - Probability Assessment of Performance and Cost (RAP-RETRO) (*)
- Annex 56: Cost Effective Energy and CO₂ Emissions Optimization in Building Renovation (*)
- Annex 57: Evaluation of Embodied Energy and CO₂ Equivalent Emissions for Building Construction (*)
- Annex 58: Reliable Building Energy Performance Characterisation Based on Full Scale Dynamic Measurements (*)
- Annex 59: High Temperature Cooling and Low Temperature Heating in Buildings (*)
- Annex 60: New Generation Computational Tools for Building and Community Energy Systems (*)
- Annex 61: Business and Technical Concepts for Deep Energy Retrofit of Public Buildings (*)
- Annex 62: Ventilative Cooling (*)
- Annex 63: Implementation of Energy Strategies in Communities (*)

- Annex 64: LowEx Communities - Optimised Performance of Energy Supply Systems with Exergy Principles (*)
- Annex 65: Long-Term Performance of Super-Insulating Materials in Building Components and Systems
- Annex 66: Definition and Simulation of Occupant Behavior in Buildings (*)
- Annex 67: Energy Flexible Buildings
- Annex 68: Indoor Air Quality Design and Control in Low Energy Residential Buildings
- Annex 69: Strategy and Practice of Adaptive Thermal Comfort in Low Energy Buildings
- Annex 70: Energy Epidemiology: Analysis of Real Building Energy Use at Scale
- Annex 71: Building Energy Performance Assessment Based on In-situ Measurements
- Annex 72: Assessing Life Cycle Related Environmental Impacts Caused by Buildings
- Annex 73: Towards Net Zero Energy Resilient Public Communities
- Annex 74: Competition and Living Lab Platform
- Annex 75: Cost-effective Building Renovation at District Level Combining Energy Efficiency and Renewables
- Annex 76: ☀ Deep Renovation of Historic Buildings Towards Lowest Possible Energy Demand and CO₂ Emissions
- Annex 77: ☀ Integrated Solutions for Daylight and Electric Lighting
- Annex 78: Supplementing Ventilation with Gas-phase Air Cleaning, Implementation and Energy Implications
- Annex 79: Occupant Behaviour-Centric Building Design and Operation
- Annex 80: Resilient Cooling

Working Group - Energy Efficiency in Educational Buildings (*)

Working Group - Indicators of Energy Efficiency in Cold Climate Buildings (*)

Working Group - Annex 36 Extension: The Energy Concept Adviser (*)

Working Group - HVAC Energy Calculation Methodologies for Non-residential Buildings

Working Group - Cities and Communities

Working Group - Building Energy Codes

Working Group - International Building Materials Database

Authors: Bjarne Olesen (Technical University of Denmark), Ogun Berk Kazanci (Technical University of Denmark), Yi Jiang (Tsinghua University), Xiaohua Liu (Tsinghua University), Youness Ajaji (University of Liege), Stefano Paolo Corgnati (Politecnico di Torino), Jerome Le Dreau (Aalborg University), Tao Zhang (Tsinghua University), Haida Tang (Tsinghua University), Xiangjian Xiang (Tsinghua University)

Editors: Ogun Berk Kazanci, Tao Zhang

Contents

1.	Characteristics of indoor heat and moisture sources.....	1
1.1.	Characteristics of indoor heat and moisture sources.....	1
1.1.1.	Types and temperature levels of heat sources.....	2
1.1.2.	Characteristics of moisture sources.....	4
1.2.	Objectives of indoor heat and moisture collecting processes.....	5
2.	Terminal units and their characteristics.....	8
2.1.	Common terminal units.....	8
2.1.1.	Hydronic radiant heating and cooling systems.....	9
2.1.2.	All-air systems.....	11
2.1.3.	Fan coil unit (FCU).....	12
2.1.4.	Beams.....	12
2.2.	Entransy dissipation analysis of common terminal units.....	14
2.2.1.	FCU+OA system.....	14
2.2.2.	THIC air-conditioning System.....	16
2.3.	Construction principles based on indoor heat and moisture collecting process.....	18
2.3.1.	Heat collection in indoor inhomogeneous thermal environment.....	18
2.3.2.	Limiting factors for choosing terminal units.....	21
2.3.3.	Construction principles for thermal built environment.....	22
3.	Characteristics of radiant terminal.....	24
3.1.	Dynamic performance of radiant floors with solar radiation.....	25
3.1.1.	Response time in the start-up process (without solar radiation).....	25
3.1.2.	Dynamic performance with solar radiation.....	30
3.1.3.	Conclusions.....	37
3.2.	Cooling capacity prediction of radiant floors in large spaces.....	37
3.2.1.	Key factors of radiant floor cooling capacity in large spaces.....	37
3.2.2.	Longwave heat exchange with different emissivity values.....	42
3.2.3.	Effect of transient solar radiation on radiant floor.....	46
3.2.4.	Results and discussion.....	50
3.2.5.	Conclusions.....	57
4.	Case studies and novel terminal systems.....	57
4.1.	Application of radiant floor in an airport.....	58
4.1.1.	Description of the radiant floor system in an airport.....	58

4.1.2. Performance on-site test in summer.....	63
4.1.3. Performance on-site test in winter	68
4.1.4. Energy performance of the total air-conditioning system.....	73
4.1.5. Conclusion	77
4.2. Novel terminal units for HTC<H systems	77
4.2.1. Hybrid system combining radiation and convection	78
4.2.2. High temperature cooling and low temperature heating AC System.....	80
4.2.3. Dehumidifying chilled radiators	83
5. Conclusions	85
Appendix A: terminal units and corresponding characteristics	87
Appendix B: numerical model of radiant floor	88
Appendix C: experimental analysis of different terminal units.....	94
References	107

List of abbreviations

AC	air-conditioning
AUST	average uncooled surface temperature
COP	coefficient of performance
EBC	Energy in Buildings and Communities Program
HTC	high temperature cooling
HVAC	heating, ventilation and air-conditioning
IEA	International Energy Agency
LTH	low temperature heating
PAQ	perceived air quality
SC	shading coefficient
TABS	thermally active building system
THIC	temperature and humidity independent control
VAV	variable air volume

0. Background

People spend 90% of their lives indoors and buildings are built for people and not to save energy. Buildings should be designed to ensure thermal comfort, health and productivity for the building occupants, and this should be achieved with the lowest possible energy use through choosing the most energy-efficient and environmentally-friendly heating, cooling and ventilation systems.

If heating and cooling systems are considered to consist of three connected parts (heating and cooling plant, the system carrying the heat transfer medium-transportation system, and heat emission/removal system-terminal unit), terminal units are the part of the system that are closest to the occupants. The choice of terminal units has a direct impact on overall and local thermal comfort. This choice also affects the whole heating and cooling system because it determines the temperature levels to be used, dimensioning of the auxiliary components (pumps, fans, etc.), heating and cooling plants, and even which heat sources and sinks could be used, which in turn determines the whole energy performance of the system.

This report (Subtask B) focuses on the terminal units while information on heat sources and sinks, transportation system and about total system analysis can be found in Subtask D. Throughout this report, the supply (in) and return (out) temperatures correspond to the temperatures entering and leaving the terminal unit, immediately out of this boundary it is considered to be the transportation system.

1. Characteristics of indoor heat and moisture sources

Within this project from the International Energy Agency (IEA), Energy in Buildings and Communities (EBC) Program, Annex 59 – High Temperature Cooling and Low Temperature Heating in Buildings is studying the currently existing heating, cooling and ventilation systems. The main objective of this project is to provide suggestions to improve currently existing heating, cooling, and ventilation systems. A sub-group within the project, Subtask B, is responsible for indoor temperature and humidity fields and indoor terminal units. Indoor terminal units are active building components that emit or remove heat and moisture from indoor spaces. These indoor terminal units mainly rely on convection (natural or forced), radiation, or a combination of both. Before the characteristics of the terminal units can be studied, indoor heat and moisture sources should be clearly identified. Currently existing literature and data were used to gather information about indoor heat and moisture sources, as well as about the indoor terminal units. Case studies and novel system applications were gathered with the help of project participants. In addition to the energy performance analyses of these systems, entransy analyses were performed to evaluate the chosen terminal units and heating, ventilation and air-conditioning (HVAC) systems in order to identify possibilities for improving the existing terminal units and systems.

1.1. Characteristics of indoor heat and moisture sources

Heat and moisture are produced in an indoor space by indoor heat and moisture sources such as human bodies and equipment, leading to the requirement for creating a comfortable thermal and humid environment. The main objective of an air conditioning system is to remove redundant heat and moisture from indoor spaces to the outside. First, an air conditioner collects heat and moisture from indoor heat and moisture sources, which is called the collection process of heat and moisture. Fig. 1-1 shows the principle of the collection process by the terminal devices of an air conditioning system. Q_a denotes the load of heat extraction and m_w denotes the load of dehumidification. In addition, an air conditioning system usually provides some fresh air to meet the requirements of indoor air quality.

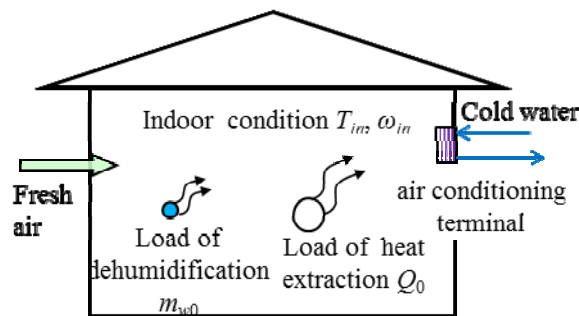


Fig. 1-1 Collection process of indoor heat and moisture by air-conditioning system.

1.1.1 Types and temperature levels of heat sources

There are various types of indoor heat and moisture sources, such as building envelopes, human bodies, equipment, and solar radiation. The spatial distribution and transfer pathways of heat sources are different: solar radiation, heat transfer through building envelope, sensible heat of air infiltration, indoor light, heat transfer from human bodies and equipment by heat conduction, and convection and radiation through building envelopes and indoor surfaces. Moisture produced by human bodies and latent heat of air infiltration transfer by moisture diffusion. Based on whether the capacity of heat transfer is influenced by the environment, indoor heat sources can be divided into two types: heat sources with constant heat flux Q and heat sources with constant temperature T , as listed in Table 1-1.

Table 1-1 Main Types of Indoor Heat Sources

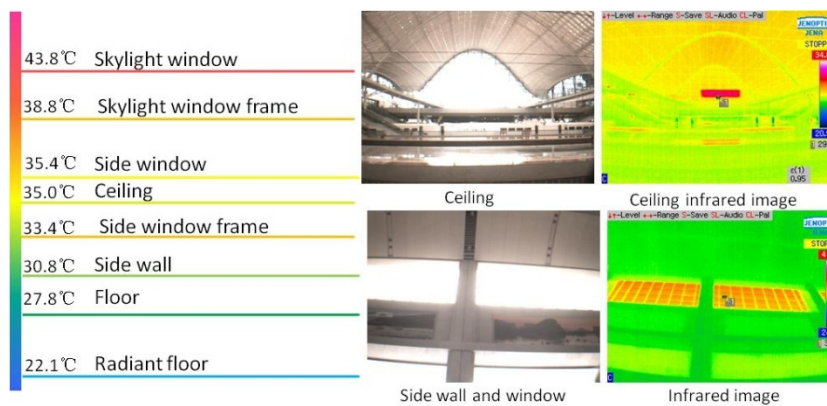
Heat sources with constant heat flux Q	 Solar radiation	 Human bodies, equipment and light
Heat sources with constant temperature T	 Surface of building envelopes	 Air infiltration

a) Heat sources with constant heat flux Q : These heat sources include solar radiation and the heat produced by light, equipment, and human bodies. The heat flux depends on the heat produced by these heat sources while the transfer process has no effect on the heat flux. Under certain indoor thermal environment, it is believed that these indoor heat sources have a constant heat flux Q . For example, at a room temperature of 26°C and relative humidity of 60%, the heat flux of a male adult at office is 86 W (the moisture gain is 109 g/h) and the heat flux of a computer is about 200 W. The heat flux of direct sunlight is over 100 W/m² and the sunlit areas are scattered, which changes with the passage of time. The surface temperature of these heat sources are closely related with the indoor environment. For example, when solar radiation is absorbed by the floor, the temperature of solar radiation is the surface temperature of the floor. The temperature of lighting devices is the equilibrium temperature attained after heat transfer between heating components and the surrounding air.

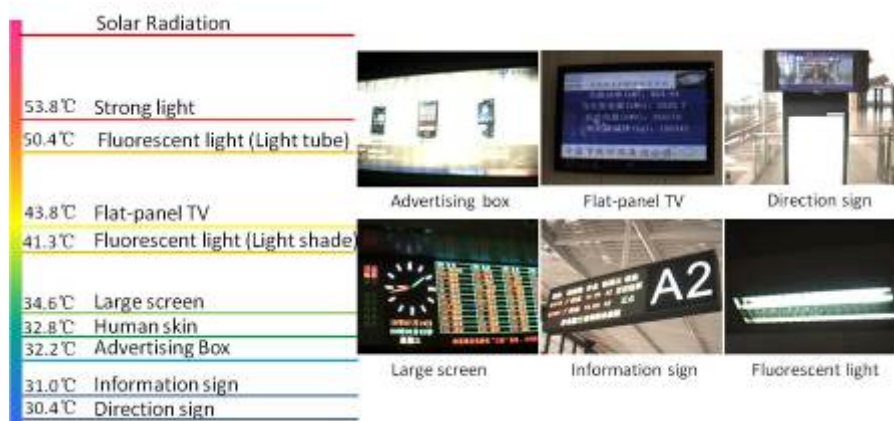
b) Heat sources with constant temperature T : These heat sources include air infiltration and heat transfer through building envelopes (light building envelopes). These heat

sources are supposed to have a constant surface temperature (e.g., inner surface temperature of building envelopes) or air temperature (e.g., temperature of air infiltration). The heat flux is closely related with temperature difference and heat transfer processes. For instance, the process of indoor heat radiation and convection will affect the heat flux through building envelopes. Further, the heat flux of air infiltration is closely related with indoor airflow organization. For a certain air infiltration rate, the heat entering an indoor space decreases as the exhaust temperature of air increases.

The space and temperature distributions of heat sources are different; thus, the environment of indoor heat sources is uneven. Fig. 1-2 shows the measured temperature levels of typical indoor heat sources. It can be seen that the temperature levels of inner surfaces of building envelopes and indoor equipment are different. The figure shows that the heat from indoor heat sources varies in heat grade.



(a)



(b)

Fig. 1-2 Indoor surface temperature distribution in large space buildings: (a) Internal wall surfaces; and (b) Indoor heat sources.

For indoor heat sources, Table 1-2 describes the temperature levels of typical indoor heat sources. Heat transfer from high-temperature surfaces to indoor air takes place directly or

indirectly. It can be seen that the temperature of indoor heat sources is high, and the temperature of some indoor sources is even higher than outdoor temperature, which is regarded as a heat sink. The heat grade of cold sources required for heat extraction depends on the temperature of heat sources. The outdoor temperature for air-conditioning design in most cities in China during summer is below 35°C; thus, outdoor natural cold sources can be used for heat extraction in theory. Moreover, different cold sources and methods can be used for different heat sources. For example, the temperature of lighting devices, as described in Table 1-2, is over 40°C; thus, theoretically, outdoor air can remove the heat directly and an air conditioning system is not necessary. However, because of the limitation of complex terminal devices, only a few methods and devices can be used for the collection of heat and moisture.

Table 1-2 Temperature levels of indoor heat sources

Temperature levels	Shortwave radiation(high temperature)	About 50°C	About 40°C	30~35°C
Typical heat sources	Direct and diffuse solar radiation through windows, shortwave radiation of lighting	Heat convection and longwave radiation of lighting, heat convection of equipment's kernel	Heat convection and longwave radiation of equipment's surface	Body surfaces

1.1.2 Characteristics of moisture sources

For normal civil buildings, the main moisture sources are human bodies. Table 1-3 lists the moisture diffusion rate of human body for slight labor intensity. When the required indoor temperature is certain, the moisture gain of human body is certain, which is similar to heat sources with constant heat flux Q . For the purpose of dehumidification, replacement of dry air (ventilation) is required for removing the moisture produced by human bodies. The grade of moisture sources can be described in terms of indoor humidity ratio. For example, for a temperature of 25°C and relative humidity of 50%, the indoor humidity ratio is 9.9 g/kg. When condensation dehumidification is adopted, the temperature of cold sources must be lower than the dew-point temperature. Thus, dew-point temperature can be used to measure the grade of moisture sources. According to the results in Table 1-3, the indoor dew-point temperature varies from 13°C to 18°C when the required indoor temperature and humidity ratio are between 24–27°C and 50–60%, respectively. The dew-point temperature is 8–11°C lower than air temperature.

Table 1-3 Moisture gain of human body with different indoor temperature

Indoor air temperature °C	24.0	25.0	26.0	27.0
Moisture diffusion rate of human body g/h	96	102	109	115

Indoor dew-point temperature* °C	12.9~15.8	13.9~16.7	14.8~17.6	15.7~18.6
Indoor humidity ratio* g/kg	9.3~11.2	9.9~11.9	10.5~12.6	11.1~13.4
Air temperature minus dew-point temperature* °C	8.2~11.1	8.3~11.1	8.4~11.2	8.4~11.3

Remark: ‘*’ means that the results are in the conditions of 50%~60% RH

1.2. Objectives of indoor heat and moisture collecting processes

Heat and moisture collection is a basic process for building an indoor thermal built environment. The entire thermal built system consists of this heat and moisture collecting process, the transportation process, and heating and cooling sources. Considering an active air-conditioning system in summer, the basic indoor heat and moisture collecting process is to collect the extra heat or moisture from sources in an indoor space and transfer it to a cooling medium such as chilled water in terminal devices, to satisfy the requirement for removing heat or moisture.

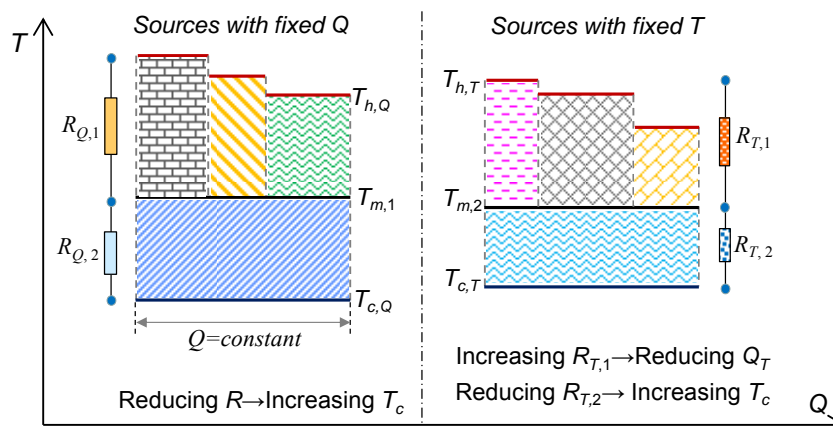


Fig. 1-3 Sensible heat collecting process shown in T - Q chart

For indoor heat collecting process, the task of an air conditioner is to remove the extra sensible heat from different heat sources. Terminal devices that are adopted in air conditioners usually include convective type and radiant type (such as radiant ceiling) devices. Sensible heat is transferred from different sources to the terminal devices of an air-conditioning system through heat convection or radiation, and the heat is removed by a cooling medium such as chilled water. The characteristics of heat sources affect the performance of indoor heat collecting process significantly. Fig. 1-3 illustrates the indoor heat collecting processes of heat sources with constant Q and constant T , respectively, in a T - Q chart. There are two heat transfer processes from heat sources to cooling medium: first, heat is transferred from the heat sources to indoor terminal devices, and second, the heat is transferred from the terminal device to a cooling medium such as chilled water. The corresponding temperature level

decreases from heat source temperature T_h to the temperature of the indoor terminal device T_m , and finally to the temperature of the cooling medium T_c . The shaded areas represent the entransy dissipation of the heat transfer process in the $T-Q$ chart.

According to the entransy dissipation and equivalent thermal resistance analysis by Subtask A, the relation between equivalent temperature difference $\Delta\bar{T}$, thermal resistance R , entransy dissipation $\Delta E_{n,dis}$, and transferred heat Q for sensible heat transfer process could be expressed by Eq. (1-1).

$$\Delta\bar{T} = \frac{\Delta E_{n,dis}}{Q} = R \cdot Q \quad (1-1)$$

According to the characteristics of the various types of indoor heat sources in a thermal built environment, the objectives for indoor heat collecting process can be categorized as following:

- For heat sources with a fixed temperature T , such as heat transfer through the internal surface of building envelope and air infiltration, it is important to reduce the transferred heat. As the temperatures of the heat sources and terminal device are fixed, i.e., the temperature difference for the heat transfer process is constant, increasing the thermal resistance $R_{T,1}$ from the heat sources to the terminal device is beneficial to reduce the entransy dissipation according to Eq. (1-1). The transferred heat Q_T from this type of heat source will also be reduced. Additionally, the heat transfer process between the terminal device and a cooling medium could be regarded as a transfer process to remove a fixed heat flux. According to Eq. (1-1), reducing the thermal resistance $R_{T,2}$ on the cooling source side helps to reduce the entransy dissipation and increase the required cooling source temperature $T_{c,T}$.
- For heat sources with a fixed heat flux Q , such as solar radiation, indoor occupants and equipment, heat flux to be removed for the heat collecting process could be regarded as constant. According to Eq. (1-1), reducing the thermal resistance $R_{Q,1}$ from the heat sources to a terminal device or $R_{Q,2}$ from the terminal device to a cooling medium is effective in reducing the entire thermal resistance R_Q for removing this type of heat. Thus, the corresponding dissipation for heat collecting process is reduced. The equivalent temperature difference $\Delta\bar{T}$ between the heat sources and cooling medium in terminal devices will also be reduced, and the required temperature of the cooling source $T_{c,Q}$ will be increased.

The corresponding optimization objectives for heat collecting processes of different sources are summarized in Table 1-4. For heat sources with a fixed heat flux Q including solar radiation and indoor equipment, it is important to reduce the thermal resistance $R_{Q,1}$ from heat sources to terminal device and $R_{Q,2}$ from terminal device to cooling medium to

increase the required temperature of the cooling source $T_{c,Q}$. For heat sources with a fixed temperature T_H , such as heat transfer through building envelope and infiltration, it is recommended to increase the thermal resistance $R_{T,1}$ from heat sources to terminal device to reduce the transferred heat Q , while the thermal resistance $R_{T,2}$ from terminal device to cooling medium should be decreased to improve the temperature of the cooling source $T_{c,T}$.

Table 1-4 Objectives for heat collecting processes of different sources

Heat source's characteristic	Fixed heat flux Q (solar radiation, devices and etc.)	Fixed temperature T (envelope, infiltration and etc.)
Objective	Increasing cooling source temperature T_c	Reducing Q_T ; increasing cooling source temperature T_c
Optimization method	Heat source Cooling medium Reducing $R_{Q,1}$ Reducing $R_{Q,2}$	Increasing $R_{T,1}$ → Reducing Q_T Reducing $R_{T,2}$ → increasing T_c

As indicated by the above analysis, there are two optimization objectives for heat collecting process: **reducing the transferred heat Q from heat sources to indoor space** (referring to Q_T by heat sources with fixed temperatures) and **increasing the required temperature of cooling source T_C** . Reducing the entransy dissipation of the heat collecting process is conducive to realize the aforementioned objectives. The heat collecting process from an indoor terminal device to a cooling medium could be regarded as a heat transfer process with a constant heat flux, irrespective of whether the heat sources have a fixed heat flux Q or a fixed temperature T . If the required heat flux to be removed is fixed, the lesser the entransy dissipation of heat collecting process, the higher the required temperature of the cooling source. The demand for the temperature grade of the cooling source is accordingly reduced, consequently helping to improve energy performance of the cooling source and realize high-temperature cooling.

Apart from removing sensible heat from heat sources, such as building envelope and indoor equipment, an air-conditioning system is also responsible for removing moisture produced by occupants. Compared with the heat collecting process, the characteristics for indoor moisture collecting process are quite different. The main distinctions between heat and moisture collecting processes are embodied as follows:

- **Characteristics of heat sources and moisture sources are quite different.** Indoor moisture sources are usually simple, moisture is mainly produced by indoor occupants, plants, and open water surfaces. In an indoor space, moisture exists in the form of water vapor; this moisture load needs to be removed by an air-conditioning

system. Moisture sources and their characteristics are simple. However, sensible heat sources are more diverse, and there are significant differences for the corresponding temperature levels.

- **Approaches to be selected for removing heat or moisture are different.** Heat removal or collection processes are realized by supplying air with a lower temperature or with the help of a cooling surface, i.e., heat convection or radiation are both feasible for removing sensible heat. However, replacement of air is necessary for removing or collecting indoor moisture. The air supplied to an indoor space should have a lower humidity ratio for removing the moisture load and realize indoor humidity control.
- **Temperature grades required for heat and moisture collecting process are different.** Theoretically, the required temperature of a cooling source is lower than the temperature of a heat source. If different heat sources having different temperature levels are first mixed in an indoor space, the required temperature of the cooling source becomes equal to the indoor air temperature in theory. To remove indoor moisture, if there is no dry air to be used from outdoor or other sources and adopting condensing dehumidification method in general use, the required temperature of the cooling source should be lower than indoor dew point temperature (which is 8-11°C lower than indoor air temperature on an average).

2. Terminal units and their characteristics

2.1. Available terminal units

Indoor terminal units are building elements that use different heat transfer mechanisms and media to emit and remove heat or moisture from indoor spaces. Indoor temperature and humidity fields depend on the chosen terminal units. In addition, the chosen terminal units affect the total energy performance of heating and cooling systems, as well as occupant thermal comfort.

Terminal units differ from each other according to certain criteria:

- Possibilities (heating, cooling, ventilation–fresh air, humidification, and dehumidification)
- Methods of heat emission or removal (convection, radiation, or a combination of both)
- Maximum heating and cooling capacities
- Medium of energy distribution (air, water, or electricity)
- Thermal mass and storage capacity

-
- Total or local volume conditioning

The main objectives of this section of the report are to summarize the basic characteristics of the chosen terminal units and to provide a simple and reliable reference tool for selection of these units. The systems were chosen with the possibility of performing low temperature heating and high temperature cooling:

- Radiant systems
- Mixing, displacement, and personalized ventilation
- Passive and active beams

2.1.1. Hydronic radiant heating and cooling systems

A hydronic (water-based) radiant heating and cooling system refers to a system where water is used as the heat carrier (medium of energy distribution) and more than half of the heat exchange within a conditioned space takes place through radiation.

It is possible to divide the radiant heating and cooling systems into three types:

- radiant heating and cooling panels
- pipes isolated from the main building structure (radiant surface systems)
- pipes embedded in the main building structure (thermally active building systems, TABS).

Hydronic systems are low-temperature heating and high-temperature cooling systems. Therefore, the heat carrier (water) circulating in the pipes has a low temperature during the heating operation and a high temperature during the cooling operation. In some TABS constructions (hollow core concrete decks), air has also been used as a heat carrier. Moreover, in some TABS, electricity can also be used in heating applications.

Floor, wall, and ceilings can be used as surfaces that provide heating or cooling to the space. Hydronic radiant surface systems are capable of addressing only sensible heating and cooling loads. Therefore, they require a ventilation system to address latent loads (to regulate humidity) and to provide the ventilation rates required for indoor air quality. Radiant heating and cooling systems enable lower airflow rates than all-air systems, where the entire heating and cooling loads are addressed by the ventilation system.

Heat emission or removal from a space is achieved by a combination of radiation and convection. Total heat exchange coefficients (combined convection and radiation) for floor heating, wall heating, and ceiling heating are 11, 8, 6 W/m²K, respectively, and for floor cooling, wall cooling, and ceiling cooling are 7, 8, and 11 W/m²K, respectively. The radiant heat transfer coefficient can be used as a constant value of 5.5 W/m²K, with an error of less than 4%. The difference in the total heat transfer coefficients is due to natural convection.

Based on the acceptable surface temperatures (comfort and dew-point concerns), and assuming an operative room temperature of 20°C and 26°C for heating and cooling, respectively, the maximum heating and cooling capacities can be obtained. The maximum floor (occupied zone) heating and cooling capacities are 99 W/m² and 42 W/m², respectively; wall heating and cooling capacities are 160 W/m² and 72 W/m², respectively; and ceiling heating and cooling capacities are 42 W/m² and 99 W/m², respectively. In the perimeter zones of the floor, it is possible to obtain a maximum heating capacity of 165 W/m². Different studies have shown that the cooling capacity of a floor cooling system increases above the given maximum capacity of 42 W/m² and may even exceed 100 W/m², when there is direct solar radiation on the floor.

Different construction types of radiant systems can be found in [9]. The design, test methods, control, and operation principles of radiant panels are provided in ISO 18566:2013, while the design, dimensioning, installation, and control principles of embedded radiant systems are provided in ISO 11855:2012.

Fig. 2-1 and Fig. 2-2 show examples of different radiant system applications.



Fig. 2-1 Examples of a cooling panel [8]

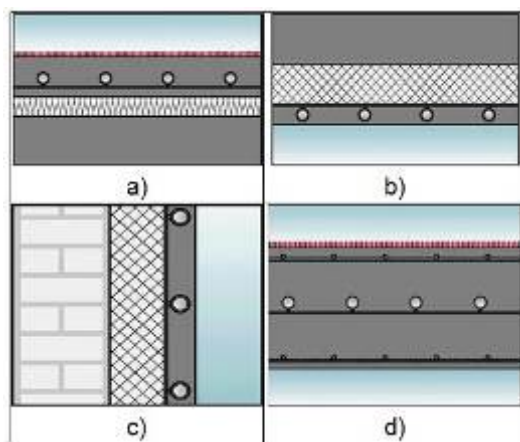


Fig. 2-2 Examples of embedded radiant systems: a) Floor, b) Ceiling, c) Wall, d) TABS [16]

2.1.2. All-air systems

Currently, there are eight commonly applied ventilation strategies in buildings. These strategies are mixing ventilation, displacement ventilation, personalized ventilation, hybrid air distribution, stratum ventilation, protected occupied zone ventilation, local exhaust ventilation, and piston ventilation. For ventilation systems, heat emission and removal takes place through convection, and the medium of energy distribution is air. Mixing, displacement, and personalized ventilation systems are further described in this report.

1) *Mixing ventilation*

Mixing ventilation (mixing room air distribution) intends to dilute the polluted and warm (or cool) room air with clean and cooler (or warmer) supply air. The aim is to achieve a uniform temperature and contaminant distribution in the occupied zone. It is possible to heat or cool a space by mixing ventilation. In addition, it is possible to provide dehumidified and conditioned outdoor air (fresh air). The typical temperature level of supply air for heating and cooling is a maximum of 34°C and a minimum of 14°C, respectively. The obtained heating and cooling effects will depend on the ventilation rate. In some countries, such as Denmark, the highest permissible supply air temperature is limited to 35°C by regulations. In order to achieve proper mixing, it is recommended that the temperature difference between the supply and room air should be limited to 10°C. According to literature, a specific cooling load of 90 W/m² can be handled with mixing ventilation systems.

2) *Displacement ventilation*

Displacement ventilation (displacement room air distribution) is based on displacing the polluted room air with fresh air (conditioned outdoor air). The cool fresh air is supplied at a low velocity (0.25~0.35 m/s) at or near the floor, and the supplied air rises because of the effects of momentum and buoyancy forces. It is possible to provide cold, dehumidified, and conditioned outdoor air with displacement ventilation. It is possible to provide warm air, which is at a higher temperature than room air, with displacement ventilation (e.g., to heat an unoccupied room before occupancy); however, it is not common. The supply of warm air by displacement ventilation is not recommended because of the short-circuiting of the supply air. Typically, the minimum supply air temperature can be 18°C. The cooling load that a floor current displacement system can handle is 30~35 W/m² according to [21] and 50 W/m² according to [20].

3) *Personalized ventilation*

Apart from the two mainly applied total volume air distribution principles (mixing and displacement air distribution), personalized ventilation is another air distribution principle that aims at supplying clean and cool air close to an occupant before it is mixed with the room air.

The most important advantage of personalized ventilation compared to total volume conditioning systems is its potential to provide clean, cool, and dry air at inhalation. According to [18], the minimum supply air temperature can be 20°C in cooling mode and a maximum of 28°C in heating mode. However, it should be noted that perceived air quality might be a problem with the increase in supply air temperature, and ventilation effectiveness may decrease depending on the chosen air supply location and terminal unit.

The required ventilation rates can be calculated based on EN 15251:2007 (this standard is currently under revision), CR 1752:1998, and ASHRAE 62.1-2013. Fig. 2-3 shows examples and principles of different ventilation approaches.

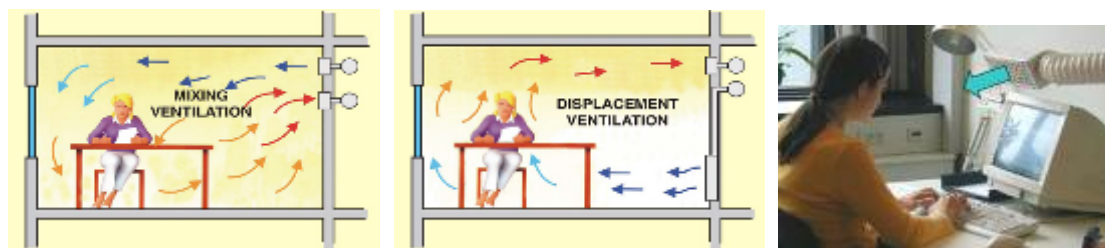


Fig. 2-3. Examples and principles of different ventilation strategies: mixing ventilation (left), displacement ventilation (middle), personalized ventilation (right) [30]

2.1.3. Fan-coil unit (FCU)

A fan-coil is another type of terminal unit that can be used for heating and cooling in buildings. Information regarding fan-coil units can be found in [12], [20].

2.1.4. Beams

Although these systems are known as chilled beams, a recent guidebook refers to them as beams; therefore, this terminology will be used in this report [31]. Beams (passive and active) are room air recirculation devices that can heat or cool (sensible) a space by using water as the energy distribution medium. In addition, beams operate on the principle of low-temperature heating and high-temperature cooling.

Active beams can provide conditioned primary air to a space because they are coupled to the main air-handling unit. Fresh air is delivered to the space by a decoupled ventilation system in passive beam applications. Beams cannot humidify or dehumidify the room air directly because they operate in dry (non-condensing) conditions. However, it is possible to control latent loads and to address ventilation requirements with active beams. Heat emission and removal from the space mainly takes place by convection.

The operation principles of beams are similar to fan-coil units. They are similar to a fan-coil unit that is installed in the ceiling, although beams benefit, and they are specially developed for, from the low temperature heating and high temperature cooling principle. In

beam systems, high chilled water temperatures of 14-18°C (typically around 14.5°C), and low heating water temperatures of 32-45°C are typically used [31: ASHRAE&REHVA Guidebook].

1) *Passive beams*

The performance of passive beams relies on natural convection [31]. In passive beams, the medium of energy distribution from the plant is water. It is possible to heat and cool a space with passive beams, but it is not possible to provide fresh air to the space. Although heating is possible with passive beams, in most applications, passive beams are used for cooling purposes only; therefore, a separate heating system should be used. In addition, ventilation needs should be addressed by a complementing system (e.g., by an air-handling unit). It is recommended to use passive chilled beams when the total sensible cooling load is in the range of 40-80 W/m².

2) *Active beams*

The performance of active beams relies on convection that is caused by induction [31]. It is possible to heat, cool, and provide fresh air to a space by active beams. In active beams, both air (fresh air from the air-handling unit) and water from heating and cooling plants can be used as the medium of energy distribution. Active beams can typically be used when the total sensible cooling (air and water) load is less than 120 W/m² in comfort conditions. The optimum operating range (for achieving thermal comfort in sedentary type occupancy) is 60-80 W/m². For the heating case, the optimum operating range is a heating load of 25-35 W/m² and a maximum heating load of 50 W/m². The specific heating and cooling capacities of beams can be expressed in W/m.

The testing and rating procedures of passive and active chilled beams are provided in EN 14518:2005 and in EN 15116:2008, respectively. Fig. 2-4 shows the airflow and operation schemes of passive and active beams. The descriptions, characteristics, operation principles, and other information regarding other terminal units that were not considered in this report (radiators, radiant tubes, convectors) can be found in [20].

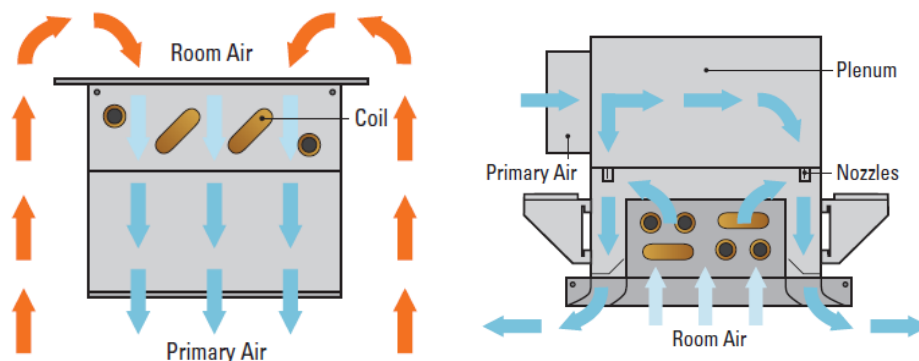


Fig. 2-4 Airflow schemes of a passive (left) and an active beam (right) [31]

Based on the presented operation characteristics of the terminal units until now, it is possible to classify them according to the heat transfer mechanisms employed and the thermal mass. Fig. 2-5. shows the classification chart.

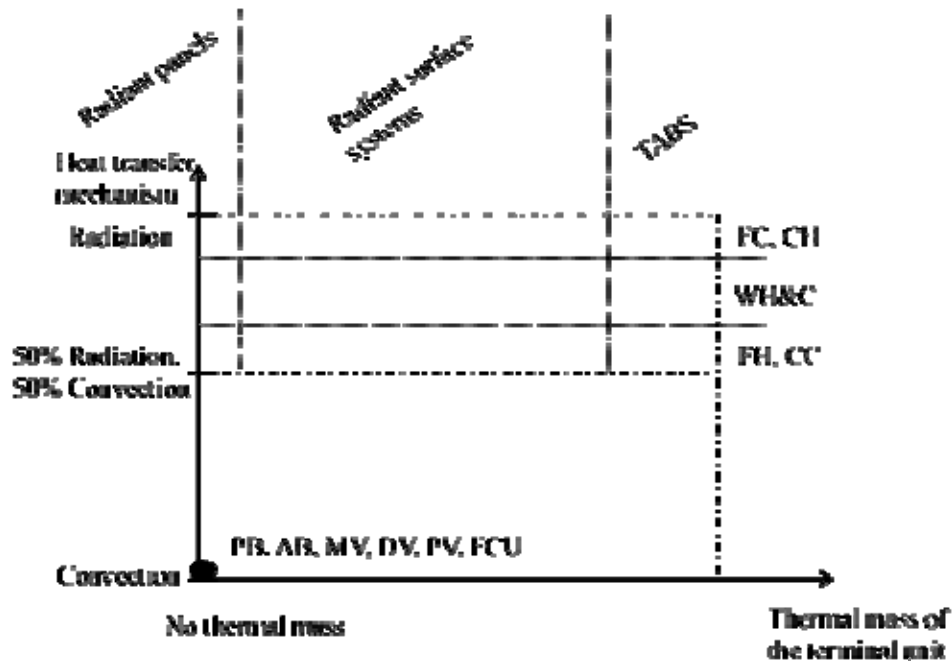


Fig. 2-5 Classification chart of terminal units according to the heat transfer mechanism and thermal mass. PB: passive beam, AB: active beam, MV: mixing ventilation, DV: displacement ventilation, PV: personalized ventilation, FCU: fan coil unit, FC: floor cooling, FH: floor heating, CH: ceiling heating, CC: ceiling cooling, WH&C: wall heating and cooling

In Fig. 2-5, it should be noted that the thermal mass is referring to the terminal unit and not the building. Although the thermal mass of the building is not considered in this report, it will play a crucial role in the thermal indoor environment and it will also interact with the terminal unit and the heating/cooling system of the building.

2.2. *Entransy dissipation analysis of common terminal units*

2.2.1. FCU+OA system

Compared with an all-air air-conditioning system, in a system consisting of a fan coil unit and an outdoor air processing unit (FCU+OA), the outdoor air is usually processed to a state that has the same humidity ratio or enthalpy as the indoor state. The air handling process in the FCU+OA system (air water system) is shown in Fig. 2-6. Both outdoor air and indoor return air are processed using the same cooling source (such as 7°C chilled water). After

condensation dehumidification, the outdoor air is usually processed from state W to state L , which has the same humidity ratio as the indoor air (state N). Meanwhile, the indoor return air is processed from state N to state L' when flowing through the FCU. The processed outdoor air (state L) and the processed return air (state L') are then mixed to state O , which is supplied to the conditioned space.

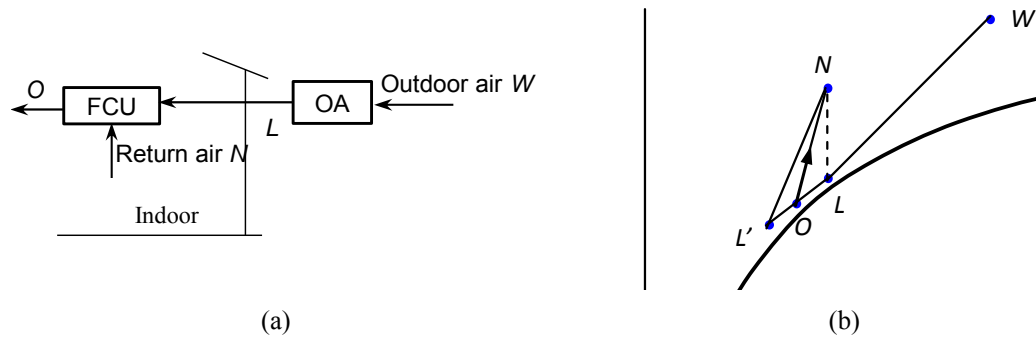


Fig. 2-6 Typical air handling process in the FCU+OA system: (a) Schematic of the air handling process; and (b) Psychrometric chart.

Fig. 2-7 shows the T - Q diagram of indoor heat exhaustion processes and the ω - m_w diagram of indoor moisture exhaustion processes. Because of the small amount of outdoor airflow rate, the influence of the processed outdoor air state on the indoor state is neglected, i.e., the indoor heat and moisture loads are similar to the heat and moisture extraction quantities in the handling process of the return air in an FCU. The supply air state in the FCU+OA system is close to that in an all-air system; therefore, the entransy dissipation caused by the mixing of the supply air and indoor air in an FCU+OA system is close to that in an all-air system. Similarly, the total entransy dissipation from chilled water to indoor state in an FCU+OA system is close to that in an all-air system because both the air-conditioning systems use low-temperature chilled water to handle the outdoor air and return air simultaneously to realize the indoor heat and moisture exhaustion processes.

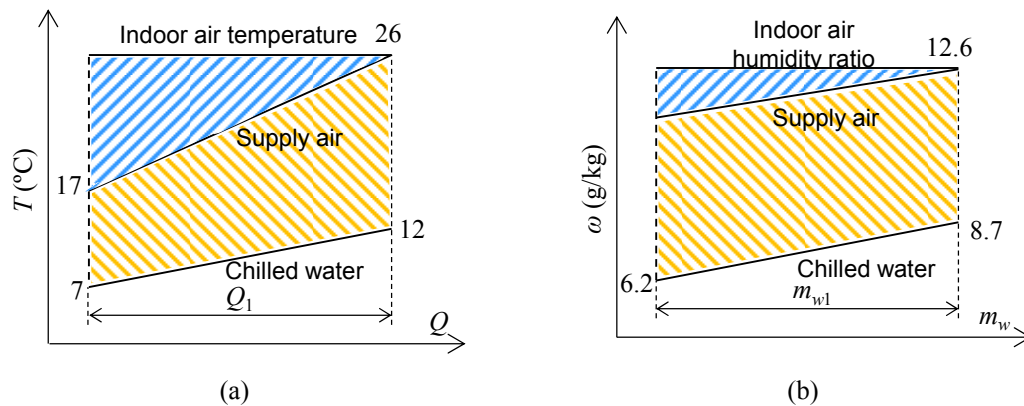


Fig. 2-7 Depiction of entransy dissipation in the indoor heat and moisture extraction in FCU+OA systems: (a) Heat extraction; and (b) Moisture extraction.

Through the entransy dissipation analysis of the indoor heat and moisture extraction processes in the FCU+OA system, a conventional air-conditioning system uses the same low-temperature chilled water to extract heat and moisture to realize the dehumidification requirement; as a result, the indoor dew point temperature limits the chilled water temperature. The entransy dissipation in the heat and moisture extraction processes is the area enclosed by the chilled water and the indoor state in $T-Q$ diagram and $\omega-m_w$ diagram. In the heat extraction process, utilization of low-temperature chilled water to handle sensible heat load limits the rise of the chilled water temperature and increases the entransy dissipation significantly. In the moisture extraction process, the difference in humidity ratio between the supply air and indoor air is small because of a larger airflow rate, and the entransy dissipation caused by the mixing between supply air and indoor air is also lower.

2.2.2. THIC air-conditioning System

In typical air-conditioning systems, the sensible heat load always occupies about 60%–80% of the total heat load. The cooling and dehumidification processes use the same low-temperature cooling sources in conventional air-conditioning systems, which leads to a waste of energy quality. In contrast to conventional air-conditioning systems, temperature- and humidity-independent control air-conditioning systems (i.e., THIC system shown as Fig. 2-8) employ different methods to control indoor temperature and humidity. THIC systems use high-temperature cooling sources for cooling processes, and low-temperature cooling sources separately for dehumidification processes (or other dehumidification methods), which could eliminate the loss of the combination of heat and moisture handling process in conventional air-conditioning system. An example of this type of system is a dry FCU that is used to control indoor air temperature, and Fig. 2-9 shows the working principle and psychrometric chart of the air handling process of a THIC system. Outdoor air is processed to a state which is dry enough remove the indoor moisture load to control indoor humidity; Dry FCUs use high-temperature chilled water to handle indoor air to control indoor temperature.

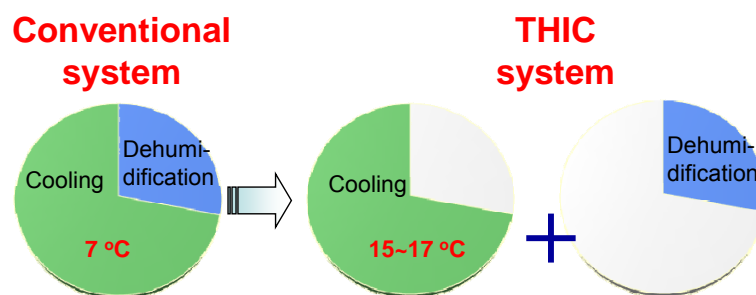


Fig. 2-8 Comparison between the THIC and conventional air-conditioning system (the sizes should be adjusted according to the energy levels)

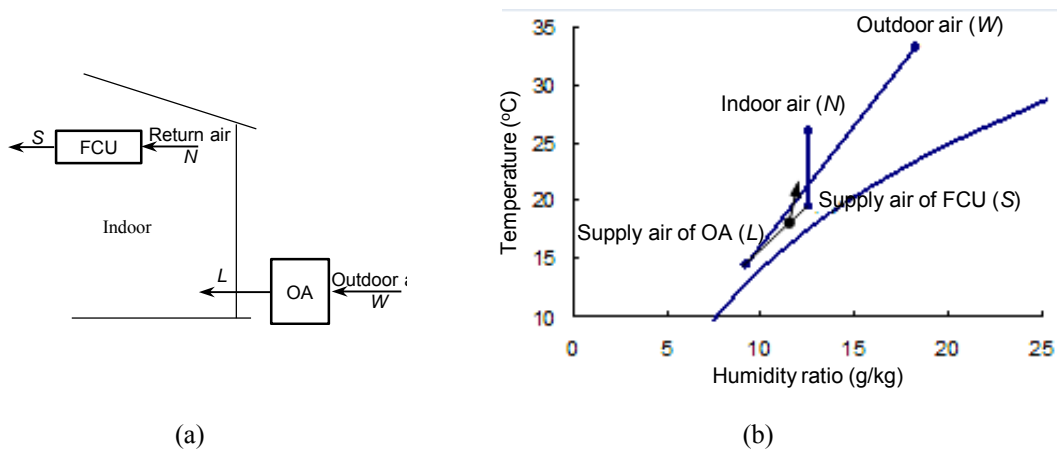


Fig. 2-9 Operating principle and air handling process of THIC system: (a) System working principle; and (b) Air handling process.

Fig. 2-10(a) shows the $T-Q$ diagram of the heat extraction process from high-temperature chilled water in dry FCUs in THIC systems to indoor state. For example, in the condensation dehumidification method, the outdoor air is first dehumidified by chilled water and is then supplied to the indoor space to control humidity. Fig. 2-10(b) shows the $\omega-m_w$ diagram of the moisture extraction process from the indoor space to the low temperature chilled water. Compared with conventional air-conditioning systems, the entransy dissipation of the heat extraction process in THIC systems decreases significantly. Take the FCU+OA system as an instance, the entransy dissipations of the conventional and THIC systems are $16.5Q_1$ and $7.5Q_1$, respectively. With regard to the moisture extraction process, compared with conventional air-conditioning system, which handles return air to remove the indoor moisture load, THIC systems always utilize outdoor air for the indoor moisture extraction process. Because of the small outdoor airflow rate, which only performs the dehumidification task, the required humidity ratio of the processed outdoor air is relatively low, which increases the entransy dissipation caused by the mixing of supplied air for dehumidification and indoor air, and raises the required performance of the outdoor air handling process. When the indoor state is designed at 26°C and a humidity ratio of 12.6 g/kg , the personal moisture load is 109 g/h and the outdoor airflow rate is $30\text{ m}^3/\text{h}/\text{person}$. The difference in the required humidity ratio between the supplied outdoor air and indoor air in THIC systems is 3.0 g/kg , i.e., the required humidity ratio of supplied air is 9.6 g/kg . Compared with conventional air-conditioning systems, the outdoor air is supposed to be processed to a lower humidity ratio in THIC systems. Thus, using a small airflow rate for dehumidification makes the humidity ratio of processed air lower, but decreases the energy

consumption of fans.

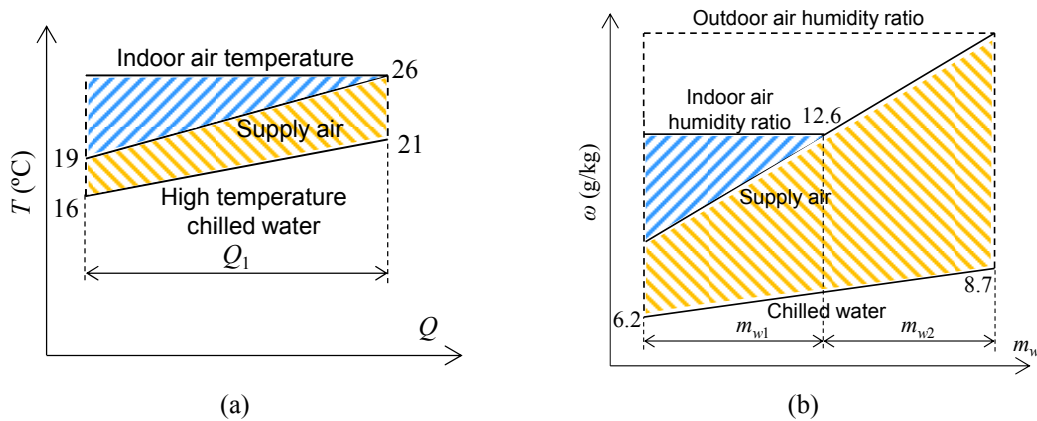


Fig. 2-10 Depiction of entransy dissipation in the heat and moisture extraction processes of THIC systems: (a) Heat extraction process; and (b) Moisture extraction process (e.g. condensation dehumidification method).

In THIC systems, the heat and moisture extraction processes are performed separately. When high-temperature cooling sources are adopted for heat extraction processes, the total entransy dissipation in heat extraction process decreases significantly. Utilizing high-temperature cooling sources for heat extraction could decrease entransy dissipation significantly and reduce the requirement of the level of cooling sources, which is beneficial to improve the cooling source efficiency. For a given heat quantity, the input of heat exchange capacity UA for the heat transfer between air and high-temperature cooling source should be increased. It is notable that increasing the heat exchange capacity could decrease both entransy dissipation and the requirement of the level of cooling sources in conventional air-conditioning system, but the cooling source temperature is limited by the condensation dehumidification method because of the utilization of the same low-temperature cooling source for cooling and dehumidification. Instead, high-temperature cooling sources are adopted for heat extraction in THIC systems. THIC and conventional systems are differentiated based on whether temperature and humidity can be controlled independently or not.

2.3. Construction principles based on indoor heat and moisture collecting process

2.3.1. Heat collection in indoor inhomogeneous thermal environment

Reducing the entransy dissipation in collection processes is beneficial for realizing heat collection processes, i.e., decreasing the heat quantity and increasing the cooling source

temperature. Through the depiction of the entransy dissipation in indoor heat collection processes, the blending of heat sources of different qualities into an indoor state contributes to significant entransy dissipation owing to blending and reduction in heat source quality. In heat exhaustion processes, the required temperature level of cooling sources is closely related to the temperature quality of heat sources: The higher the temperature level of heat sources, the higher is the temperature level of cooling sources required to exhaust heat quantity; in theory, the lower the temperature quality requirement of cooling sources, the wider is the range of optional natural cooling sources. Therefore, an approach involving the direct heat extraction from high-temperature heat sources and heat removal is efficient for increasing the required cooling source temperature in heat collection processes, by eliminating the blending of high-temperature heat sources in different temperature qualities into the indoor state.

In indoor illumination and facilities, for example, the heat sources can be regarded as given heat flux and their temperature levels are always considerably higher than the required indoor temperature level. As for an active air-conditioning system in summer, the extraction of heat due to illumination and facilities is an important component of indoor heat collection processes. In this heat collection process, the conventional idea is to blend the heat sources into an indoor state, extract the heat quantity from the indoor air by a unified supply air, and finally exhaust the heat via the air-conditioning systems. Fig. 2-11(b) shows the heat collection processes, from the heat sources to the chilled water of the air-conditioning system, including the blending of heat sources and indoor air (process ①), the blending of supply air and indoor air (process ②), and the transfer of heat between supply air and chilled water (process ③). The typical temperature of a heat source is $T_h = 33^\circ\text{C}$, and the required heat extraction Q_0 is given. The indoor air temperature is $T_r = 26^\circ\text{C}$, and the supply air temperature is 18°C ; considering the requirement of heat extraction, the supply/return chilled water temperature is $16^\circ\text{C}/21^\circ\text{C}$. When the heat quantity Q_0 is exhausted after blending into the indoor state, the entransy dissipation in processes ①–③ under typical parameters is $7Q_0$, $4Q_0$, and $3.5Q_0$, and the corresponding thermal resistances R_1 – R_3 are $7/Q_0$, $4/Q_0$, and $3.5/Q_0$. The total entransy dissipation and thermal resistance in heat collection processes are $14.5Q_0$ and $14.5/Q_0$, respectively.

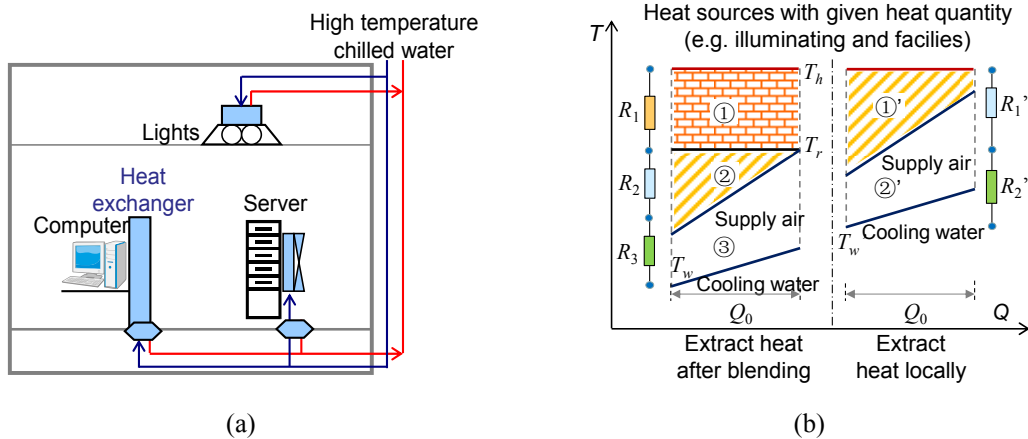


Fig. 2-11 Utilization of high temperature cooling sources to directly extract heat due to illumination and facilities: (a) System working principle; and (b) T - Q diagram of the handling process.

Heat exhaustion through a unified supply air after the blending of heat in different temperatures into the indoor state leads to a significant blending of the heat quantity of sources with indoor air; this mixing process leads to mixing thermal resistance, which accounts for 48% of the total thermal resistance. Though the heat quantity required to be extracted in the heat collection process is still Q_0 , the temperature level of the heat sources is decreased (from 33°C to 26°C). Fig. 2-11(a) shows the working principle of the system utilizing high-temperature cooling sources to extract heat from indoor illumination and facilities; this system is employed to decrease the blending loss in the heat collection processes for different indoor heat sources. With regard to lights, computers, servers, etc., the heat source temperatures are much higher than the required indoor temperature, and chilled water can be transported directly to the heat sources; an air-water heat exchanger is used to transfer heat between the chilled water and heat sources. Thus, through separate collections and processes of heat quantity produced by illumination and facilities, the heat source can be efficiently used with a higher temperature level and the cooling sources can be used with a higher temperature for heat exhaustion.

From the T - Q diagram of the different handling processes in Fig. 2-11(b), compared with the manner in which unified heat extraction takes place after blending the heat quantity produced by illumination and facilities into the indoor state, the manner in which high-temperature cooling sources are used to extract heat locally eliminates the blending process. The heat collection processes includes heat exchange between the heat sources and supply air ①' and heat exchange between the supply air and chilled water ②'; a decrease in the temperature level owing to the blending process and the blending entransy dissipation is prevented. Under the same condition of heat sources, when the temperature and heat quantity

of the heat source are still 33°C and Q_0 , respectively, and the flow rate of supply air and chilled water and the heat transfer area are identical, after preventing the blending of heat quantity from heat sources into the indoor state and considering a certain temperature difference in the heat transfer process between air and heat sources, the temperature of the supply/return air could be increased to 22°C/30°C; the temperature of the corresponding supply/return chilled water could be increased to 20°C/25°C. The equivalent thermal resistance of processes ①' and ②' are $7/Q_0$ and $3.5/Q_0$, respectively, and the total thermal resistance of the heat collection processes is decreased to $10.5/Q_0$.

Therefore, through separate collections of heat quantity produced by illumination and facilities, the characteristic of the temperature level of heat sources being higher than indoor state could be made the most of, and entransy dissipation during blending of heat with indoor air could be prevented. This effective process is beneficial for improving the entire heat collection process, decreasing the entransy dissipation and thermal resistance, and significantly increasing the temperature level of cooling sources in the heat extraction process. Raising the required temperature level of cooling sources creates favorable conditions for a wider use of natural cooling sources and improving the efficiency of the mechanical cooling sources.

2.3.2. Limiting factors when choosing terminal units

When considering the operation of different heating and cooling systems and selection of terminal units, there are certain limiting factors, depending on the occupant thermal comfort (overall and local), dew point, and occupant safety and health.

The thermal comfort of occupants in a space is directly influenced by the choice of the terminal unit in that space. Human thermal comfort can be considered to consist of two parts, overall and local. The overall thermal comfort depends on the air temperature and the mean radiant temperature in the space, which is usually expressed as operative temperature. Different thermal indoor environment categories are defined based on the operative temperature in international standards. Although the overall thermal comfort may be satisfactory, the local thermal discomfort can cause dissatisfaction with the thermal environment.

In addition to providing the required overall thermal comfort, the following phenomena should also be considered:

- Draft
- Vertical air temperature difference
- Warm or cool floors
- Radiant asymmetry

Additionally, the temperature drifts in buildings should also be controlled, and they should not exceed the limits given in respective standards. The same applies for noise; noise from terminal units should be limited and the sound pressure levels should not be exceeded for the given type of space.

The international standards (EN 15251:2007, EN ISO 7730:2005, ASHRAE 55-2010) should be followed to provide an optimal indoor environment for the occupants, considering indoor air quality, thermal indoor environment, acoustics, and lighting.

When considering the surface temperatures for radiant surface heating and cooling systems, in addition to the surface temperature and radiant asymmetry limitations given in international standards, the dew point is another limiting factor. The formation of dew on the cooled surfaces should be prevented, and it is good practice to maintain the supply temperature to the radiant loops below the dew point.

Occupant safety and health also puts certain limitations on permissible surface temperatures. The wall surface temperatures in wall heating systems should be designed such that the risk of pain caused by touching with bare skin is minimized. This happens when the surface temperature exceeds approximately 40°C. The perception of high surface temperature will depend on the thermal properties (thermal conductivity and specific heat capacity) of the surface material. The dew point and draft concerns should be considered when designing a wall cooling system.

On the supply-side, the choice of heat source and sink for the heating and cooling system will depend on the terminal unit, geographical conditions, and the regulations (location-specific opportunities such as district heating/cooling, utilization of seawater for cooling, etc.). A holistic approach that considers the supply, distribution, and terminal units (emission) is required for system and component selection.

2.3.3. Construction principles for thermal built environment

As the most fundamental process in creating a proper thermal and humid built environment, the indoor heat and moisture extraction process is supposed to collect extra indoor heat and moisture with terminal units; the extraction process is significantly influenced by the inhomogeneous property of the indoor heat source temperature and moisture sources. The indoor heat and moisture extraction could be realized by various methods: heat quantity produced by indoor heat sources can be extracted by convection, radiation, etc.; the moisture produced by moisture sources can only be extracted by ventilation. In the heat and moisture collection and transportation processes from indoor heat and moisture sources to coolants in air-conditioning systems (e.g., chilled water and refrigerant), various types of losses are

expected owing to blending, heat transfer, a combination of heat and moisture handling process, etc. Improving the indoor heat and moisture extraction process is essential for enhancing the performance of the creation of thermal and humid built environments. Starting from the characteristics of indoor heat and moisture sources, through a thermal analysis on the transportation property of the indoor heat and moisture collection process, the effective approaches for reducing the consumption of driving force (temperature difference) and entransy dissipation in heat and moisture collection processes are derived.

Through the loss property of indoor heat and moisture collection processes, the construction principles of terminal units to extract extra indoor heat and moisture are derived, as well as the approaches to reduce entransy dissipation in the indoor collection process.

1) Temperature and humidity independent control

The required temperature levels of cooling sources differ for indoor heat and moisture extraction. For the heat extraction process, heat extraction could be realized in theory as long as the cooling source temperature is lower than the indoor heat source temperature. For the moisture extraction process, the cooling source temperature should be lower than the indoor dew point if the condensation dehumidification method is adopted. The required cooling source temperature for dehumidification is much lower than that for removing sensible heat. Conventional air-conditioning systems generally use the same cooling source for the simultaneous removal of heat and moisture, which reduces the quality of the low-temperature cooling source and increases the entransy dissipation in heat extraction processes.

A THIC system is used to eliminate losses caused by a combination of heat and moisture handling processes. Through temperature- and humidity-independent control, the cooling source temperature used for heat extraction increases significantly, and the entransy dissipation in the heat collection processes decreases significantly. The temperature control process achieves high-temperature cooling, reduction in entransy dissipation, reduction in the requirement of the temperature level of cooling sources, and improvement in the energy efficiency level of cooling sources. In addition, the temperature- and humidity-independent control overcomes the limitation of the combination of the heat and moisture handling processes and meets the demand of indoor temperature and humidity control better.

2) Decreasing the blending loss in indoor collection processes

The distribution of indoor heat sources is inhomogeneous, and the temperature levels of indoor heat sources are variable. The blending of heat quantity in different temperature levels into an indoor state causes significant blending entransy dissipation. Theoretically, the extraction of heat in variable temperature levels could be achieved by cooling sources of

variable temperatures. Practical air-conditioning systems generally use a single cooling source (a single ventilation of a single terminal unit) to remove heat load. Heat extraction can be achieved by convection, radiation, and other methods. Based on the inhomogeneous property of indoor heat sources, different terminal units could be adopted to meet the demand of heat extraction. Compared with convective terminal units (e.g., FCUs), radiant terminal units can reduce heat transfer processes, decrease the blending entransy dissipation, and improve the performance of the heat extraction process.

Though the blending process will not cause a loss in the cooling and heating quantity, the blending process increases the entransy dissipation in the indoor heat extraction process. Through an analysis of the loss property, with a given condition of indoor heat and moisture sources (quantity and temperature level), reducing the blending of heat and moisture as well as the blending of heat quantity from heat sources and indoor air could decrease the total entransy dissipation in the entire heat and moisture collection process, which is beneficial for lowering the requirement of the temperature level of cooling sources used in air-conditioning systems. Through improving the transportation property of the indoor heat and moisture collection process, a proper system to create thermal and humid built environments could be established.

In built environments, the thermal conditions are created by heat transfer between several heat sources (computers, lights, commercial boards, etc.) and heat sinks (e.g. radiant floor cooling). Regardless of the nature of the heat sources (constant heat flux or constant temperature, as explained in 1.1.1), there are two crucial issues to consider when analyzing the built environment; resistance between heat sources and terminal units, and occupant thermal comfort. Both of these are functions of the chosen terminal unit, and they require careful consideration together with the factors given in 2.3.2.

3. Characteristics of radiant terminal

In this Annex cooperation project focusing on high temperature cooling and low temperature heating in buildings, radiant terminal is regarded as an important approach to construct a HTC<H system. To investigate the characteristics of radiant terminals, typical concrete core radiant floors and light floors are examined and analyzed in this chapter. Their variant dynamic behaviors during intermittent operation and the impact of transient solar radiation are illustrated through numerical calculation. The concept of the time constant is used to estimate quantitatively the thermal inertia of the different types of radiant floors in the start-up period of the cooling/heating systems. Dynamic equivalent heat resistance is defined to reflect the thermal behavior of radiant floor. At the same time, the influence of material emissivity on longwave radiant heat exchange between the radiant floor surface and the

indoor wall surfaces is estimated. The location and duration of solar radiation on the floor surface through skylights and side windows in large spaces are depicted quantitatively. The following will give the detailed analysis on dynamic performance and cooling capacity prediction of radiant terminal, aiming to clarify the radiant terminal's characteristics and provide convenience for real applications.

3.1. Dynamic performance of radiant floors with solar radiation

3.1.1. Response time in the start-up process (without solar radiation)

1) Cool-down/heat-up process

Numerical models of radiant floors are given and validated as Appendix B, and the parameters of the radiant floor are also described in Appendix B. In the start-up process of radiant floor cooling/heating, it takes some time for the radiant floor to cool/heat itself. Here, supposing radiant floors I(a) and II(a) in cooling mode (chilled water temperature $\bar{T}_w=16^\circ\text{C}$, initial temperatures of radiant floors are equal to environmental temperature $T_z=28^\circ\text{C}$, and the integrated heat exchange coefficient at the floor surface $h_z=7\text{ W/m}^2\text{K}$) as examples. According to the results calculated with the numerical model introduced above, the floor surface temperature T_s gradually decreases from the initial temperature, and then cooling output q_s increases, as exhibited in Fig. 3-1 and Fig. 3-2, respectively.

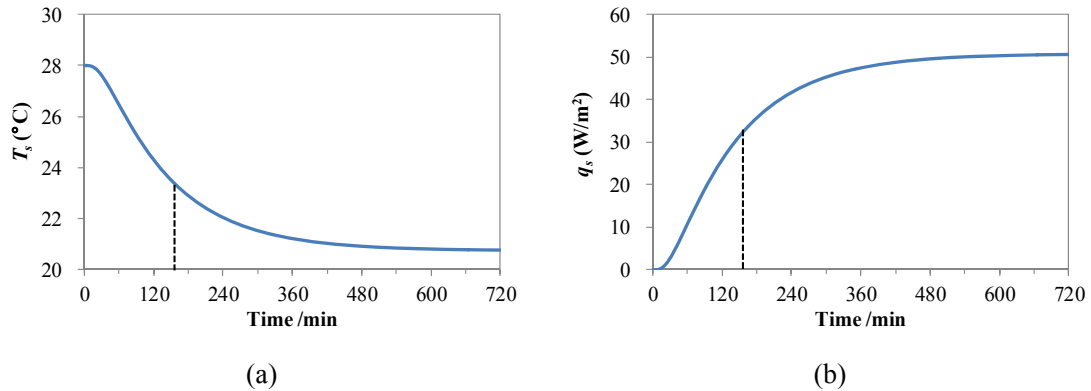


Fig. 3-1 Surface temperature and cooling capacity changes of concrete core radiant floor

I(a): (a) Surface temperature; and (b) cooling capacity at floor surface

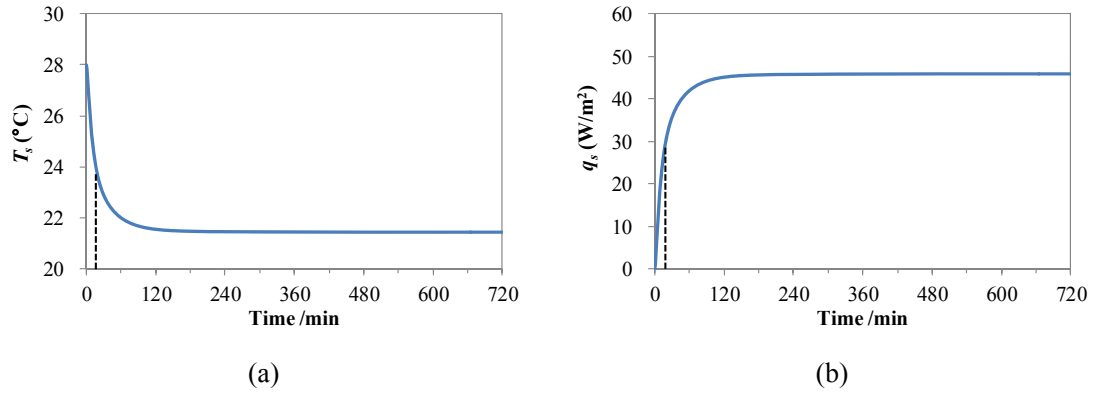


Fig. 3-2 Surface temperature and cooling capacity changes of light floor II(a): (a) Surface temperature; and (b) Cooling capacity at floor surface

It can be seen that the cool-down processes of concrete core radiant floor I(a) and light floor II(a) are considerably different in terms of stability time. For concrete core radiant floor I(a), it takes about 2.4h for its surface temperature to approach its steady state, and the cooling capacity reaches 63% of its maximum cooling output. Under the same conditions, it takes only 15~20 min for light radiant floor II(a) to cool itself down, which is significantly faster than radiant floor I(a).

Table 3-1 Time constant of typical radiant floors (Cooling mode: $h_z=7 \text{ W}/(\text{m}^2 \cdot \text{K})$, heating mode: $h_z=11 \text{ W}/(\text{m}^2 \cdot \text{K})$)

	I(a)	I(b)	I(c)	II(a)	II(b)
Heat resistance R ($\text{m}^2 \cdot \text{K}/\text{W}$)	0.094	0.219	0.264	0.119	0.200
Equivalent heat capacity C ($\text{kJ}/(\text{m}^2 \cdot \text{K})$)	148.4	128.9	107.0	17.4	9.1
Stability Cooling mode	2.4	3.1	2.8	0.3	0.2
time τ_c (h) Heating mode	1.9	2.3	2.0	0.2	0.2

The cool-down/heat-up times of concrete core radiant floors and light floors are indeed quite different. Even for radiant floors with similar structures, the response time varies based on pipe spacing, floor thickness, and surface material. In actual applications, a simple indicator that can reflect the response time of each radiant floor in the start-up process during intermittent cooling/heating is beneficial for system design and operation. Equivalent heat capacity C is defined according to the heat storage propriety of the radiant floor, and time constant τ_c in automatic control indicates the response time of “heavy floors” and “light floors.”

2) Equivalent heat capacity

The actual heat storage capacity of a radiant floor is not only dependent on its material

properties, but also on its internal temperature distribution, which is related to the structure of the radiant floor (pipe spacing, thickness, etc.). Hence, equivalent heat capacity C is introduced to reflect the heat storage capacity per unit of temperature difference between the water pipe and the floor surface; both the material properties of the radiant floor's components and the structure of the radiant floor (pipe spacing, etc.) are taken into consideration.

Fig. 3-3 (a) shows the representative domain of a radiant floor, which is divided into a layer with embedded water pipes and other slabs. The calculation methods for the heat capacities of the layer with embedded water pipes and the other slabs are introduced separately.

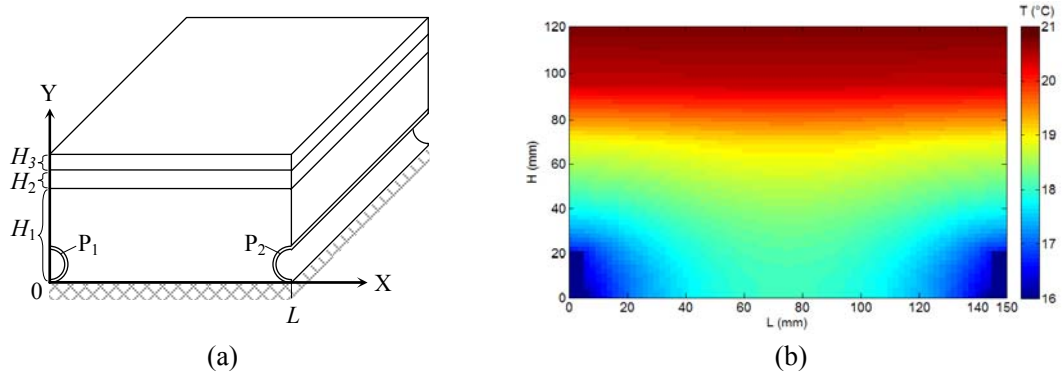


Fig. 3-3 Representative domain of radiant floor: (a) Physical model; and (b) Temperature distribution

(1) Heat capacity of a slab with embedded water pipes (C_1)

Around the water pipes, there is a filling layer, the heat conduction problem of which can be solved by a slab with embedded parallel circular pipes. The stored energy (Q_{stored} , measured in J/m^2) of the slab in steady state is acquired from the literature (Larsen, 2010).

Define the equivalent heat capacity (C_1) of the slab with embedded water pipes as Eq. (3-1):

$$C_1 = \frac{Q_{stored}}{T_w - T_s} \quad (3-1)$$

Equivalent heat capacity C_1 is expressed as

$$C_1 = \frac{\pi \rho_1 c_{p,1} \Gamma}{L^2} \left[L(d_1 + d_2) \left(\frac{2k_1}{U} - \frac{d_1^2}{d_1 + d_2} \right) + \delta^2 \left(\frac{\delta}{4} - \frac{2k_1}{U} \right) \right] + \frac{\rho_1 c_{p,1} \Gamma L}{2\pi^2} \sum_{s=1}^{\infty} \frac{\sin(\pi s \delta / L)}{s^3} \left[2 - G(s) \left(e^{\frac{\pi s \delta}{L}} - e^{-\frac{\pi s \delta}{L}} \right) - 2e^{-\frac{\pi s \delta}{L}} \right] \quad (3-2)$$

with

$$\Gamma = \left[\ln\left(\frac{L}{\pi\delta}\right) + \frac{2\pi k_1}{LU} + \sum_{s=1}^{\infty} \frac{G(s)}{s} \right]^{-1} \quad (3-3)$$

$$U = \left(\frac{1}{h_z} + \frac{d_1}{k_1} \right)^{-1} \quad (3-4)$$

$$G(s) = \frac{\frac{Bi + 2\pi s}{Bi - 2\pi s} e^{-\frac{4\pi s}{L}d_2} - 2e^{-\frac{4\pi s}{L}(d_1+d_2)} - e^{-\frac{4\pi s}{L}d_1}}{\frac{Bi + 2\pi s}{Bi - 2\pi s} + e^{-\frac{4\pi s}{L}(d_1+d_2)}} \quad (3-5)$$

where Bi is the Biot number of the slab surface ($Bi=h_zL/k_1$).

(2) Heat capacity of a uniform slab (C_2, C_3)

In radiant floors, there is a toweling layer and a surface layer above the pipe-embedded layer. Both the toweling layer and the surface layer can be considered to be slabs with uniform thermal diffusivity that satisfy the following equations:

$$\frac{\partial T}{\partial \tau} = a \left(\frac{\partial^2 T}{\partial x^2} + \frac{\partial^2 T}{\partial y^2} \right) \quad (3-6)$$

The boundary conditions of the governing equation are

$$\left. \frac{\partial T}{\partial x} \right|_{x=0} = \left. \frac{\partial T}{\partial x} \right|_{x=L} = 0 \quad (3-7)$$

$$\lambda \left. \frac{\partial T}{\partial y} \right|_{y=H_i} = h_z (T_z - T) \quad (3-8)$$

$$T|_{y=0} = f(x) \quad (3-9)$$

$$T|_{t=0} = T_0 \quad (3-10)$$

By solving the heat transfer equation, the equivalent heat capacity of a uniform slab can be obtained by Eq. (3-11):

$$C_i = \frac{\frac{1}{L} \int_0^{H_i} \int_0^L \rho_i c_{p,i} (T(\infty) - T_0) dx dy}{\frac{1}{L} \int_0^L (T(\infty)|_{y=0} - T(\infty)|_{y=H_i}) dx} = \frac{\rho_i c_{p,i} H_i}{2} \quad (3-11)$$

(3) Heat capacity of a radiant floor (C)

According to the principle of superposition of heat capacity, the total heat capacity of the radiant floor is

$$C = C_1 + \sum_{i=1}^n C_i \quad (3-12)$$

The equivalent heat capacities of the concrete core radiant floors and light floors are shown in Table 3-1. It can be seen from the table that the heat capacities of the concrete core radiant floors are 60~150 kJ/(m²·K), and those of the light floors are only 9~18 kJ/(m²·K).

3) Time constant (τ_c)

Based on equivalent heat capacity C , the concept of the time constant in automatic control is used as the time scale to measure the time required to stabilize the heat transfer.

First, an energy equation is used to describe radiant floor surface T_s exchanging heat with its surroundings in the dynamic process:

$$\begin{cases} C \frac{dT_s}{d\tau} = \frac{1}{R} (\bar{T}_w - T_s) + h_z (T_z - T_s) = (h_z + R^{-1}) (T_e - T_s) \\ T_s|_{\tau=0} = T_z \end{cases} \quad (3-13)$$

with

$$T_e = \frac{h_z T_z + R^{-1} \bar{T}_w}{h_z + R^{-1}} \quad (3-14)$$

By solving the heat transfer equation, the excess temperature coefficient ($\theta_s=0\sim 1$) can be obtained by Eq. (3-15):

$$\theta_s = \frac{T_s - T_z}{T_e - T_z} = 1 - \exp\left(-\frac{h_z + R^{-1}}{C} \tau\right) \quad (3-15)$$

Here choose the surface temperature changes of radiant floors I(a) and II(a) as examples. The heat exchange coefficient $h_z=7$ W/m²K, and the values of equivalent heat resistance R and heat capacity C are listed in Table 3-1. The excess temperature coefficients (θ_s), calculated according to Eq. (3-15), are shown in Fig. 3-4 (dotted line), conforming well to the results (full line) that transformed from the floor surface temperatures shown in Fig. 3-1 and Fig. 3-2. Thus, the simple calculation results accurately reflect the changes of surface temperature T_s .

On this basis, the radiant floor is considered to be equivalent to a lumped system with equivalent heat capacity C . Time constant τ_c , calculated according to Eq. (3-16), represents the time it takes the system's step response to reach 63% of its final (asymptotic) value ($\theta_s=0.63$):

$$\tau_c = \frac{C}{h_z + R^{-1}} \quad (3-16)$$

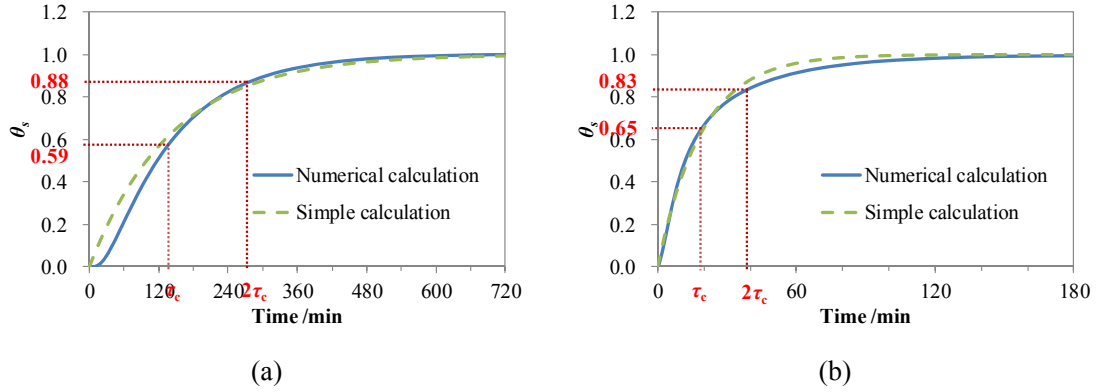


Fig. 3-4 Excess temperature coefficient of radiant floor: (a) Type I(a); and (b) Type II(a)

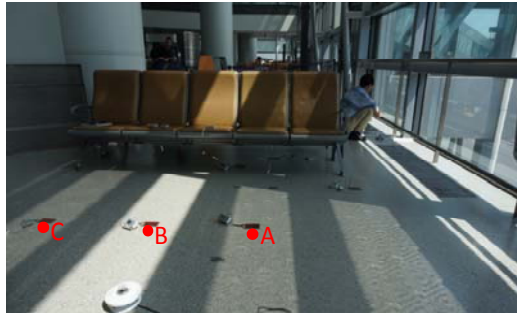
As shown in Fig. 3-4, the time constants of radiant floors I(a) and II(a) in cooling mode ($h_z=7 \text{ W}/(\text{m}^2\cdot\text{K})$) are 143 min and 19 min, respectively. During that time, the excess temperature coefficients (θ_s) are in the range of $63\pm 5\%$. And at time $2\tau_c$, the excess temperature coefficients are in the range of $86\pm 3\%$.

The time constants of the typical types of radiant floors are listed in Table 3-1. The values for the concrete core radiant floors are about 1~3 h. In contrast, those for the light floors are only 10~20 min, representing a much quicker response. Using the time constant as an indicator makes it easy to determine the advanced launch time of the cooling/heating system before the occupancy period during intermittent operation.

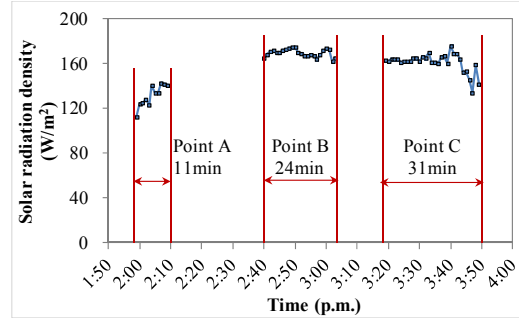
3.1.2. Dynamic performance with solar radiation

1) Effect of solar radiation

In summer, solar radiation on the floor surface may exceed over $100 \text{ W}/\text{m}^2$, especially in the space with large glass surface (such as airport, atrium), so that the cooling capacity of the radiant floor increases remarkably. Hence, the solar heat's intensity and duration are the key factors that influence the radiant floor cooling performance. Fig. 3-5 shows the solar radiation intensity tested on the radiant floor in the Xi'an Xianyang International Airport, which ranges from 120 to $170 \text{ W}/\text{m}^2$ when the outdoor solar radiation intensity is $500\sim 750 \text{ W}/\text{m}^2$ (measured on July 16th, 2013). The solar radiation absorption factor of the radiant floor surface is $0.6\sim 0.7$, and about $80\sim 120 \text{ W}/\text{m}^2$ of heat caused by solar radiation is absorbed by the radiant floor. At different points (Points A, B, and C shown in Fig. 3-5(a)), the duration of the direct solar radiation (through a band of transparent glass with a height of 1.2 m) is 10~30 min.



(a)



(b)

Fig. 3-5 Direct solar radiation on radiant floor: (a) test points; and (b) solar radiation intensity

The performances of radiant floors I(a) and II(a) with solar radiation were simulated by numerical calculation. In its original state, the radiant floor is stable within the environment $T_z=28^\circ\text{C}$ (no solar radiation, $h_z=7 \text{ W/m}^2\text{K}$), and chilled water temperature $\bar{T}_w=16^\circ\text{C}$, with a corresponding floor surface temperature (T_s) of

$$T_s(\infty) = \frac{h_z T_z + R^{-1} \bar{T}_w}{h_z + R^{-1}} \quad (3-17)$$

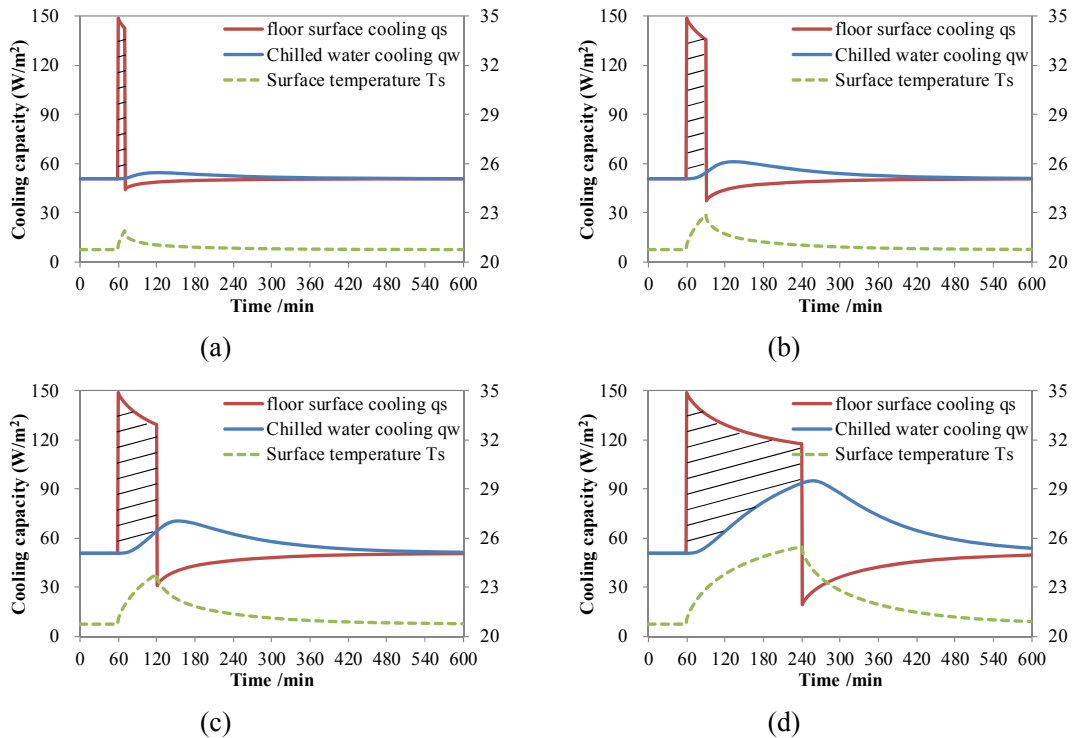


Fig. 3-6 Cooling capacity and surface temperature changes of concrete core radiant floor I(a) with solar radiation: (a) 10 min; (b) 30 min; (c) 1h; and (d) 3h

Fig. 3-6 (concrete core radiant floor) and Fig. 3-7 (light floor) illustrate the changes of floor surface temperature T_s and cooling capacity q_s (at the floor surface) when direct solar

radiation is 100 W/m^2 , with durations of 10 min, 30 min, 1 h, and either 3 h or 2 h. In the start-up phase, the heat absorbed by the floor surface (q_s) increases immediately. As time elapses, floor surface temperature T_s increases and the cooling capacity at the floor surface (q_s) decreases, approaching their equilibrium temperature and cooling capacity, as shown in Eqs. (3-18) and (3-19), respectively:

$$T_s^{sr}(\infty) = \frac{h_z T_z + q_{sr} + R^{-1} \bar{T}_w}{h_z + R^{-1}} \quad (3-18)$$

$$q_s^{sr}(\infty) = \frac{h_z T_z + q_{sr} - h_z \bar{T}_w}{1 + h_z R} \quad (3-19)$$

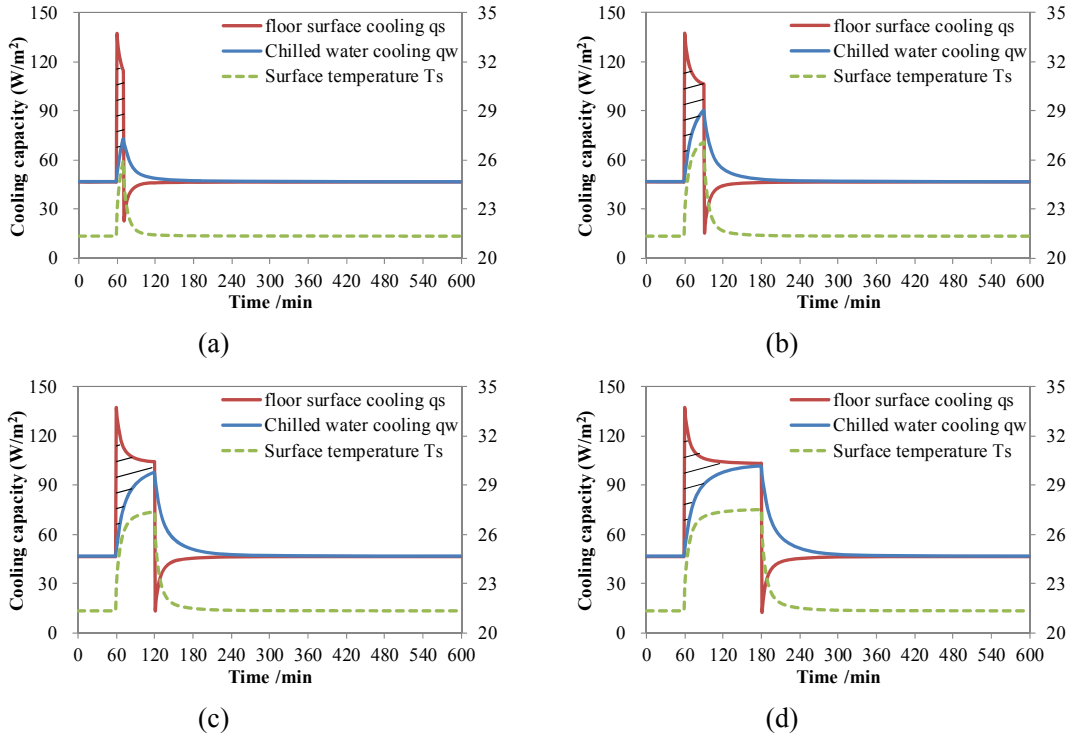


Fig. 3-7 Cooling capacity and surface temperature changes of light radiant floor II(a) with solar radiation: (a) 10 min; (b) 30 min; (c) 1h; and (d) 2h

By comparing the processes of change for the concrete core radiant floors and the light floors, it can be seen that the surface temperature (T_s) of concrete core radiant floor I(a) increases slowly. The heat absorbed by the floor surface (q_s) decreases slowly as well, and is maintained at a higher level than $q_s^{sr}(\infty)$ for a considerable amount of time; T_s of the light floor increases quickly, and the heat absorbed by the floor surface (q_s) is equal to $q_s^{sr}(\infty)$.

2) Dynamic heat resistance

The detailed cooling capacity of the radiant floor is related not only to the structure of the radiant floor, but also to the intensity and duration of the solar radiation. Similar to the

equivalent heat resistance in steady state R , a dynamic equivalent heat resistance R^{sr} is defined to reflect the radiant floor cooling capacity at the floor surface when it is exposed to transient solar radiation.

According to the definition of the equivalent heat capacity (C), the actual maximum heat storage per unit of temperature difference between the water pipe and the floor surface during solar radiation is rC , where r is the ratio of the heat storage caused by the solar radiation (Q^{sr}_{stored}) to the total heat storage ($Q_{stored} + Q^{sr}_{stored}$):

$$r = \frac{Q^{sr}_{stored}}{Q^{sr}_{stored} + Q_{stored}} = \frac{T_s^{sr}(\infty) - T_s(\infty)}{T_s^{sr}(\infty) - \bar{T}_w} = \frac{q_{sr}}{h_z(T_z - \bar{T}_w) + q_{sr}} \quad (3-20)$$

Similar to the analysis of the start-up process, the radiant floor can be considered to be equivalent to a lumped system in the analysis of floor surface temperature and cooling capacity changes. The change in radiant floor surface temperature T_s when there is transient solar radiation with duration $\Delta\tau^{sr}$ is

$$T_s(\tau) = \begin{cases} T_s(\infty) + (T_s^{sr}(\infty) - T_s(\infty)) \left(1 - \exp(-\tau/r\tau_c)\right) & (\tau \leq \Delta\tau^{sr}) \\ T_s(\Delta\tau^{sr}) + (T_s(\infty) - T_s(\Delta\tau^{sr})) \left(1 - \exp(-(\tau - \Delta\tau^{sr})/r\tau_c)\right) & (\tau > \Delta\tau^{sr}) \end{cases} \quad (3-21)$$

The corresponding cooling capacity at the floor surface (q_s) is obtained by Eq. (3-22), with the maximum value $q_{s,max}$ shown in Eq. (3-23) when $\tau=0$.

$$q_s(\tau) = \begin{cases} h_z \left[T_z - T_s(\infty) - (T_s^{sr}(\infty) - T_s(\infty)) \left(1 - \exp(-\tau/r\tau_c)\right) \right] + q_{sr} & (\tau \leq \Delta\tau^{sr}) \\ h_z \left[T_z - T_s(\Delta\tau^{sr}) - (T_s(\infty) - T_s(\Delta\tau^{sr})) \left(1 - \exp(-(\tau - \Delta\tau^{sr})/r\tau_c)\right) \right] & (\tau > \Delta\tau^{sr}) \end{cases} \quad (3-22)$$

$$q_{s,max} = h_z (T_z - T_s(\infty)) + q_{sr} \quad (\tau = 0) \quad (3-23)$$

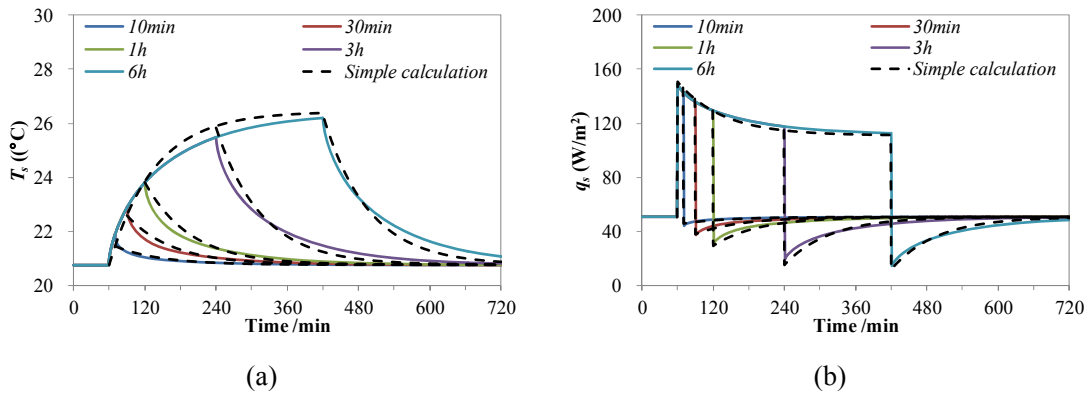


Fig. 3-8 Simple calculation of surface temperature and cooling capacity for concrete core radiant floor I(a): (a) T_s ; and (b) q_s

Under the same conditions as those in Fig. 3-6 and Fig. 3-7, the calculation results for the surface temperature and cooling capacity changes of radiant floors I(a) and II(a) with solar radiation are shown in Fig. 3-8 and Fig. 3-9, respectively (dotted lines). It can be seen that the simple calculation results accord well with the numerical calculation results.

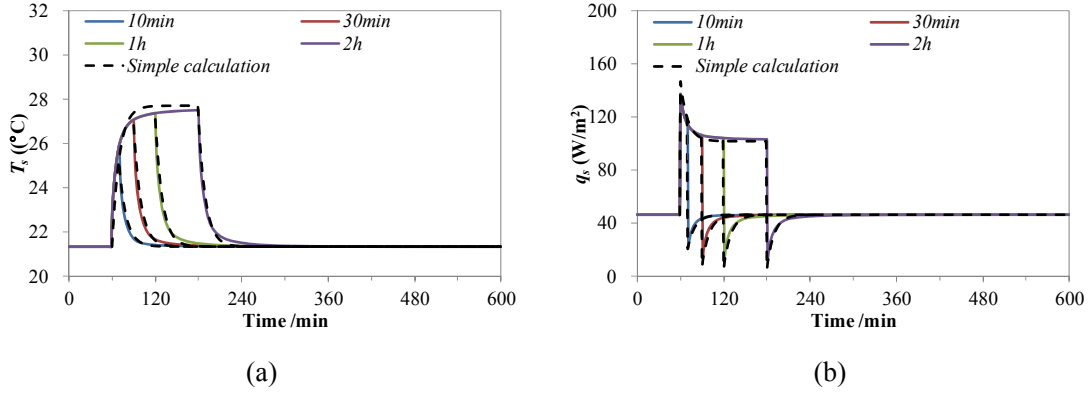


Fig. 3-9 Simple calculation of surface temperature and cooling capacity for light radiant floor II(a): (a) T_s ; and (b) q_s

Form Eqs. (3-20)-(3-21), the dynamic heat resistance R^{sr} is the product of the heat resistance in steady state R and corresponding factor α , displayed in Eq. (3-24).

$$R^{sr}(\tau) = \frac{T_s(\tau) - \bar{T}_w}{q_s(\tau)} = R \cdot \alpha \quad \text{where } \alpha = \frac{1 - r \exp(-\Delta\tau^{sr}/r\tau_c)}{1 - Rh_z r \exp(-\Delta\tau^{sr}/r\tau_c)} \quad (3-24)$$

Fig. 3-10 depicts the varying tendency of factor α with the solar radiation duration time under the same conditions with Fig. 3-6 and Fig. 3-7. The value of factor α is always less than 1 (upper limit value), which means that the heat absorption capacity of the radiant floor is strengthened when exposed to transient solar radiation. The factor α of concrete core radiant floor I(a) is smaller than that of light radiant floor, and it increases more slowly as well. Combined with the changes of the cooling capacity and surface temperature shown in Fig. 3-6 and Fig. 3-7, it can be seen that the smaller of the factor α , the relative higher cooling capacity of the radiant floor with solar radiation. Therefore, the radiant floor with high heat capacity and low value of α , such as the concrete core radiant floor, is more suitable for application with solar radiation.

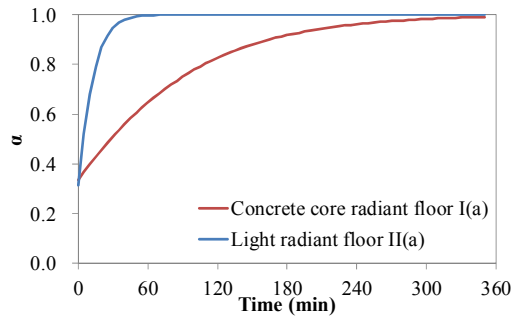


Fig. 3-10 Dynamic heat resistance factor α

Table 3-2 Cooling capacity at radiant floor surface with transient solar radiation

	τ_c (min)	$T_s(\infty)$ (°C)	q_{sr} (W/m ²)	$T_s^{sr}(\infty)$ (°C)	$q_{s,max}$ (W/m ²)	$q_s^{sr}(\infty)$ (W/m ²)	Average cooling capacity with solar radiation \bar{q}_s^{sr} (W/m ²)								
							10 min	30 min	1 h	2 h	3 h				
I(a)	140	20.8	100	26.4	150.7	111.0	Numerical calculation	145.4	141.1	136.7	131.0	127.2			
							Simple calculation	148.2	143.8	138.4	131.0	126.2			
							Error	+1.9%	+1.9%	+1.2%	-0.0%	-0.8%			
			50	23.6	100.7	80.8	Numerical calculation	98.1	96.0	93.8	90.9	89.0			
							Simple calculation	99.4	97.2	94.6	90.8	88.4			
							Error	+1.4%	+1.3%	+0.8%	-0.1%	-0.6%			
			II(a)	19	21.5	100	27.9	145.8	100.4	Numerical calculation	123.0	113.9	109.6	106.7	105.5
										Simple calculation	128.6	114.6	107.8	104.1	102.9
										Error	+4.5%	+0.5%	-1.6%	-2.4%	-2.5%
50	24.7	95.8				73.1	Numerical calculation	84.8	80.3	78.2	76.7	76.2			
							Simple calculation	87.2	80.2	76.8	75.0	74.3			
							Error	+2.8%	-0.2%	-1.7%	-2.3%	-2.4%			

* $T_z=28^\circ\text{C}$, $\bar{T}_w=16^\circ\text{C}$, $h_z=7 \text{ W}/(\text{m}^2\cdot\text{K})$, $r=0.54$ when $q_{sr}=100 \text{ W}/\text{m}^2$, and $r=0.37$ when $q_{sr}=50 \text{ W}/\text{m}^2$

Also, the average cooling capacity \bar{q}_s^{sr} during solar radiation with duration $\Delta\tau^{sr}$ can be obtain according to Eq. (3-25).

$$\bar{q}_s^{sr} = q_s^{sr}(\infty) + h_z (T_s^{sr}(\infty) - T_s(\infty)) \frac{r\tau_c}{\Delta\tau^{sr}} \left(1 - \exp\left(-\Delta\tau^{sr}/r\tau_c\right) \right) \quad (3-25)$$

The calculation results for the average cooling capacity (\bar{q}_s^{sr}) of radiant floors I(a) and II(a) with solar radiation of 100 W/m² and 50 W/m² are shown in Table 3-2. It can be seen that the simple calculation results are consistent with the numerical calculation results, with an error of $\pm 5\%$. The simple calculation method can be used for estimate the cooling capacity of radiant floor when applied with high-intensity solar radiation.

3.1.3. Conclusions

The cool-down/heat-up time in the start-up period and the change of the cooling capacity with solar radiation are two core factors in the application of radiant floor. In this section, the dynamic behaviors of radiant floors are investigated quantitatively with a numerical calculation model: The time constant, which is related to the heat capacity of radiant floors, is a convenient way to reveal the thermal response properties of radiant floors in the start-up period; the values for the concrete core radiant floor and the light floor are 1~3 h and 10~20 min, respectively. Using the time constant as an indicator makes it easy to determine the advanced launch time of the cooling/heating system before the occupancy period during intermittent operation. When exposed to solar radiation, the cooling capacity of radiant floors increases dramatically compared to applications without solar radiation. The dynamic equivalent heat resistance is defined to reflect the thermal behavior of radiant floor with transient solar radiation; concrete core radiant floor has lower values than the light radiant floor when the heat resistances in steady state are the same, which means that it owns high cooling capacity with solar radiation and more suitable for the application with high-intensity solar radiation.

3.2. Cooling capacity prediction of radiant floors in large spaces

3.2.1. Key factors of radiant floor cooling capacity in large spaces

1) Typical large spaces and radiant floor cooling

Check-in hall and departure hall, as shown in Fig. 3-11, are typical large spaces in airports. The former is structured with large spatial depth, so that skylights are adopted to improve indoor natural lighting; and the latter is usually designed with glass curtain walls for

a wide field of vision. In building design, there are also limits for fenestration and necessary sun shading technology in order to prevent excessive sunlight from coming into the indoor space. For examples, the check-in hall (shown in Fig. 3-11(a)) is 280 m in length, 114 m in depth, and 22 m in height. On the roof, 2-m-wide skylights with a shading coefficient of 0.3 are arranged in a row 20 m apart. The roof expands to deep overhangs, so that little direct sunlight comes into the indoor space through the glass curtain wall. The departure hall (shown in Fig. 3-11(b)) is 190 m in length, 39 m in width, and 16 m in height. The building façades are dominated by double glass curtain walls, the majority of which are furnished with colored glaze for sunshade, except for two bands in the middle and bottom (with a height of 1.5 m and 2.0 m, respectively, and a shading coefficient of 0.3) through which direct solar radiation shines on the radiant floor.

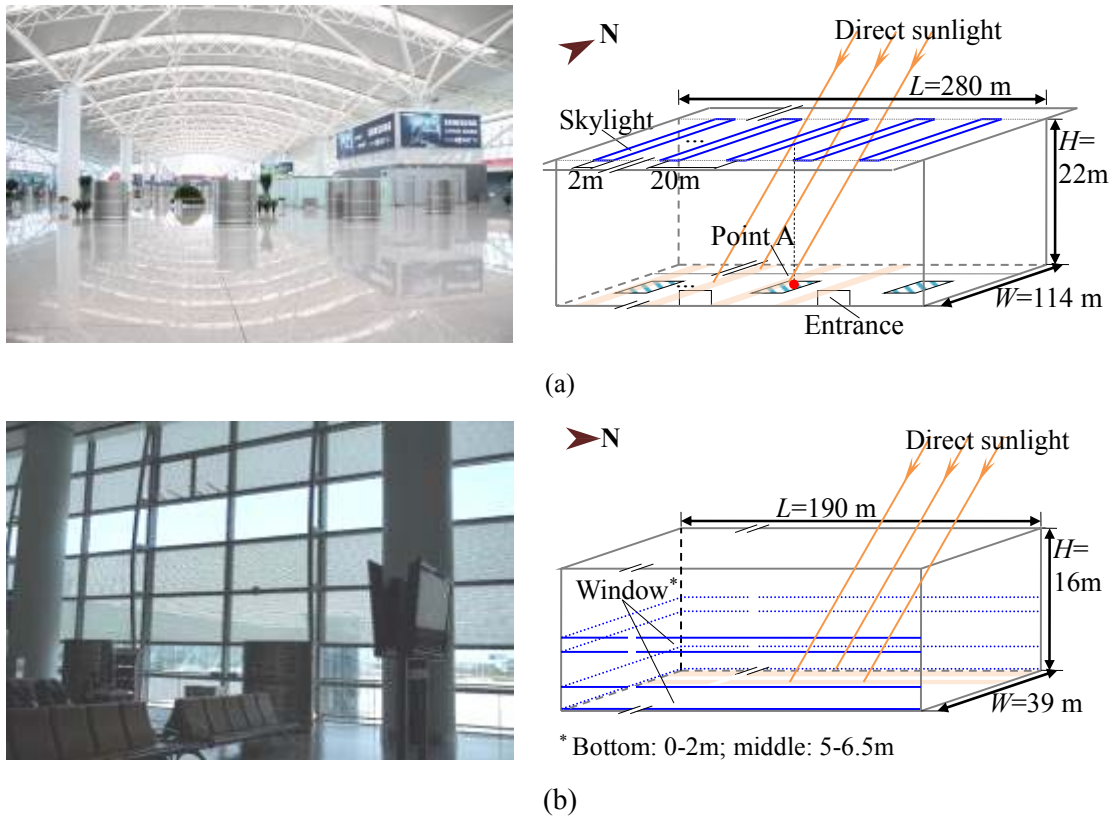


Fig. 3-11 Large spaces in an airport: (a) check-in hall; and (b) departure hall

For radiant cooling floor in large spaces, it exchanges heat with indoor air and wall surfaces by convection and longwave radiation, and also absorbs sunlight passing through the transparent glass falling on the floor surface, as depicted in Fig. 3-12(a). In cooling capacity calculation, the complex heat transfer process of a radiant floor can be divided into two parts as shown in Fig. 3-12(b): transfer from the indoor space to the radiant floor surface, and then to the chilled water inside the radiant floor. The heat transfer from the indoor space to the radiant floor surface is composed of convection (q_c), longwave radiation (q_{lr}), and absorption

of shortwave radiation (q_{sr}). Hereinto, the convective heat flux (q_c) and longwave radiant heat flux (q_{lr}) can be achieved when the convective heat exchange coefficient (h_c), longwave radiant heat exchange coefficient (h_{lr}), and corresponding indoor air temperature (T_a) and wall surface temperature ($AUST$) are known. The heat transfer from the floor surface to the chilled water is mainly determined by the construction parameters of the radiant floor (R) and the difference between the chilled water temperature (\bar{T}_w) and the radiant floor surface temperature (T_f). Thereout, the cooling capacity (q) of the radiant floor in steady state can be represented by Eq. (3-26):

$$\begin{aligned} \text{Indoor space} \rightarrow \text{radiant floor surface: } q &= q_c + q_{lr} + q_{sr} \\ &= h_c(T_a - T_f) + h_{lr}(AUST - T_f) + q_{sr} \end{aligned} \quad (3-26)$$

$$\text{Radiant floor surface} \rightarrow \text{chilled water: } q = \frac{T_f - \bar{T}_w}{R}$$

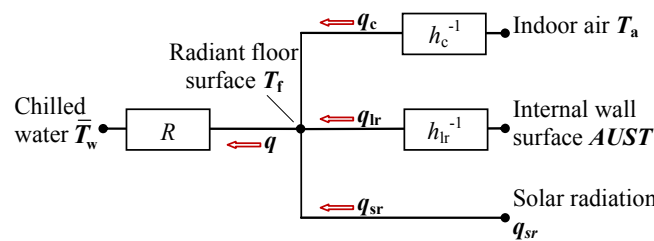
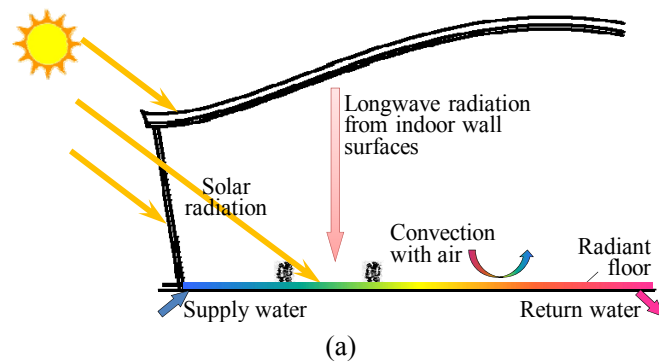


Fig. 3-12 Heat transfer of radiant cooling floor in a large space: (a) simple graph; and (b) simple analytical method with heat resistance

Usually, longwave radiant heat exchange coefficient (h_{lr}) has an almost constant value of 5.2-5.5 W/(m²·K) with an emissivity of 0.90-0.95. However, in large spaces, h_{lr} may change when low-emissivity materials are adopted. And the effect of solar radiation is usually a transient process of limited duration. As longwave radiation heat transfer q_{lr} and absorption of shortwave radiation of sunlight q_{sr} represent a significant proportion of the total cooling capacity of the radiant floor, these factors are worthy of deeper analysis.

2) Influence of emissivity on longwave radiation

Indoor surfaces exchange heat by longwave radiation with a delta pattern, such as the radiant network shown in Fig. 3-13. The net heat flux q_{lr} at the radiant floor surface can be calculated using the radiosity method, which solves the radiant exchange matrix, as shown in Eq. (3-27):

$$\begin{bmatrix} \frac{1}{\varepsilon_f - 1} & F_{f-1} & \cdots & F_{f-n} \\ F_{1-f} & \frac{1}{\varepsilon_1 - 1} & \cdots & F_{1-n} \\ \cdots & \cdots & \cdots & \cdots \\ F_{n-f} & F_{n-2} & \cdots & \frac{1}{\varepsilon_n - 1} \end{bmatrix} \begin{bmatrix} J_f \\ J_1 \\ \vdots \\ J_n \end{bmatrix} = \begin{bmatrix} \frac{\varepsilon_f}{\varepsilon_f - 1} \sigma T_f^4 \\ \frac{\varepsilon_1}{\varepsilon_1 - 1} \sigma T_1^4 \\ \vdots \\ \frac{\varepsilon_n}{\varepsilon_n - 1} \sigma T_n^4 \end{bmatrix} \quad (3-27)$$

$$q_{lr} = \frac{\sigma T_f^4 - J_f}{(\varepsilon_f - 1)/\varepsilon_f}$$

where T_j , ε_j , A_j and J_j are the temperature, emissivity, area and radiosity of surface j (radiant floor is denoted by subscript f), F_{i-j} is the view factor between the surface i and surface j , and σ is the Stefan-Boltzman constant, $5.67 \times 10^{-8} \text{ W}/(\text{m}^2 \cdot \text{K}^4)$.

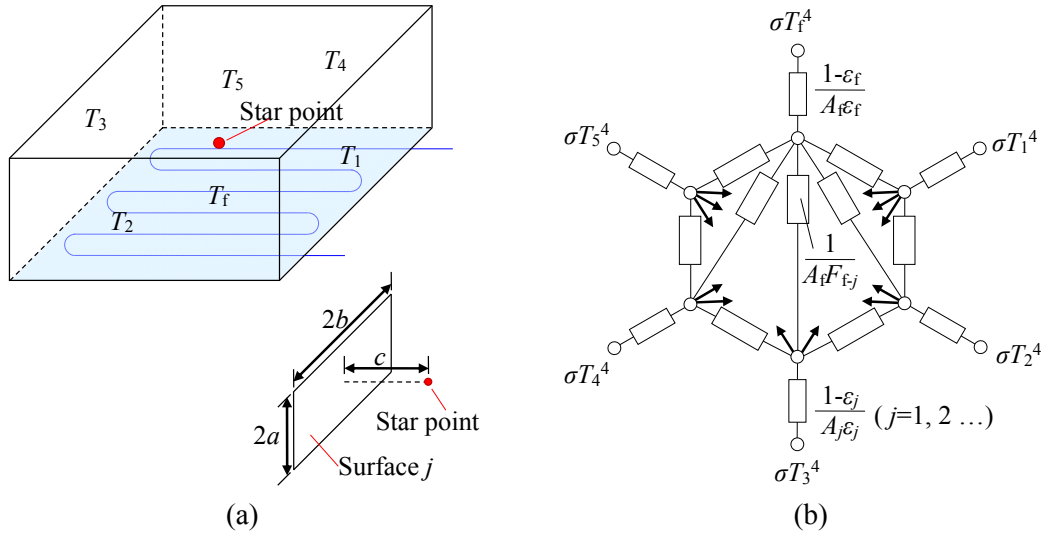


Fig. 3-13 Longwave radiant links in rectangular space: (a) rectangular enclosure; and (b) longwave radiant network with delta pattern

As shown in Eq. (3-27), emissivity is a critical parameter in the longwave radiant heat exchange process, which affects the radiant floor's cooling capacity. The surface emissivities of several ceiling, wall, and floor surface materials used in large spaces are listed in Table 3-3. The emissivity of sheet metal is 0.2-0.4, and the emissivities of heat-reflecting and low-e coatings (covering the indoor side) are 0.4-0.7 and 0.1, respectively. The emissivities of sheet metal and (indoor side) coated glass are obviously lower than those of common building

materials.

Table 3-3 Surface emissivity of common materials in large space buildings

Material	Emissivity	Condition
Al alloy	0.24~0.33	38°C; 3SO and 24ST types are 0.24 and 0.33, respectively
Stainless steel	0.21~0.39	23.9°C; Types 301, 306, and 347 are 0.21, 0.28, and 0.39 respectively
Ti alloy	0.24~0.31	T _{A7} plate (80°C): 0.26; Titanium plate (27°C): 0.31
Polycarbonate	0.95	
FRP	0.88~0.92	50°C
Glass	0.90~0.95	38°C
Heat-reflecting glass	0.40~0.70 (Lu, 2008)	Heat-reflecting coating covers the indoor side
Low-e glass	0.08~0.15 (Lu, 2008)	Low-e coating is covered at the indoor side
Marble	0.90~0.95	22~38°C
PVC	0.89~0.94	80°C; rigid and soft types are 0.89 and 0.94, respectively
Rubber	0.86~0.94	80°C; rigid and soft types are 0.94 and 0.86, respectively

The large spaces in Fig. 3-11 are taken as examples to illustrate the influence of emissivity on longwave radiation. For simplicity, the materials of the radiant floor surface, walls, and ceiling are kept uniform; the emissivities of both the walls and floor surface are fixed at 0.9. The temperatures of the ceiling, walls, and radiant floor surface are 32°C, 30°C, and 22°C, respectively. When the emissivity of the ceiling surface is 0.1, the heat fluxes at the radiant floor surface in the check-in hall and departure hall are only 21 W/m² and 28 W/m², respectively. However, they are about 49 W/m² when the emissivity is 0.9. Hence, the impact of material emissivity cannot be ignored in the calculation of the longwave heat exchange, especially when low-emissivity materials are adopted in large spaces.

In this conventional method, the longwave heat fluxes are calculated by solving the radiant exchange matrix. Unfortunately, this method is inconvenient for many engineering applications of radiant floor cooling, as it is difficult to jointly calculate with the convective heat transfer and directly absorbed solar radiation as shown in Fig. 3-12. Therefore, a new linearized simple calculation method for the longwave radiant heat exchange with different surface emissivities would be preferable.

3) *Transient solar radiation*

When the radiant floor is exposed to solar radiation, its cooling capacity increases sharply, while the floor surface temperature increases gradually. During this dynamic process, the equivalent heat resistance of radiant floor $R^{sr}(\tau)$ is much lower than the equilibrium value R . For example, for a concrete radiant floor with an equivalent heat resistance (R) of 0.1

(m²·K)/W and a heat capacity (C) of 138 kJ/(m²·K), the ratio of $R^{sr}(\tau)$ to R ranges from 0.3 to 1.0 as time elapses, as shown in Fig. 3-14. Therefore, in addition to solar radiation intensity, the duration of solar radiation is a key factor influencing the radiant floor's cooling capacity.

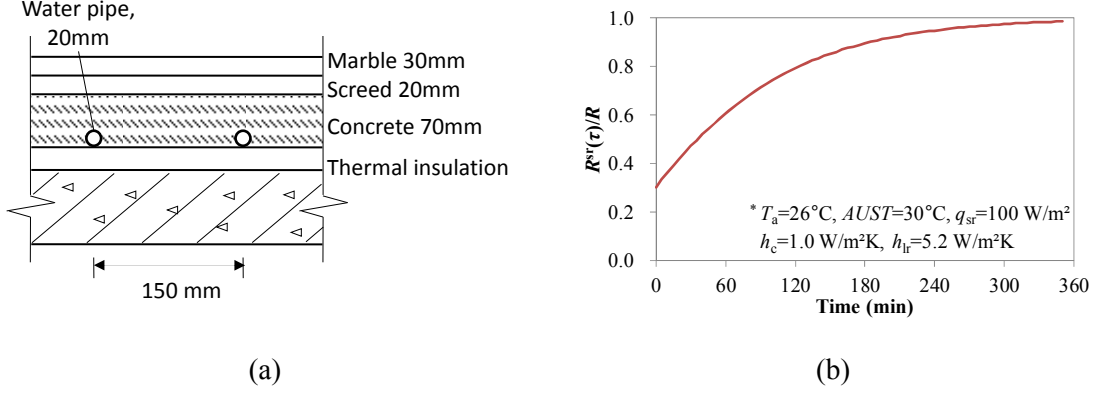


Fig. 3-14 Dynamic heat resistance of radiant floor: (a) structure; and (b) dynamic heat resistance $R_{sr}(\tau)$ with solar radiation

When there is transient solar radiation with a duration of $\Delta\tau^{sr}$, the average cooling capacity of the radiant floor (\bar{q}^{sr}) can be calculated according to Eq. (3-28). $q^{sr}(\infty)$ and $T_f^{sr}(\infty)$ are the equilibrium values of the radiant floor's cooling capacity and surface temperature, respectively, with solar radiation q_{sr} , and are calculated with Eq. (1). $T_f(\infty)$ is the equilibrium value under the condition without solar radiation.

$$\bar{q}^{sr} = q^{sr}(\infty) + (h_c + h_{lr})(T_f^{sr}(\infty) - T_f(\infty)) \frac{\gamma\tau_c}{\Delta\tau^{sr}} \left(1 - \exp\left(-\frac{\Delta\tau^{sr}}{\gamma\tau_c}\right) \right) \quad (3-28)$$

$$\text{where } \gamma = \frac{q_{sr}}{h_c(T_a - \bar{T}_w) + h_{lr}(AUST - \bar{T}_w) + q_{sr}}, \quad \tau_c = \frac{C}{h_c + h_{lr} + R^{-1}}$$

Furthermore, the location of the sunlight shining on the floor can guide both the placement of the cooling pipes inside the radiant floor and the partition of subsystems according to the cooling load caused by solar radiation.

3.2.2. Longwave heat exchange with different emissivity values

1) Methodology of new approach

First, the delta-based surface-surface pattern in Fig. 3-13 is transformed into the star-based pattern in Fig. 3-15(a), as the heat resistance between any two nodes in a star-based pattern should be equal to those in a delta-based pattern. The β_j value has to be adjusted so that the external effect of the star circuit resembles that of the delta circuit. Previous research has demonstrated that in a spherical cavity, $\beta_j = 1 - F_{rs-j}$, in which F_{rs-j} is the view factor

between the star point and surface j . For a rectangular room where the vertices of each surface are located in the same sphere, the values of β_j can be derived using the same equation. Combined with the view factor between a sphere and a surface, the β_j value can be calculated according to Eq. (3-29):

$$\beta_j = 1 - F_{rs-j}, \text{ where } F_{rs-j} = \frac{1}{\pi} \arctan \frac{abc^{-1}}{\sqrt{a^2 + b^2 + c^2}} \quad (j=f, 1, 2 \dots 5) \quad (3-29)$$

where a and b are the length and width of surface j respectively, c is the distance between the star point and surface j , and F_{rs-j} is the view factor.

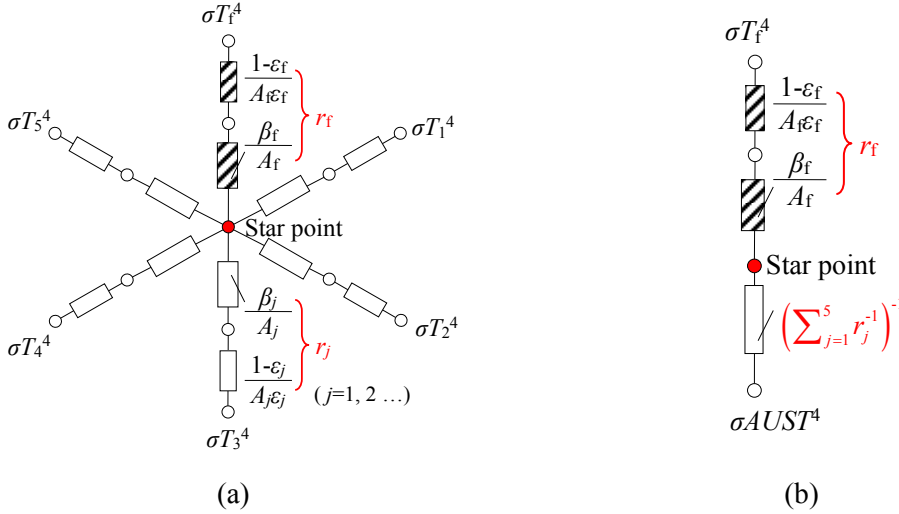


Fig. 3-15 Transformation of longwave radiant network: (a) star pattern; and (b) simplification

Second, the total heat flux at the radiant floor (denoted by subscript f) from other surfaces in Fig. 3-15(a) can be simplified into Fig. 3-15(b). The resistance between the radiant floor and an equivalent of uncooled surfaces is composed of two parts: r_f between the radiant floor and the star point, and $(\sum_{j=1}^5 r_j^{-1})^{-1}$, which is the sum of the resistances between the radiant star point and the other uncooled surfaces. Hence, the heat flux per square meter at the radiant floor surface can be determined with Eq. (3-30):

$$q_{lr} = \frac{1}{A_f} \cdot \frac{\sigma(AUST^4 - T_f^4)}{r_f + (\sum_{j=1}^5 r_j^{-1})^{-1}} \quad (3-30)$$

$$\text{where } AUST = \left(\frac{\sum_{j=1}^5 r_j^{-1} T_j^4}{\sum_{j=1}^5 r_j^{-1}} \right)^{0.25}, \quad r_j = \frac{1 - \varepsilon_j}{A_j \varepsilon_j} + \frac{\beta_j}{A_j} = \frac{\varepsilon_j^{-1} - F_{rs-j}}{A_j} \quad (j=f, 1, 2 \dots 5)$$

Based on these results, surface j ($j=f, 1, 2 \dots 5$) in Fig. 3-13 can be subdivided when the

surface materials and temperatures are different, as shown in Fig. 3-16(a). The transformed star-based network is shown in Fig. 3-16(b), in which the $\beta_{j,i}$ value for each patch can be calculated according to Eq. (3-31):

$$\beta_{j,i} = A_{j,i} \frac{\beta_j F_{rs-j}}{A_j F_{rs-j,i}}, \text{ where } F_{rs-j,i} = \frac{g(a,b) + g(a_0,b_0) - g(a_0,b) - g(a,b_0)}{4\pi} \text{ with} \quad (3-31)$$

$$g(a,b) = \arctan \frac{abc^{-1}}{\sqrt{a^2 + b^2 + c^2}} \quad (j=f, 1, 2 \dots 5; i=1, 2 \dots n_j)$$

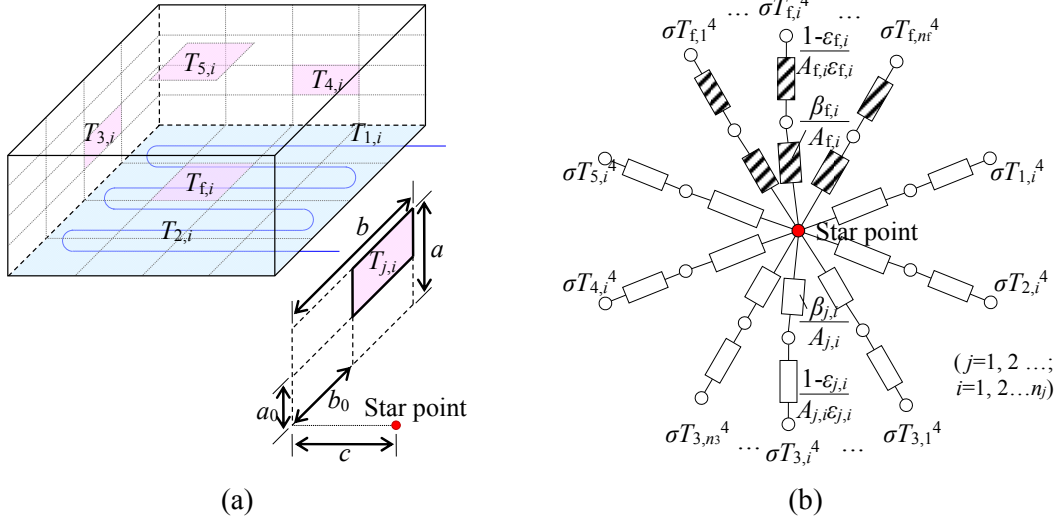


Fig. 3-16 Longwave radiant links with subdivided patches: (a) rectangular enclosure with subdivided surfaces; and (b) longwave radiant network with star pattern

The average heat flux at the radiant floor also can be calculated with Eq. (3-30), in which the temperature and heat resistance values are from Eq. (3-32):

$$\bar{T}_f = \left(\frac{\sum_{i=1}^{n_f} r_{f,i}^{-1} T_{f,i}^4}{\sum_{i=1}^{n_f} r_{f,i}^{-1}} \right)^{0.25}, \quad AUST = \left(\frac{\sum_{j=1}^5 \sum_{i=1}^{n_j} r_{j,i}^{-1} T_{j,i}^4}{\sum_{j=1}^5 \sum_{i=1}^{n_j} r_{j,i}^{-1}} \right)^{0.25}, \quad \text{and } r_j = \left(\sum_{i=1}^{n_j} r_{j,i}^{-1} \right)^{-1} \quad (3-32)$$

$$\text{where } r_{j,i} = \frac{1 - \epsilon_{j,i}}{A_{j,i} \epsilon_{j,i}} + \frac{\beta_{j,i}}{A_{j,i}} \quad (j=f, 1, 2 \dots 5; i=1, 2 \dots n_j)$$

And the heat flux of each patch ($q_{lr,j,i}$) can be expressed as Eq. (3-33):

$$q_{lr,j,i} = \frac{\sigma (T_{rs}^4 - T_{j,i}^4)}{A_{j,i} r_{j,i}} \quad \text{where } T_{rs} = \left(\frac{\sum_{j=1}^5 r_j^{-1} T_j^4 + r_f^{-1} \bar{T}_f^4}{\sum_{j=1}^5 r_j^{-1} + r_f^{-1}} \right)^{0.25} \quad (3-33)$$

$$(j=f, 1, 2 \dots 5; i=1, 2 \dots n_j)$$

2) Longwave heat transfer coefficient

For convenience, Eq. (3-30) can be linearized into Eq. (3-34), which represents the

product of the equivalent radiant heat exchange coefficient (h_{lr}) and the temperature difference between the radiant floor and the average uncooled surface ($AUST - T_f$):

$$q_{lr} = h_{lr}(AUST - T_f) \quad (3-34)$$

$$\text{where } h_{lr} = \frac{\sigma(T_f^2 + AUST^2)(T_f + AUST)}{A_f \left(r_f + \left(\sum_{j=1}^5 r_j^{-1} \right)^{-1} \right)} \approx \frac{\sigma(295^2 + 303^2)(295 + 303)}{A_f \left(r_f + \left(\sum_{j=1}^5 r_j^{-1} \right)^{-1} \right)}$$

The value of h_{lr} varies only slightly with the temperature levels of T_f and $AUST$. Therefore, T_f and $AUST$ can adopt constant values, e.g., 295 K and 303 K, respectively, in radiant floor cooling. Under this condition, the value of h_{lr} is only determined by the building geometry and surface emissivity of enclosure surfaces.

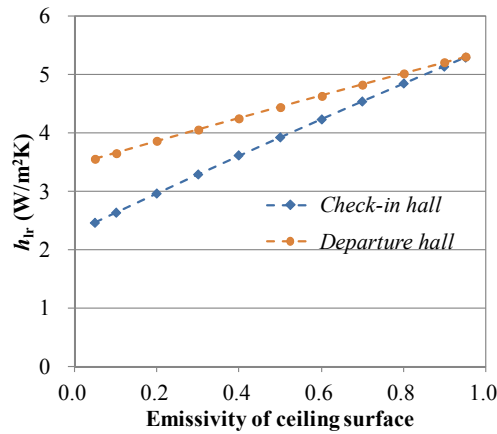


Fig. 3-17 Equivalent longwave radiant heat transfer coefficient h_{lr}

For the check-in hall and departure hall shown in Fig. 3-11, when the emissivities of both the walls and floor surface are fixed at 0.9 and the ceiling surface emissivity ranges from 0.05-0.95, the values of h_{lr} are presented in Fig. 3-17. It can be seen that the values of h_{lr} are decreases as the ceiling surface emissivity decreases. They are only 2.5 W/(m²·K) and 3.6 W/(m²·K) in the check-in hall and departure hall, respectively, when the emissivity of the ceiling surface is 0.05-0.1. In contrast, h_{lr} is in the range of 5.1-5.3 W/(m²·K) when the emissivity of the ceiling surface is 0.9-0.95.

Applying the equivalent radiant heat exchange coefficient h_{lr} , the calculation results of the longwave radiant heat flux at the radiant floor surface are shown in Fig. 3-18 (denoted by dots), where the temperatures of the ceiling, walls, and radiant floor surface are 32°C, 30°C, and 22°C, respectively. Compared with the exact results from the radiosity method in Eq. (3-27) (denoted by rhombuses), the calculation results calculated according to new method in Eq. (3-34) are very similar, with an error of less than 6%.

According to an analysis on 121 enclosures having ratios of L/H and W/H in the ranges

of 1 to 100 and 1 to 10 respectively, the root mean product deviations between the β_j value in Eq. (4) and the optimal values are less than 2%. Using constant temperature values of 295 K and 303 K in radiant floor cooling in the equation of h_{lr} , involves a maximum error of 2%. Therefore, this new method has an error within 6%.

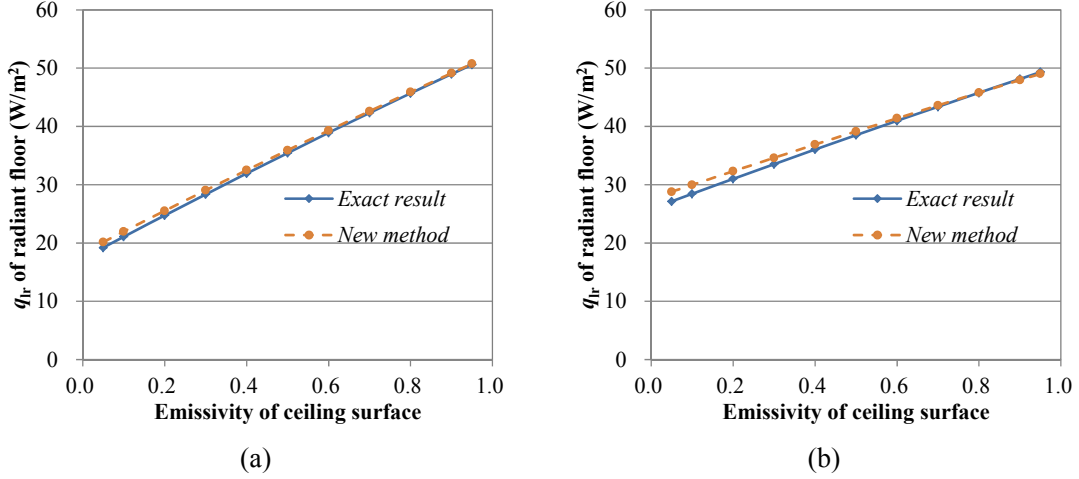


Fig. 3-18 Longwave radiant heat exchange of radiant floor with different ceiling surface emissivity values: (a) check-in hall; and (b) departure hall

As the values of h_{lr} and $AUST$ are independent of radiant floor surface temperature T_f , it is advantageous to select a proper T_f for the radiant floor in any engineering design. As shown in Eqs. (3-32) and (3-34), h_{lr} and $AUST$ have constant values when the building geometry, surface emissivity, and temperature of enclosure surfaces are known. On this occasion, linearized Eq. (3-34) allows for the expeditious selection of a proper radiant cooling floor surface temperature (T_f) for the required cooling capacity.

3.2.3. Effect of transient solar radiation on radiant floor

1) Location of sunlight on floor

The location of the sunlight shining on the floor can be calculated with the location of the window, the local solar elevation angle (θ), and the azimuth angle (α). For the sunlight shining through Point i in Fig. 3-19(a), the distances between its incident point on the floor surface (Point i') and Point i on the horizontal plane in the east-west and north-south directions are $D_{i,EW}$ and $D_{i,NS}$, respectively. The distances can be calculated according to Eq. (3-35), where H_i is the height of Point i :

$$D_{i,EW} = H_i \frac{\sin \alpha}{\tan \theta}, \quad D_{i,NS} = H_i \frac{\cos \alpha}{\tan \theta} \quad (3-35)$$

For instance, for the point located in Xi'an, China (34.3°N, 108.9°E) at a height of 20 m, the sunlight shining through it at 14:00 (UTC+08:00) on July 16th is located on its northeast side, with $D_{i,EW}$ and $D_{i,NS}$ equaling 6.5 m and 4.2 m, respectively. The detailed locations of the sunlight shining on the floor are shown in Fig. 3-19(b). Hereinto, $D_{i,EW}$ is counted as positive

for afternoon hours and negative for morning hours.

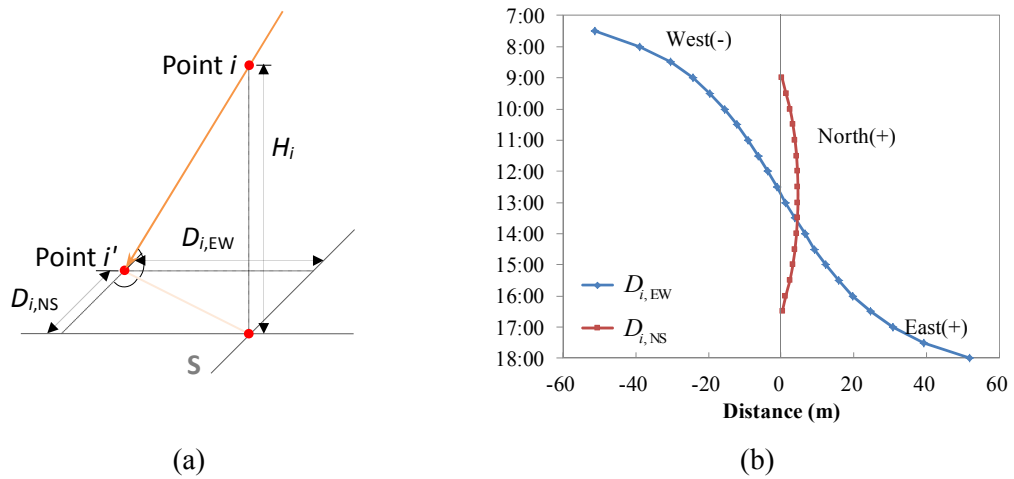
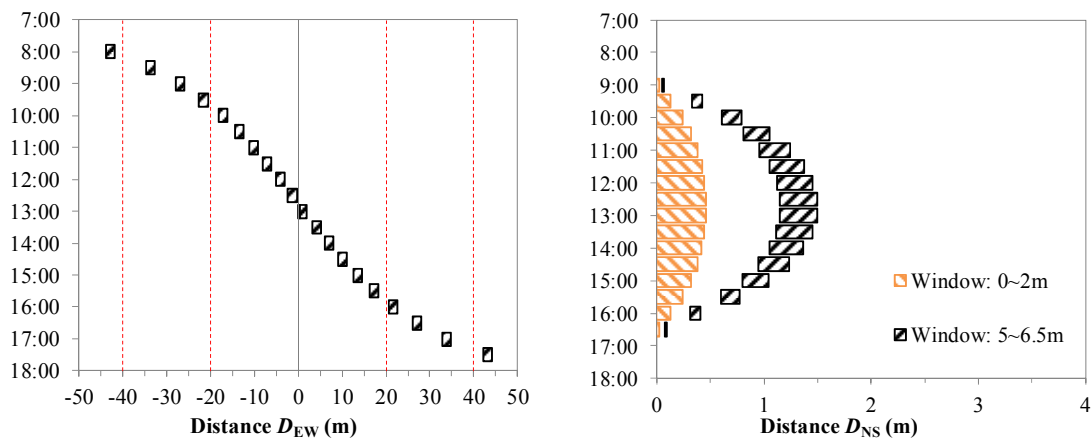


Fig. 3-19 Location of sunlight on floor: (a) schematic diagram; and (b) distances for a point at a height of 20 m (in Xi'an on July 16th; similar hereinafter)

The sunlight shining on the floor that arrives through typical windows, such as the skylights and side windows shown in Fig. 3-11, is illustrated in Fig. 3-20. For the skylights in the check-in hall (2 m wide, spaced 20 m apart, and 22 m above the floor), the sunlight shining through moves from the west side to the east side each day, as shown in Fig. 3-20(a). For Point A located under the skylight in Fig. 3-11(a), sunlight shines directly on it from 8:00-8:30, 9:30-10:00, 12:30-13:00, 15:30-16:00, and 17:00-17:30.

For the side windows in the departure hall that are either 0-2 m or 5-6.5 m above the floor, the sunlight shining through the south window will be located on the floor at distance D_{NS} , as shown in Fig. 3-20(b). For the side windows on the east and west walls, the sunlight will be located on the floor at distance $|D_{EW}|$, as shown in Fig. 3-20(c). By comparison, the distances for the sunlight shining through the east and west side windows (i.e., 0.5-22 m) are greater than they are for the south side windows (i.e., 1.5-0.3 m).



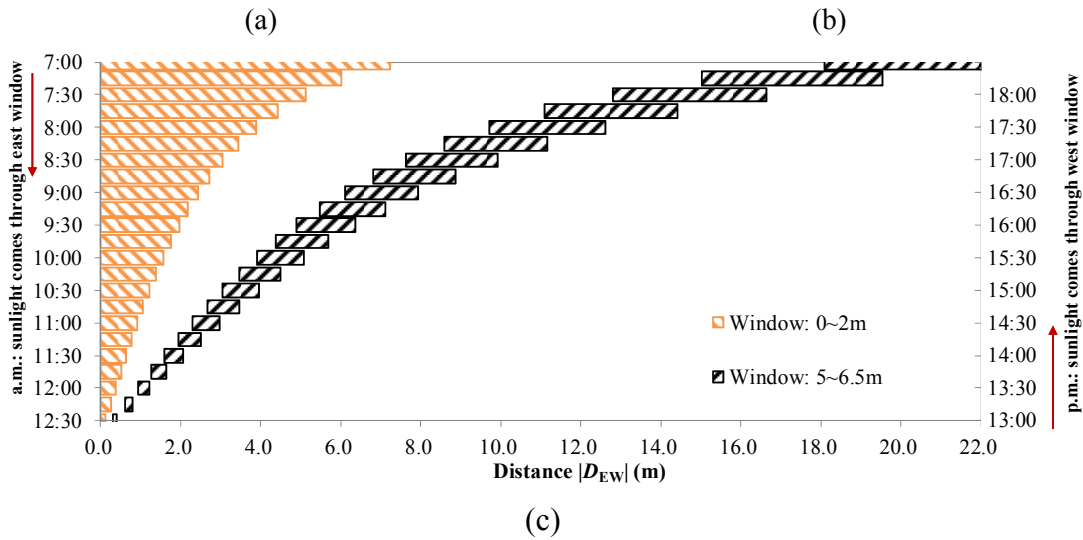


Fig. 3-20 Sunlight through skylight and side windows: (a) skylight; (b) south window; and (c) east/west window

2) Duration of sunlight on floor

The moving speed of the incident point on the floor surface (Point i') can also be calculated with the location of the window and sun, written as Eq. (3-36):

$$s_{i,EW} = H_i \left| \cos \delta \frac{\cos \varphi \cos \delta + \sin \varphi \sin \delta \cos t}{\sin^2 \theta} \right|, \quad s_{i,NS} = H_i \left| \frac{\sin \delta \cos \delta \sin t}{\sin^2 \theta} \right| \quad (3-36)$$

where φ is the local latitude, δ is the current declination of the sun, t is the hour angle, and θ is the solar elevation angle.

For the point at a height of 20 m in Xi'an, the moving speed of its projection on the floor is shown in Fig. 3-21. The speed from west to east ranges from 8-50 cm/min, while the speed from south to north ranges from -6 cm/min to 6 cm/min, which is quite a bit slower than the former.

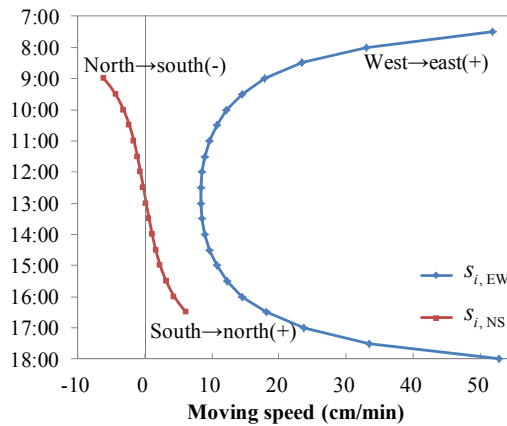


Fig. 3-21 Moving speed of sunlight passing through a 20-m-high point

Once the moving speed of the sunlight shining on the floor is known, obtaining the

irradiation time at a specific point is straightforward. For example, for the skylights in the check-in hall, the sunlight shining on the floor at 12:00 on July 16th, 2013 is shown in Fig. 3-22(a), which moves toward the east side with a speed about of 8 cm/min, and its width is the same as the width of the skylight. Hence, for Point A in Fig. 3-22(a), the duration of the solar radiation is 20-25 min.

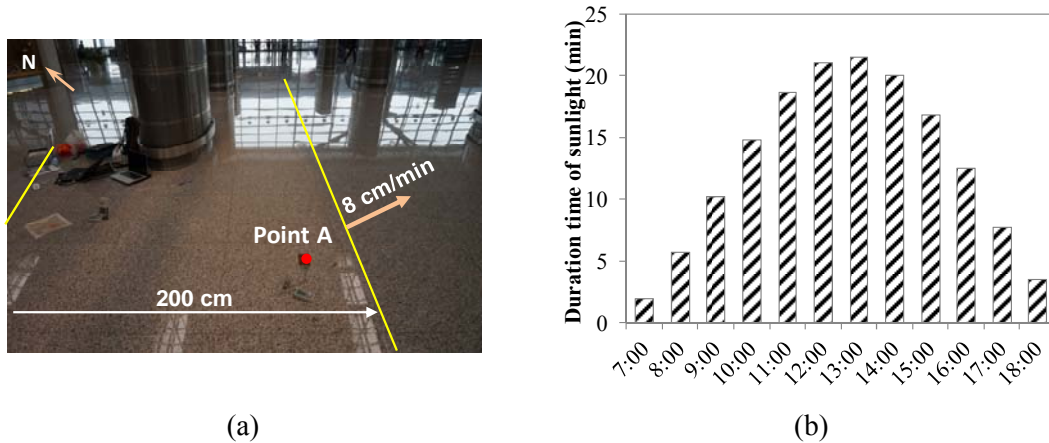


Fig. 3-22 Duration of sunlight on floor through skylight: (a) field test; and (b) duration

In engineering design, the irradiation time can be calculated according to Eq. (3-37). The duration of the sunlight shining through the skylight on the floor at different times is shown in Fig. 3-22(b). In the morning or evening, the duration of the sunlight shining on a given point is 5-10 min, while at noon, the duration is about 20 min, which fits the field test results well.

$$\Delta \tau^{sr} = \frac{w}{\bar{s}} \quad (3-37)$$

where w is the width of the skylight and \bar{s} is the average moving speed in the direction along with the width of the skylight.

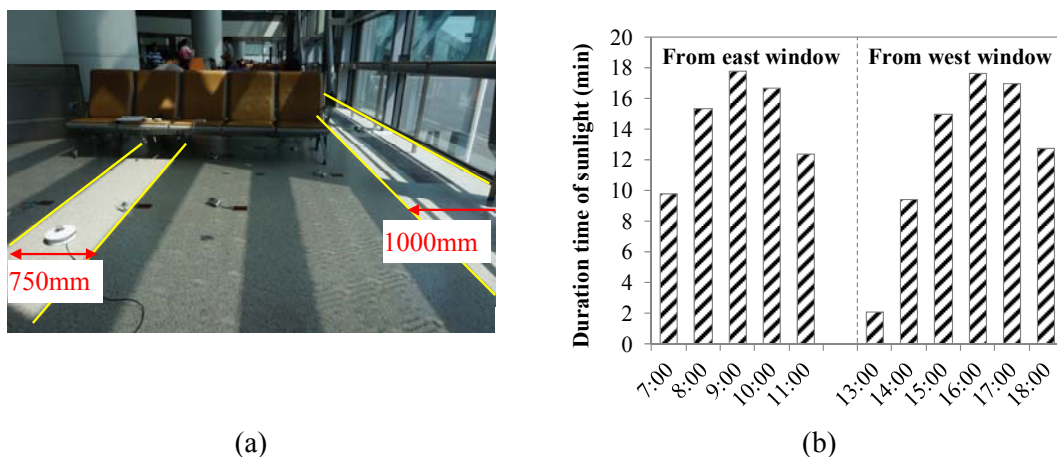


Fig. 3-23 Duration of sunlight on floor through side windows: (a) field test; and (b) duration

For the side windows, the width of the sunlight shining on the floor is related to the height of the window (H') and the location of sun, as shown in Eq. (3-38). For example, the

widths of the sunlight shining on the floor through the middle and bottom windows in the departure hall at 14:00 on July 16th, 2013 are 750 mm and 1000 mm, respectively, as shown in Fig. 3-23(a).

$$\text{East-west direction: } w = H' \left| \frac{\sin \alpha}{\tan \theta} \right|, \text{ north-south direction: } w = H' \left| \frac{\cos \alpha}{\tan \theta} \right| \quad (3-38)$$

Based on Eq. (3-37), the duration of the sunlight shining on the floor through the east and west side windows in the departure hall at different times is shown in Fig. 3-23(b). In the morning or afternoon, the duration of the sunlight shining on a given point is 10-18 min, but it is less than 5 min at noon.

3) Impact of transient solar radiation

In the above analysis, the location and irradiation time of the sunlight shining on the floor are examined. With this analysis, the impact of transient solar radiation on the cooling capacity of the radiant floor can be determined.

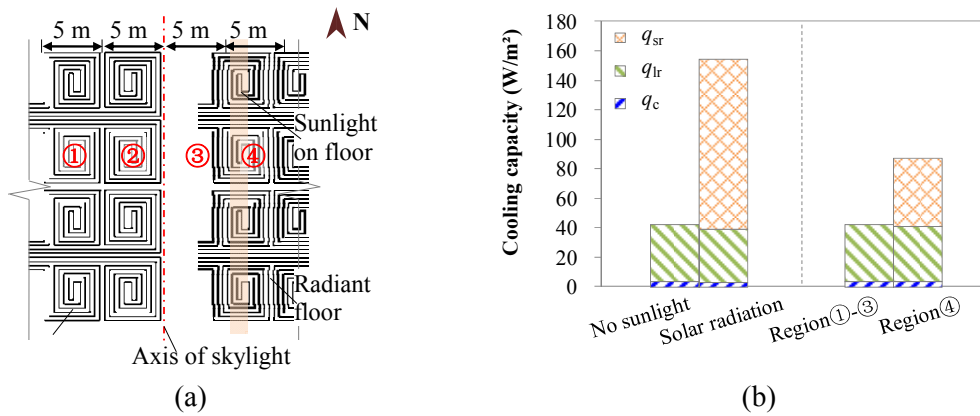


Fig. 3-24 Impact of transient solar radiation on radiant floor's cooling capacity: (a) pipe loops of radiant floor; and (b) cooling capacity with/without solar radiation

For example, the sunlight passing through the 2-m-wide skylight in the check-in hall is located on the floor surface at the east side of the skylight at a distance of 6.5 m at 14:00, as shown in Fig. 3-24. For a given point of floor surface exposed to the sunlight, the duration is about 20 min. If the solar radiation absorbed by the radiant floor surface (q_{sr}) is 116 W/m² when $T_a=26^\circ\text{C}$, $AUST=32.3^\circ\text{C}$, $\bar{T}_w=18^\circ\text{C}$, $h_c=1.0 \text{ W}/(\text{m}^2\cdot\text{K})$, $h_{lr}=3.8 \text{ W}/(\text{m}^2\cdot\text{K})$, and R and C of the radiant floor are $0.1 \text{ (m}^2\cdot\text{K)}/\text{W}$ and $138 \text{ kJ}/(\text{m}^2\cdot\text{K})$, respectively, then the cooling capacity calculated with Eq. (2) is 155 W/m². In contrast, it is only 42 W/m² without solar radiation. At this moment, for the pipe loops illuminated by sunlight (region ④ in Fig. 3-24(a)), the average cooling capacity is 87 W/m², which is higher than the 45 W/m² for regions ①-③.

3.2.4. Results and discussion

With the analytical method introduced above, the cooling capacity of a radiant floor in actual practice can be predicted in detail. The large spaces of an airport shown in Fig. 3-11 are taken as examples.

The airport is located in Xi'an, China, and its outdoor air temperature and solar radiation during a typical summer day is shown in Fig. 3-25(a). The radiant floor shown in Fig. 3-14(a) is employed for cooling with the mean chilled water temperature (\bar{T}_w) of 18°C. Its heat resistance (R) and heat capacity (C) are 0.1 (m²·K)/W and 138 kJ/(m²·K), respectively, and in cooling mode, the floor surface convective heat exchange coefficients (h_c) is about 1.0 W/(m²·K) (Olesen et al., 2000). Apart from the radiant floor, fan coil units provide supplemental cooling to maintain the air temperature in the occupied zone (T_a) at 26°C.

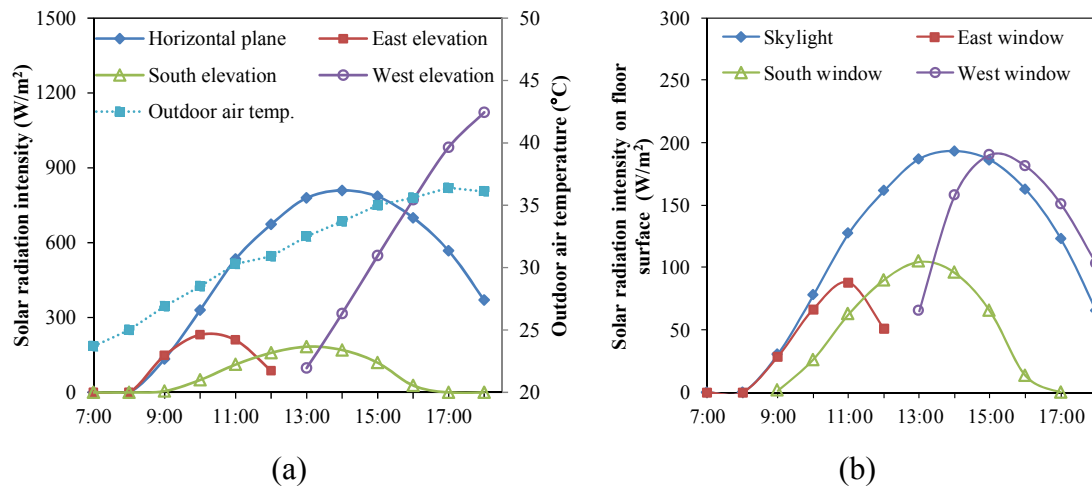


Fig. 3-25 Outdoor air temperature and solar radiation in Xi'an (July 16th): (a) outdoor conditions; and (b) solar radiation intensity on indoor floor surface

The cooling capacities of radiant floor illuminated by solar radiation or not are quite different, which will be introduced respectively.

1) Cooling capacity without sunlight

In check-in hall shown in Fig. 3-11(a), the ceiling is composed of alloy plates and polycarbonate skylights, with the emissivities of 0.4 and 0.95, respectively. The walls and floor surface adopt double glass curtain (with a low-e coating covering in the gap) and marble, respectively, the emissivities of which are all 0.9. According to the building geometry and surface emissivity of enclosure surfaces listed in Table 3-4, the equivalent longwave radiant heat transfer coefficient (h_{lr}) is calculated by Eq. (3-34) to be about 3.8 W/(m²·K).

The cooling performance of radiant floor at a typical condition is illustrated in Table 3-4. When the temperatures of the metal ceiling, skylights, and walls are 32.8°C, 38.0°C, and 30.4°C, respectively, the calculated $AUST$ with Eq. (3-32) is 32.3°C. Then according to Eq. (3-26), the calculated values for cooling capacity (q) and floor surface temperature (T_f) are

42.4 W/m² and 22.2°C respectively, where the radiant floor is not exposed to sunlight ($q_{sr}=0$ W/m²). Hereinto, the heat fluxes through convection (q_c) and longwave radiation (q_{lr}) are 3.8 W/m² and 38.6 W/m², respectively. Under these circumstances, T_{rs} is 26.7°C, with which the heat flux of each patch can be acquired with Eq. (3-33). For example, the radiant heat fluxes at the metal and skylight parts of the ceiling are 18.6 W/m² and 118.2 W/m², respectively, while those at the walls are about 21 W/m².

The calculation results were compared with a control group that assumes the emissivity of the majority of the ceiling is 0.9 (case ②). The value of h_{lr} is 5.2 W/(m²·K) and corresponding q_{lr} of radiant floor is 48.6 W/m². By comparison, it can be seen that the longwave radiant heat flux at the ceiling surface with low-emissivity is lower, which then results in a decrease in the cooling capacity of the radiant floor.

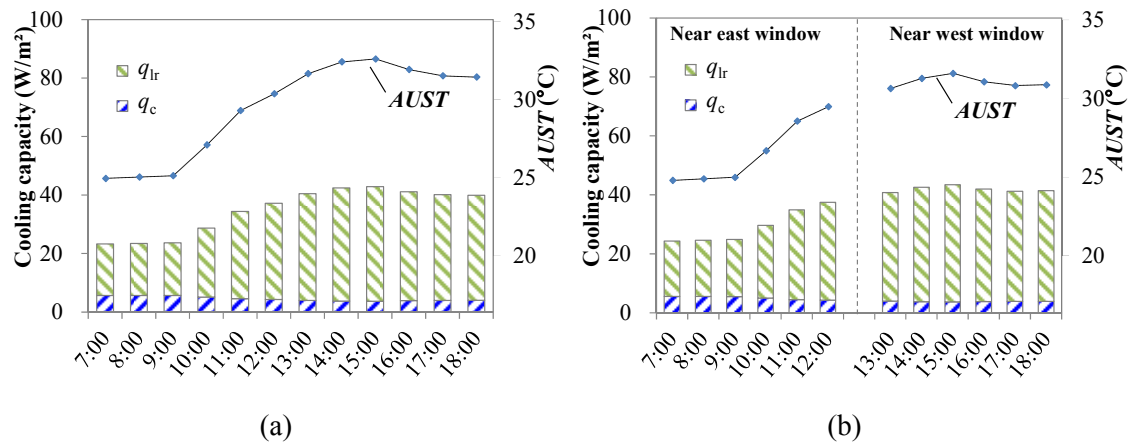


Fig. 3-26 Cooling capacity of radiant floor (without sunlight): (a) in check-in hall; and (b) in departure hall

Table 3-4 Cooling capacity of radiant floor in check-in hall without sunlight at 14:00*

		Ceiling		Wall				Radiant floor
		Majority	Skylight	East	South	West	North	
Parameters of indoor wall surfaces	Area $A_{j,i}$ (m ²)	28956	2964	6160	2508	6160	2508	31920
	Emissivity $\varepsilon_{j,i}$	0.4/0.9	0.95	0.9	0.9	0.9	0.9	0.9
	View factor $F_{rs-j,i}$	0.39	0.04	0.06	0.01	0.06	0.01	0.43
	Factor β_j	0.57	0.57	0.94	0.99	0.94	0.99	0.57
	$A_{j,i} \cdot r_{j,i}$	2.07/0.68	0.62	1.05	1.10	1.05	1.10	0.68
	Temperature $T_{j,i}$ (°C)	32.8	38	30.4	30.4	30.3	30.4	
① $\varepsilon(\text{majority of ceiling})=0.4$: $AUST=32.3^\circ\text{C}$, $h_{lr}=3.8 \text{ W}/(\text{m}^2 \cdot \text{K})$; $T_{rs}=26.7^\circ\text{C}$	Floor surface T_f (°C)	22.2						
	Floor cooling capacity q (W/m ²)	42.4 ($q_c=3.8 \text{ W}/\text{m}^2$ and $q_{lr}=38.6 \text{ W}/\text{m}^2$)						
	Longwave radiation $q_{lr,j,i}$ (W/m ²)	-18.6	-118.2	-21.8	-20.9	-21.2	-20.9	38.6
② $\varepsilon(\text{majority of ceiling})=0.9$: $AUST=32.6^\circ\text{C}$, $h_{lr}=5.2 \text{ W}/(\text{m}^2 \cdot \text{K})$; $T_{rs}=28.7^\circ\text{C}$	Floor surface T_f (°C)	23.1						
	Floor cooling capacity q (W/m ²)	51.5 ($q_c=2.9 \text{ W}/\text{m}^2$ and $q_{lr}=48.6 \text{ W}/\text{m}^2$)						
	Heat flux $q_{lr,j,i}$ (W/m ²)	-38.7	-98.3	-10.2	-9.8	-9.6	-9.8	48.6

* Indoor air $T_a=26^\circ\text{C}$, $h_c=1.0 \text{ W}/(\text{m}^2 \cdot \text{K})$, and radiant floor $R=0.1(\text{m}^2 \cdot \text{K})/\text{W}$, $\bar{T}_w=18^\circ\text{C}$

With the longwave radiant heat transfer coefficient (h_{lr}) equaled to $3.8 \text{ W}/(\text{m}^2 \cdot \text{K})$, it is convenient to calculate the cooling capacity of radiant floor at each condition. Fig. 3-26(a) illustrates the calculation results when the wall surface temperature $AUST$ ranges from 25°C to 32°C . The heat fluxes through convection and longwave radiation are in the range of $23\text{-}43 \text{ W}/\text{m}^2$, of which the convection portion (q_c) is $4\text{-}6 \text{ W}/\text{m}^2$ and the longwave radiation portion (q_{lr}) is $18\text{-}39 \text{ W}/\text{m}^2$.

As with the check-in hall, the emissivity of the indoor ceiling surface in departure hall is 0.4 , while the emissivities of the remaining surfaces are all 0.9 . According to the building geometry and surface emissivities, the values of h_{lr} is $4.3 \text{ W}/(\text{m}^2 \cdot \text{K})$. The calculation results of the cooling capacity of radiant floor is shown in Fig. 3-26(b), which ranges from 24 to $44 \text{ W}/\text{m}^2$.

2) Cooling capacity of radiant floor exposed to sunlight

For the radiant floor shone by direct solar radiation, its cooling capacity is remarkably higher than that without solar radiation. Fig. 3-25(b) shows the intensity of the solar radiation passing through the skylight in the check-in hall ($SC=0.3$) and that of the side windows in the departure hall ($SC=0.3$) reaching the indoor floor surface. The peak intensities of the solar radiation shining through the skylight, the east windows, and the west windows are $193 \text{ W}/\text{m}^2$, $88 \text{ W}/\text{m}^2$, and $190 \text{ W}/\text{m}^2$, respectively. When the surface layer of the radiant floor is gray marble, about 60% of the direct solar radiation reaching the floor can be absorbed.

In the check-in hall, combined with the solar radiation intensity and duration shown in Fig. 3-25(b) and Fig. 3-22(b), respectively, the cooling capacity of the radiant floor with transient solar radiation can be obtained with Eq. (3-27), as shown in Fig. 3-27(a). The increase in cooling capacity caused by transient solar radiation is remarkably high. When the solar radiation intensity at the floor surface ranges from $30 \text{ W}/\text{m}^2$ to $190 \text{ W}/\text{m}^2$, the total cooling capacity increases to $40\text{-}155 \text{ W}/\text{m}^2$, with absorption of $18\text{-}115 \text{ W}/\text{m}^2$ of direct solar radiation.

In the departure hall, the direct solar radiation comes into the indoor space mainly through the unshaded glass in the middle and bottom areas. Fig. 3-27(b) shows the cooling capacity of the radiant floor calculated by combining the solar radiation intensity and duration illustrated in Fig. 3-25(b) and Fig. 3-23(b), respectively. Before noon, the sunlight is rather gentle, with a heat intensity of $30\text{-}90 \text{ W}/\text{m}^2$. The cooling capacity of the radiant floor with solar radiation ranges from $41 \text{ W}/\text{m}^2$ to $86 \text{ W}/\text{m}^2$, with q_c , q_{lr} , and q_{sr} equaling $4\text{-}6 \text{ W}/\text{m}^2$, $19\text{-}29 \text{ W}/\text{m}^2$, and $17\text{-}53 \text{ W}/\text{m}^2$, respectively. By comparison, in the afternoon, the sunlight shining on the floor surface is much stronger, with a heat intensity of $65\text{-}190 \text{ W}/\text{m}^2$. Under this condition, the cooling capacity of the radiant floor is significantly enhanced to $80\text{-}155$

W/m². Hereinto, the absorption of direct solar radiation (q_{sr}) is in the range of 40-115 W/m².

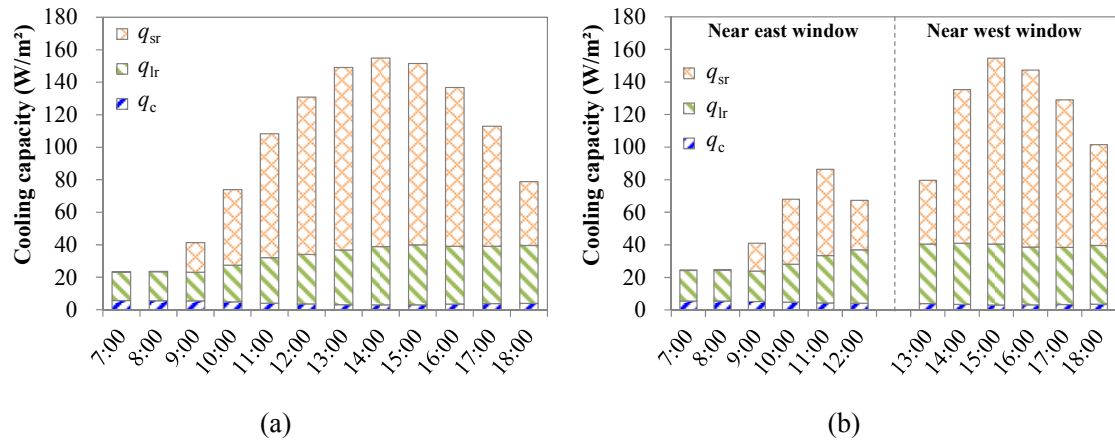


Fig. 3-27 Cooling capacity of radiant floor with solar radiation: (a) in check-in hall; and (b) in departure hall

3) Overall cooling capacity

The incident solar radiation on the radiant floor causes a difference in cooling capacity between illuminated and shaded areas. Hence, the average cooling capacity for the entire radiant floor is related to the floor area that is exposed to sunlight.

In check-in hall, the average cooling capacity for the total floor area is about 23-53 W/m², as shown in Fig. 3-28(a). Hereinto, the cooling capacity increase caused by solar radiation for the total floor area is about 2-10 W/m², as the skylight to roof area ratio is about 9%. For example, at 14:00, the cooling capacity of the radiant floor exposed to direct solar radiation is 155 W/m², while that of the rest of the radiant floor is 42 W/m². The average cooling capacity of the total radiant floor is 52.6 W/m², with q_c , q_{lr} , and q_{sr} equaling 3.7 W/m², 38.1 W/m², and 10.8 W/m², respectively, as shown in Fig. 3-28(b). Therefore, for the overall radiant floor cooling system, the heat load caused by direct solar radiation represents about 20% of the total.

In departure hall, as time goes on, the sunlight shining through the transparent glass changes locations. Hence, the heat loads for the sub-branches of the radiant floor with different distances from the outer wall are quite disparate, which results in the variance in cooling capacity. For instance, Fig. 3-29(a) illustrates the pipes in the radiant floor, in which the sub-branches numbered ①-④ measure 5 m in width from the west side (adjoining the west wall) to the east side. At 16:00, the sunlight passing through the transparent glass in the bottom and middle is located in regions ① and ②, respectively; the widths of the sunlight shining on the floor are 2.0 m and 1.5 cm respectively, with ratios of 40% and 30%,

respectively, of the width of each pipe loop. On average, for the pipe loops in regions ① and ②, the average cooling capacities of the radiant floor are 84 W/m² and 73 W/m², respectively, while those in regions ③ and ④ are both about 41 W/m². At that moment, the direct sunlight shining on the floor contributes to the cooling capacity with an enhancement of 43 W/m² and 32 W/m² for region ① and region ②, respectively.

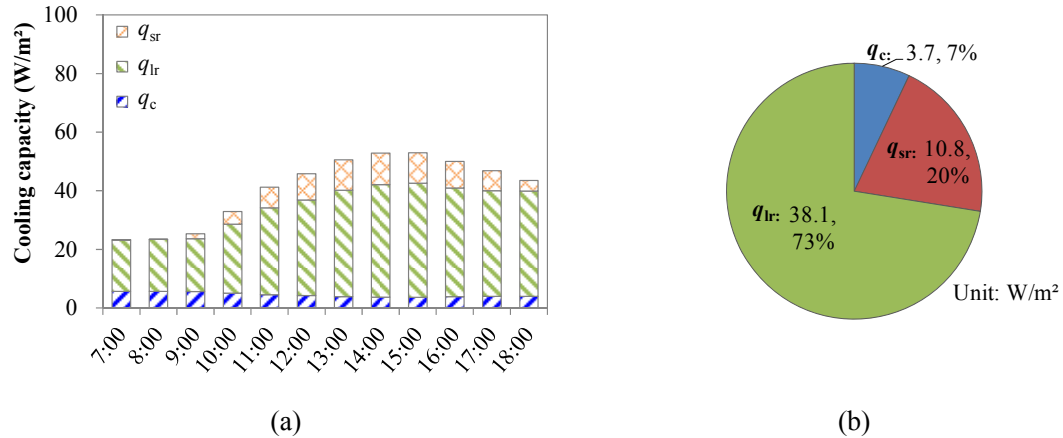


Fig. 3-28 Average cooling capacity of total radiant floor in check-in hall: (a) average cooling capacity; and (b) proportion of each part at 14:00

The cooling capacity increases caused by solar radiation for sub-branches ①-④ at different times are summarized in Fig. 3-29(b). It can be seen that the radiant floors in region ① are always exposed to solar radiation, so their heat fluxes are maintained at a high level, i.e. 65-110 W/m². The radiant floors in regions ②-④ are exposed to sunlight after 16:00, with cooling capacities of 60-70 W/m² and a duration of 1-2 h. Due to the different characteristics of the solar radiation and cooling capacity of the radiant floors, it is appropriate to design the pipe loops to be in separate regions.

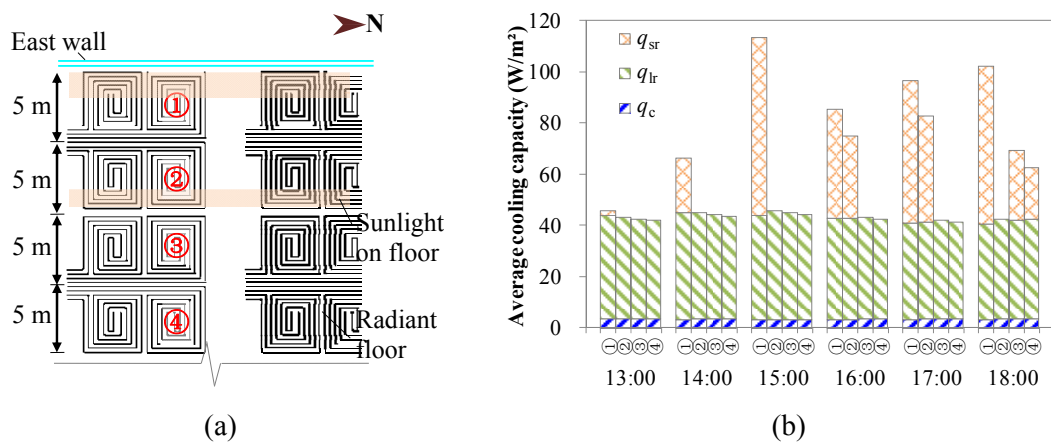


Fig. 3-29 Cooling capacity of radiant floor in each subregion in departure hall: (a) pipe loops of radiant floor; and (b) cooling capacity of each subregion

Through the above mentioned analysis, it is important to identify these two categories of

cooling capacity, i.e., the local cooling capacity of the radiant floor with transient solar radiation and the average cooling capacity of the total radiant floor, in engineering design. The former features the heat removal ability of the radiant floor on its surrounding microenvironment, while the latter is the key parameter in the capacity design of the radiant floor cooling system.

3.2.5. Conclusions

Due to a remarkable increase in cooling capacity, radiant floor cooling is suitable for large space buildings such as check-in halls and departure halls in airports, which feature high-intensity solar radiation and high-temperature internal wall surfaces. In this section, the influence of material emissivity on indoor longwave radiation and the impact of transient solar radiation on the radiant floor's cooling capacity are examined closely. The main conclusions can be summarized as follows:

- (1) Longwave radiation, an important component of the radiant floor's cooling capacity, is influenced by the emissivity of the indoor surfaces. A new simple calculation method for the longwave radiant heat exchange with different emissivity values is proposed. It is revealed that the equivalent longwave heat transfer coefficient h_{lr} decreases with lower emissivity, i.e., from a baseline of 5.2-5.5 W/(m²·K) to 3.8 W/(m²·K) when the emissivity of the ceiling is 0.4.
- (2) The location and duration of the direct sunlight on the indoor floor surface are depicted quantitatively. Combining these factors makes it possible to estimate both the location of the transient solar radiation and the extent of its effect on the cooling capacity of the radiant floor with greater precision.
- (3) An application of radiant floor cooling in the large spaces of an airport is analyzed. In the check-in hall with skylights, the peak cooling capacity of the radiant floor exposed to sunlight (9% of the total area) is 155 W/m² with q_c , q_{lr} , and q_{sr} equaling 3 W/m², 37 W/m², and 115 W/m², respectively. For the total radiant floor, the average cooling capacity is 52.6 W/m², with a q_{sr} of 10.8 W/m². In the departure hall with side windows, the cooling capacity of the radiant floor irradiated by sunlight is significantly enhanced to 80-155 W/m², with a q_{sr} of 40-115 W/m² in the afternoon. In particular, the radiant floor adjoining the west wall is always exposed to the sun, so the heat fluxes are maintained at a high level, i.e., 65-110 W/m².

4. Case studies and novel terminal systems

In this subtask, radiant terminal is regarded as an important approach to construct a HTC<H system. Several applications have been conducted and promoted in this Annex 59

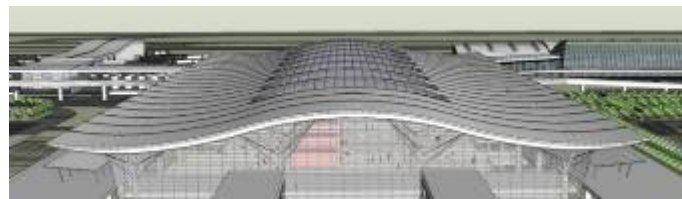
project. This chapter consists of case studies and novel system applications globally. An experimental investigation on different terminal units including entransy dissipation analysis is given in Appendix C of this subtask report. Applications of radiant heating and cooling systems in plus-energy houses and TABS with diffuse ceiling ventilation will be introduced in Subtask D report. Application of radiant floor in an airport will be given as follows, as well as performances of several novel terminal units.

4.1. Application of radiant floor in an airport

4.1.1. Description of the radiant floor system in an airport

1) Basic information

Terminal 3 of Xi'an Xianyang International Airport (Fig. 4-1), located in Shanxi Province, was designed by China Northwest Architectural Design and Research Institute. The terminal has been in use since May 2012, and it has a total building area of 258,000 m². Terminal 3 has three floors: one underground floor and two that are above ground. As a typical airport terminal, the building includes a check-in hall, a departure hall, a baggage claim area, offices, etc. Fig. 4-1(b) gives an outlook of the check-in hall. The maximum height of the terminal is 37.0 m, and the underground depth is 8.6 m.



(a)



(b)

Fig. 4-1 Terminal 3 in Xi'an Xianyang International Airport: (a) building outlook; (b) check-in hall.

The outdoor environmental conditions in Xi'an are shown in Fig. 4-2, including annual outdoor air temperature, relative humidity, and humidity ratio. The average relative humidity of the outdoor air in summer is around 60%, and the humidity ratio is 15-20g/kg. The cooling season for Terminal 3 is from May 15th to September 15th; according to the daily operating schedule of the airport terminal, the air-conditioning system is from 6:00 a.m. to 12:00 a.m.

midnight.

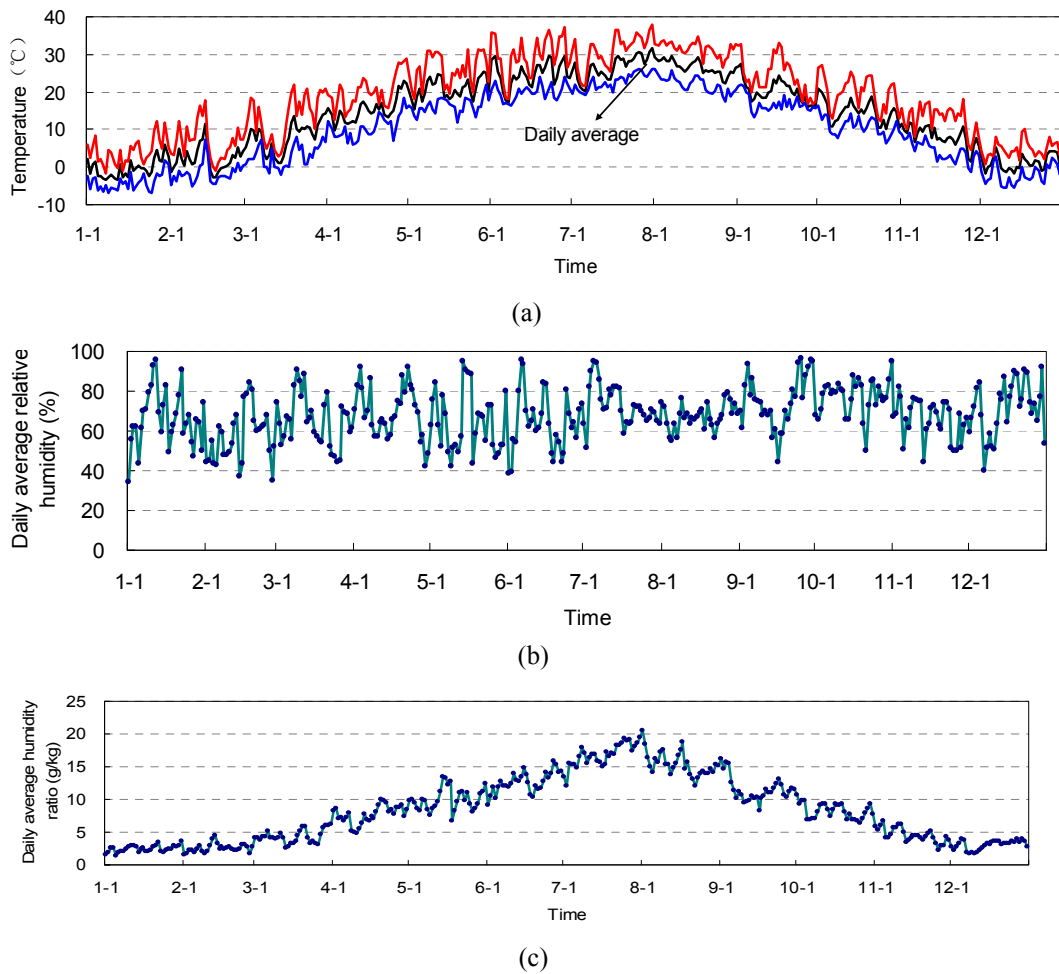


Fig. 4-2 Annual weather data of Xi'an: (a) daily maximum, average, and minimum temperatures; (b) daily average relative humidity; (c) daily average humidity ratio.

Because of the extremely large spaces in this airport terminal, radiant floors and displacement ventilation were selected for the THIC system to conserve air distribution energy during operation. Moreover, since electricity prices in Xi'an vary tremendously (the off-peak price is only about one-third of the peak price), ice storage technology was utilized in order to maximize operating cost savings.

2) THIC air-conditioning system

The building envelope is dominated with large glass walls with the internal shade. There are several typical large open spaces, including check-in hall and departure waiting hall on the second floor. The check-in hall is a large steel structure building, with a public area of 32,000 m² and a maximum height of 26.5 m (the average height is 22 m). The building envelope is dominated by double glass curtain walls, which are composed with double 6-mm-thick glazing with a low-e coating and a 12 mm gap filled with argon. The visible transmittance is 0.39, the heat transfer coefficient is 2.3 W/(m²·K), and the shading coefficient is 0.3. On the

roof, a daylighting band composed of polycarbonate sheeting (with a heat transfer coefficient of $2.7 \text{ W}/(\text{m}^2 \cdot \text{K})$ and a shading coefficient of 0.4) takes up 10% of the roof area, and the remainder is composed of an insulated alloy plate with a heat transfer coefficient of $0.55 \text{ W}/(\text{m}^2 \cdot \text{K})$. The roof also expands to deep overhangs on the east and west sides of the building, so that little sunlight comes into the indoor space through the façades.

The departure hall is located on the south side of the check-in hall; the waiting area is $15,000 \text{ m}^2$ with a height of 11.0 m. In the departure hall, the majority of the glass curtain is finished with colored glaze for sunshade, except for two bands in the middle and bottom (at 2.4 m and 1.2 m, respectively, above the floor) through which direct solar radiation shines on the radiant floor (shown in Fig. 4-3).



Fig. 4-3 Building envelope of the departure hall: (a) Glass curtain wall; and (b) Solar radiation through the glass on the floor.

The THIC air-conditioning system is employed in the large spaces of the airport terminal (i.e., the check-in hall and the departure hall), as shown in Fig. 4-4, with a total area of about $47,000 \text{ m}^2$.

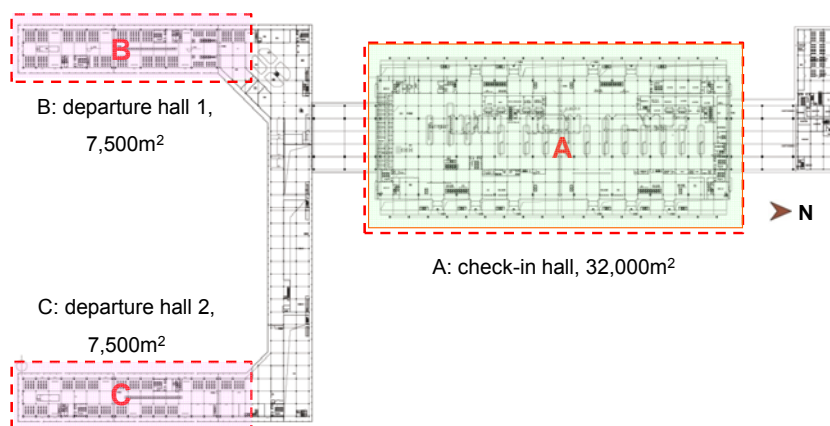


Fig. 4-4 THIC air-conditioning system application region.

Fig. 4-5 shows the operating schematic of the THIC system in the airport terminal. In this THIC system, outdoor air is dehumidified by a heat pump-driven liquid desiccant processor, and high-temperature chilled water is used to precool the air. Displacement

ventilation is utilized as the air supply terminal, and dry air is supplied into the indoor environment for humidity control. Dry FCUs (fan coil units) and radiant floors are used for temperature control in the THIC system, and dry FCUs with condensing plates are placed near the doors and windows instead of radiant floors to avoid condensation.

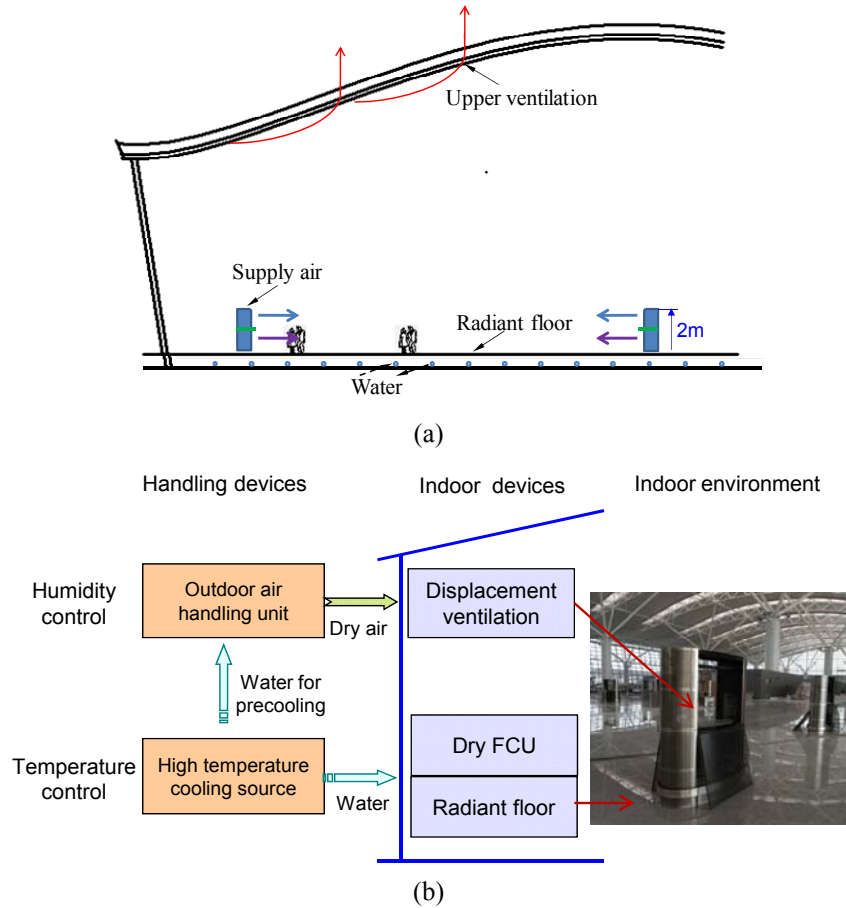


Fig. 4-5 Operating schematic of the THIC system in Terminal 3: (a) schematic; (b) principle in cooling mode.

Fig. 4-6 and Fig. 4-7 show the operating schematic of the terminal devices in the check-in hall and the departure hall, respectively. There are a variety of combinations of the terminal devices in the THIC air-conditioning system, as listed in Table 4-1. The radiant floors is designed for cooling with supply and return water temperature of 14°C/19°C in summer (designed cooling capacity of 60W/m²), and heating with supply and return water temperature of 40°C/30°C in winter. To be mentioned, the air is returned through the grilles located in the middle of the building in summer, and the top skylight is used to expel the high temperature air dirty; in winter, the air is returned through at the top of the building, weakening the temperature gradient of indoor air in the vertical direction; and in the transition season, top skylight is open for mechanical and natural ventilation.

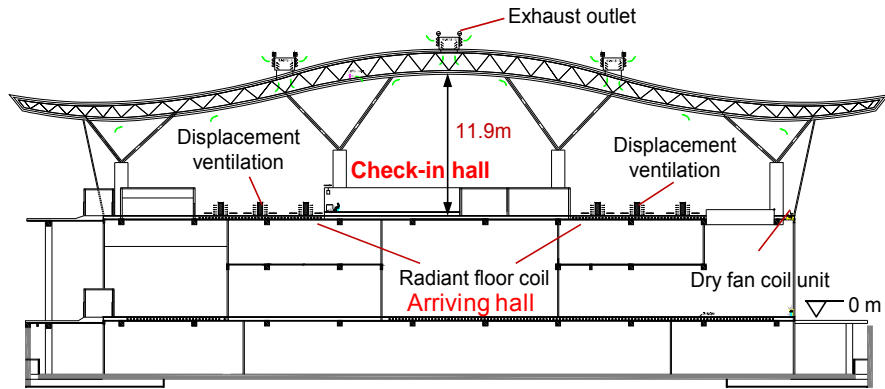


Fig. 4-6 Indoor terminals of the check-in hall.

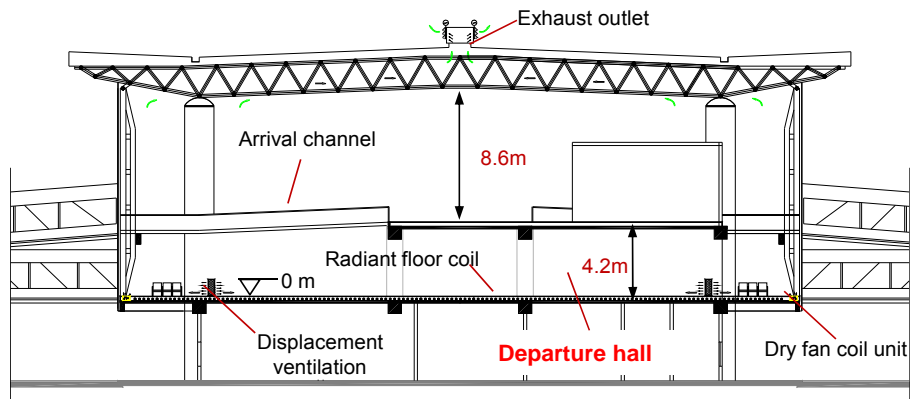


Fig. 4-7 Indoor terminals of the departure hall.

Table 4-1 Components and functions of the THIC system

	Terminal devices	Air supply	Functions
Temperature control subsystem	Radiant floor	-	1) undertake the basic sensible cooling load; 2) increase the long-wave radiation heat transfer, reduce the indoor cooling load and improve the thermal comfort; 3) reduce air-conditioning investment; 4) increase the return water temperature, reduce the transportation energy consumption and cooling energy consumption
	Radiant floor + dry fan coil units	Bottom ventilation beside the curtain wall	1) provide supplemental cooling capacity; 2) reduce the outer zone cooling load and improve the thermal comfort; 3) reduce air-conditioning investment; 4) increase the return water temperature, reduce the transportation energy consumption and cooling energy consumption
	Dry fan coil units	Bottom displacement ventilation	1) provide supplemental cooling capacity; 2) make full use of the replacement air for free cooling in transition season, reduce the cooling energy consumption; 3) increase the return water temperature, reduce the transportation energy consumption and cooling energy consumption
Humidity	Liquid	Bottom	1) undertake the latent cooling load for indoor humidity

control subsystem	desiccant outdoor air handling units	displacement ventilation	control; 2) provide fresh air for air quality; 3) make full use of replacement air for free cooling in transition season, reduce the cooling energy consumption; 4) reduce transportation energy consumption.
-------------------	--------------------------------------	--------------------------	---

4.1.2. Performance on-site test in summer

1) Indoor thermal environment

Terminal 3 has been in use since May 2012, and its indoor environment was examined in terms of the large spaces adopting the THIC system. The measured indoor parameters of the check-in hall are shown in Fig. 4-8. The temperatures of these areas were mainly between 22~24°C, while the humidity ratios were concentrated in a range of 10~11g/kg. These suitable thermal conditions showed that the indoor environment was comfortable for occupants.

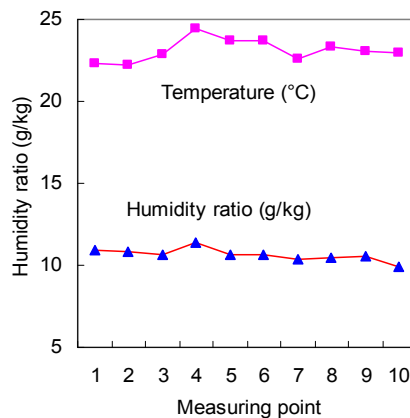


Fig. 4-8 Indoor air parameters of Terminal 3 (the check-in hall).

2) Operating performance of radiant floors

Two kinds of radiant floors are utilized in Terminal 3: a marble type and a plastic cement type. The main structure of the radiant floors applied in this building is shown in Fig. 4-9(a). It is composed of an insulating layer (30 mm), concrete core slabs (70 mm), a screed coat (25 mm/45 mm), and a surface layer; the pipe spacing is 200 mm. The detailed parameters of the radiant floors in the check-in hall and departure hall are listed in Table 4-2, the main difference being the material of the surface layer. As shown in Fig. 4-9(b), the floor surface layer in the check-in hall is marble, while that in the departure hall is PVC flooring; according to the structure parameters in Table 4-2, their equivalent heat resistance (R) values are 0.105 ($\text{m}^2\cdot\text{K}/\text{W}$) and 0.155 ($\text{m}^2\cdot\text{K}/\text{W}$), respectively. The former is lower than the latter due to the superior thermal conductivity of marble compared to PVC flooring.

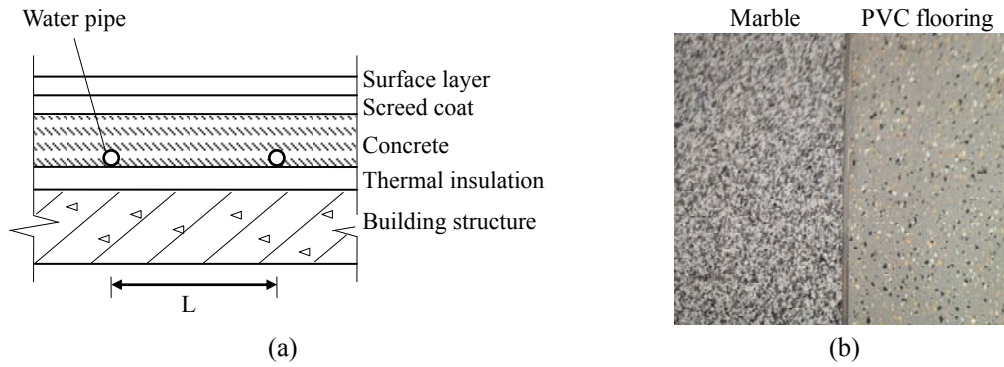


Fig. 4-9 Structure of the radiant floors: (a) Structure; and (b) Different surface layers.

Field tests of the performance of the radiant floor cooling system were conducted from July 8~22, 2013, the hottest period of the year (the outdoor conditions are shown in Fig. 4-10). In the check-in hall, direct solar radiation is minimal due to the ample sunshade from the building structure. In contrast, high-intensity solar radiation in the departure-hall has a significant impact on the performance of the radiant floor cooling system. Hence, the performances of the radiant floors in the check-in hall and departure hall are quite different. The measuring parameters, instruments and corresponding accuracy are listed in Table 4-3, in which the accuracies of the indoor air, floor surface and water temperatures are $\pm 0.2^{\circ}\text{C}$, the accuracies of the wall surface temperatures are $\pm 2^{\circ}\text{C}$, etc.

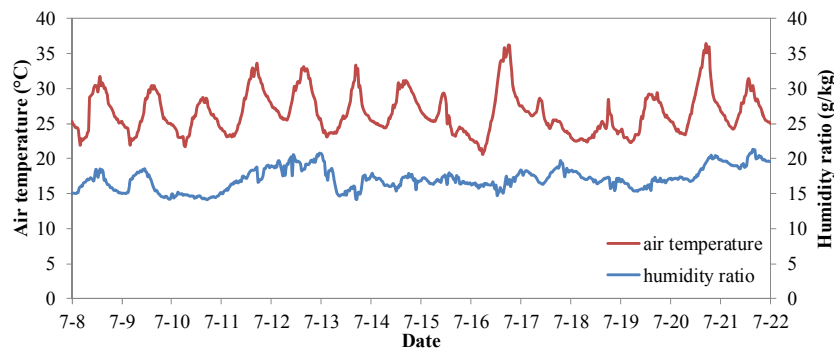


Fig. 4-10 Outdoor air temperature and humidity ratio from July 8~22, 2013.

Table 4-2 Structure of the radiant floors

Structure of radiant floor		Density ρ (kg/m ³)	Heat conductivity k (W/(m·K))	Specific heat c_p (kJ/(kg·K))	Thickness H (mm)	Pipe diameter δ and spacing L	Heat resistance R_i ((m ² ·K)/W)	Heat capacity C_i (kJ/(m ² ·K))
	Marble	2600	3.84	750	30		0.008	19.5
Check-in hall	Cement mortar	1800	0.93	840	20	$\delta=25$ mm	0.021	15.1
	Concrete	2344	1.84	800	70	$L=200$ mm	0.059	102.3
	Water pipe	1200	0.38	1400	2.5		0.017	0.8
	PVC flooring	1380	0.16	900	5		0.031	27.9
Departure hall	Cement mortar	1800	0.93	840	45	$\delta=25$ mm	0.048	34.0
	Concrete	2344	1.84	800	70	$L=200$ mm	0.059	102.3
	Water pipe	1200	0.38	1400	2.5		0.017	0.8

Table 4-3 Measuring parameters and instruments

Parameter	Instrument	Accuracy
Air temperature and humidity ratio	Self-recording hygro-thermometer	Temperature: $\pm 0.2^\circ\text{C}$; Relative humidity ratio: $\pm 2\%$
Wall surface temperature	Infrared thermal imager	$\pm 2^\circ\text{C}$
Radiant floor surface temperature and heat flux	Self-recording thermometer and heat-flow meter	Temperature: $\pm 0.2^\circ\text{C}$; Heat flux: $\pm 5\%$
Water temperature	Self-recording thermoscope	$\pm 0.2^\circ\text{C}$
Solar radiation intensity	Solar pyranometer	$\pm 2\%$
Air velocity	Hot ball anemograph	± 0.1 m/s
CO ₂ concentration	CO ₂ concentration detector	± 50 ppm

(a) No direct solar radiation (check-in hall)

The on-site test of the check-in hall was conducted in July, 2013, which was a cloudy day with an outdoor air temperature of 28~32°C. The indoor air and surface temperature distribution at a typical condition is illustrated in Fig. 4-11. The indoor air temperature (measured at a height of 1.1 m) is 23.5~23.7°C; the temperatures of the glass curtain walls on the west and east sides are 28~32°C; and the temperatures of the main roof (non-transparent) and PVC membrane are about 28°C and 38°C, respectively. The floor surface temperature is 22.1~22.6°C when the supplied and return chilled water temperatures are 16.9°C and 19.1°C, respectively. According to the heat-flow meter, the cooling capacity of the radiant floor is 37~39 W/m², with accuracy of ±5%.

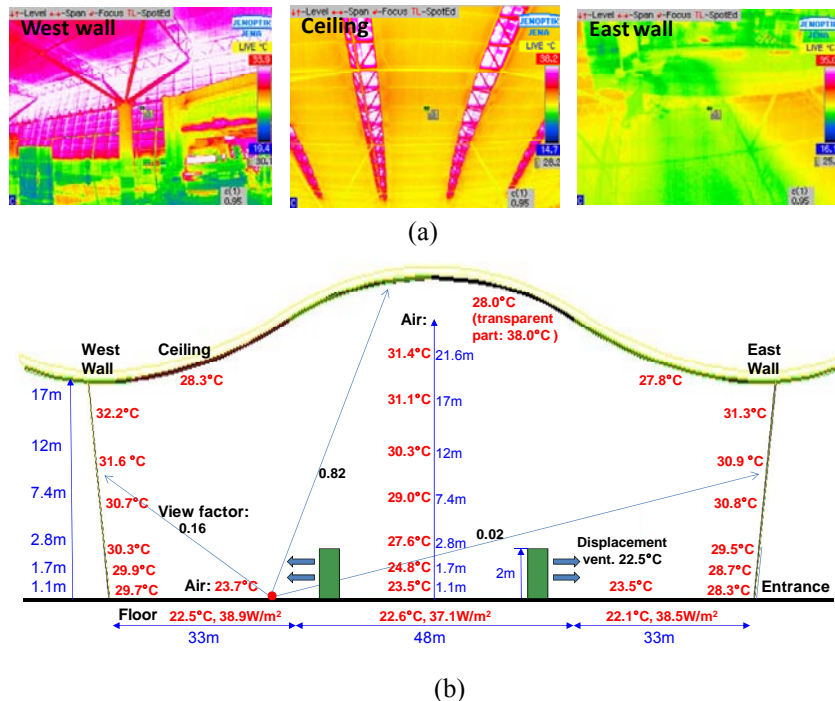


Fig. 4-11 Indoor temperature distribution in the check-in hall at 13:30 on July 8, 2013: (a) Thermal imaging of wall surfaces; and (b) Indoor temperature distribution.

The test results during the day (9:30~17:30) are shown in Fig. 4-12, in which indoor air and floor surface temperatures are the values of the west point in Fig. 4-11. In general, the indoor air is kept at 23.0~24.0°C, while the building envelope surface temperature (*AUST*, the view factors between the radiant floor and the roof, west wall, and east wall are 0.82, 0.16, and 0.02, respectively) is 26~29°C, with accuracy of ±2°C. Under such conditions, a cooling capacity of 25~40 W/m² is provided by the radiant floor, with a mean chilled water temperature of 18.0°C and a floor surface temperature of 22~23°C. The cooling capacities of the radiant floor are influenced by its surrounding air temperature and wall surface temperatures.

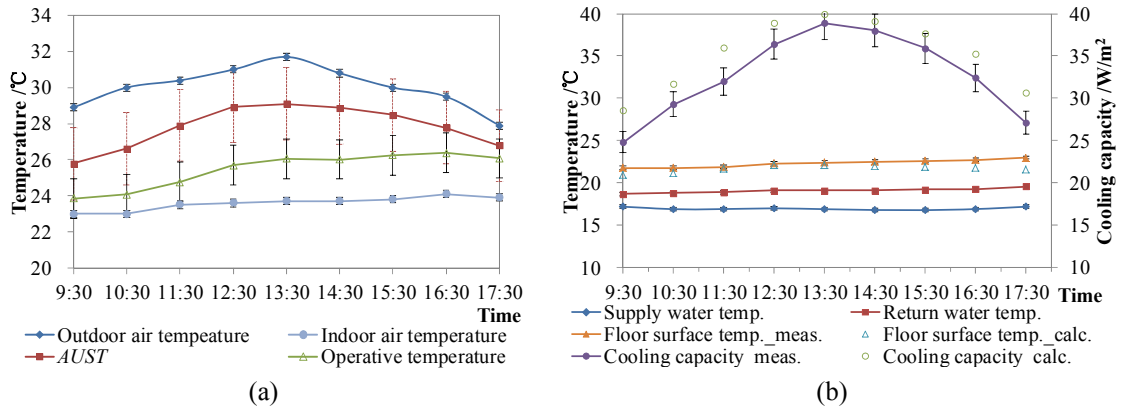


Fig. 4-12 Performance of radiant floor cooling in the check-in hall: (a) Indoor air and surface temperatures; and (b) Surface temperature and cooling capacity of the radiant floor.

(b) High-intensity solar radiation (departure hall)

The radiant floor cooling performance in the departure hall (with high-intensity solar radiation) was measured on July 16, 2013, which was a sunny day with an outdoor air temperature of 28~36°C and a solar radiation intensity of 300~750 W/m². The distribution of direct sunlight shining on the surface of the radiant floor through the transparent glass curtain is illustrated in Fig. 4-13. In the morning, the solar radiation intensity on the floor near the east wall ranges from 20~130 W/m²; at noon, there is no sunlight coming into the indoor space; and in the afternoon, it moves to the floor near the west wall and ranges from 120~170 W/m².

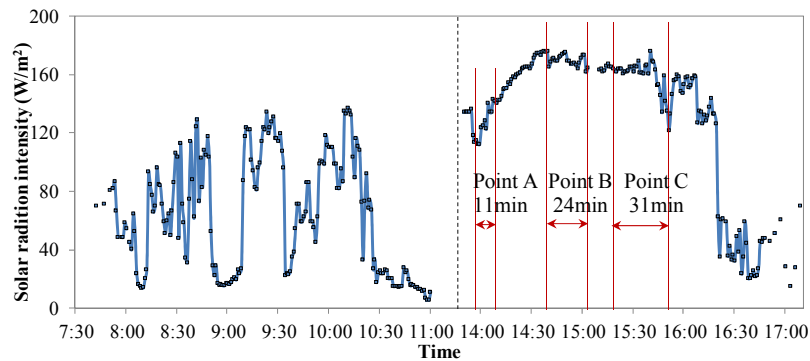


Fig. 4-13 Direct solar radiation on the radiant floor surface in the departure hall.

The solar radiation intensity in the afternoon is relatively high and stable, so it will be used to analyze the effect of solar radiation intensity on the performance of the radiant floor. The test points are shown in Fig. 4-3(b); Points A, B, and C are exposed to solar radiation for a duration of 10~30 min, and Point D is located under some chairs (i.e., without exposure to the high-temperature envelope and solar radiation). The indoor air and surface temperatures during the test are 23.4~24.3°C and 29~32°C, respectively, as shown in Table 4-4. The surface temperature and cooling capacity of each point of the radiant floor are illustrated in Fig. 4-14.

Table 4-4 Indoor air and wall surface temperatures in the departure hall (July 16, 2013)

Time	Air temperature (°C)	Wall surface temperature (°C)			AUST* (°C)	Lower surface of chair (°C)
		West wall	Roof	Internal wall surfaces		
14:10	23.4	30.0	30.1	23.4	29±2	22.7
14:40	23.7	33.2	30.7	23.7	31±2	23.2
15:10	24.3	34.4	31.4	24.3	32±2	24.0
15:50	24.1	35.4	31.6	24.1	32±2	24.5
Instrument precision	±0.2	±2	±2	±2	-	±0.2

* View factors between the radiant floor and the west wall, roof, and other internal walls are 0.5, 0.3, and 0.2, respectively.

When there is no direct solar radiation (e.g., Point B before 14:40 in Fig. 4-14), the radiant floor surface temperature is about 22.4°C with a mean chilled water temperature of 17.3°C, and the corresponding cooling capacity is 35~40 W/m². Once exposed to sunlight with an intensity of 160~175 W/m², the cooling capacity of the radiant floor increases sharply to 130~140 W/m². The floor surface temperature increases slowly due to the heat storage properties of the radiant floor itself; the temperature rises about 3°C in half an hour. As for the radiant floor under the chairs, the surface temperature and cooling capacity are only 20~21°C and 15~25 W/m², respectively, which are obviously lower than those at non-shaded points due to the lower temperature of the bottom surface of the chair (22.7~24.5°C). From these test results, it can be seen that the performance of the radiant floor will vary significantly depending on whether solar radiation is present or not.

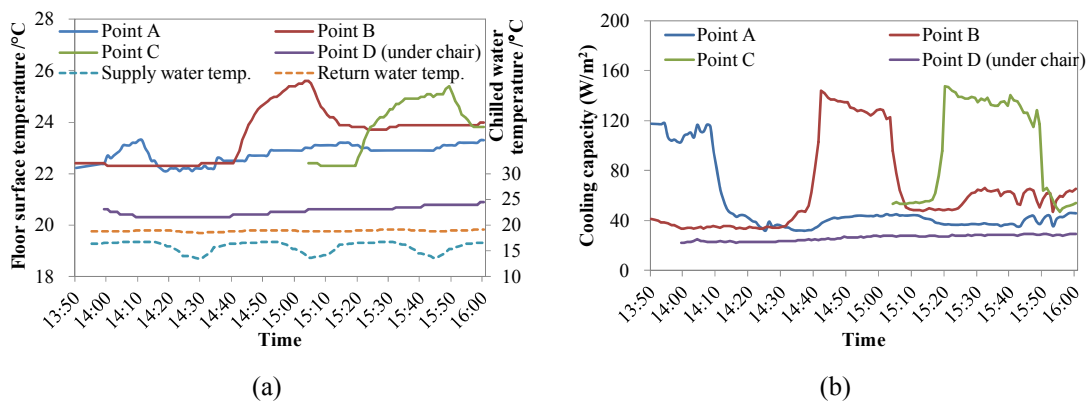


Fig. 4-14 Performance of radiant floor cooling in the departure hall: (a) Surface temperature and chilled water temperature; and (b) Cooling capacity.

4.1.3. Performance on-site test in winter

1) Indoor thermal environment

In winter, as to this THIC system for Terminal 3, radiant floor is responsible for indoor heating where hot water with a relative low temperature (about 35~40°C) is adopted to realize “low temperature heating”. The performance test of this THIC system with radiant floor for heating was carried out in December, 2012. Fig. 4-15 gives the outdoor temperature during the test, indicating that the mean outdoor temperature of Dec. 19th was about 2°C while of Dec. 20th was lower than 0°C.



Fig. 4-15 Outdoor climate during the test in winter.

Taking the check-in hall as an example, A representative indoor air and surface temperature distribution (19:00 on December 19, 2012) is illustrated in Fig. 4-16. The indoor air temperature, measured at a height of 1.5 m, is 22.5~23.4°C, and the temperatures of the glass curtain walls and roof are 18~24°C. In addition, the floor surface temperatures are 26.7~28.5°C with a mean hot water temperature of 32.5°C and a heating capacity of 38~46 W/m².

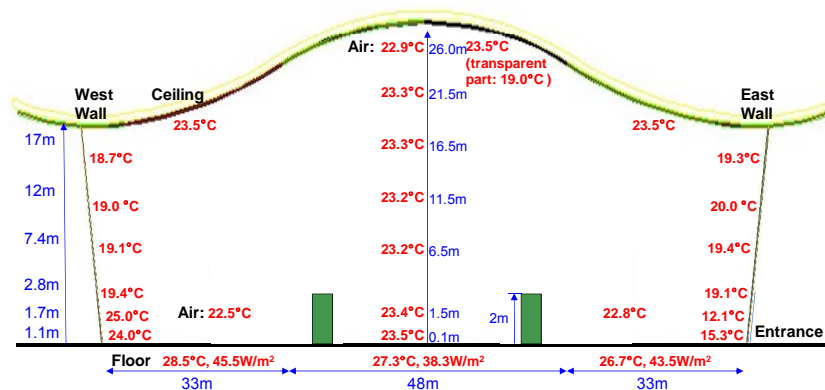


Fig. 4-16 Indoor temperature distribution in the check-in hall at 19:00 on December 19, 2012.

Fig. 4-17(a) gives the indoor air temperatures of three measuring points with the same height of about 1.8m above the floor. It shows that in Dec 19th, the air temperatures for different points was about 22.5°C, while in Dec. 20th the air temperature was about 22°C, a bit lower due to a lower outdoor air temperature as indicated by Fig. 4-15. As the height of the check-in hall is very high (about 26.5m), to investigate the indoor air temperature distribution

further, Fig. 4-17(b) gives the temperature variances during the test period. The supply water temperature T_{sup} was about 35°C in Dec. 19th while it was about 40°C during Dec. 20th and 21th. The range of the temperature variance was about 21~24°C and the vertical temperature distribution was almost uniform. It shows that the temperature was lower during the night (from 0:00~6:00) due to the operating mode of this terminal, that the supply water for the radiant floor was turned off at around 0:00 at midnight and restarted at about 6:00 in the morning according to the schedule. On basis of the testing results of the temperature distributions in the horizontal and vertical directions using radiant floor for heating, the indoor thermal environment was appropriate and comfortable.

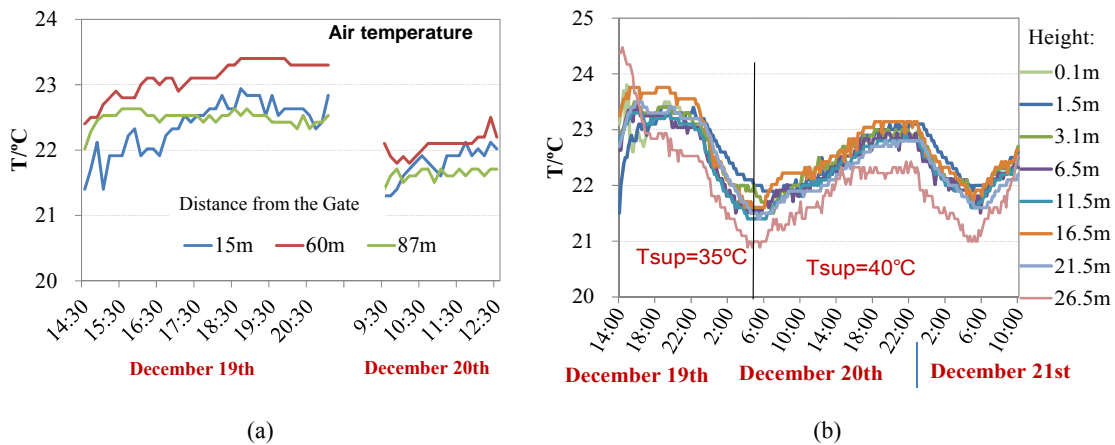


Fig. 4-17 Temperature distributions of indoor environment in the departure hall: (a) horizontal direction; (b) vertical direction.

2) Operating performance of radiant floors

Fig. 4-18 gives the supply and return water temperatures in two branches of the radiant floors, where the supply water temperature was about 35°C for Dec. 18th and 19th, and about 40°C for Dec. 20th and 21st due to a lower outdoor air temperature. As indicated by this figure, the operating temperature difference was about 3°C as the supply water temperature was about 35°C and was about 5°C as the supply water temperature of the north branch was increased to around 40°C, mainly due to a lower outdoor air temperature.

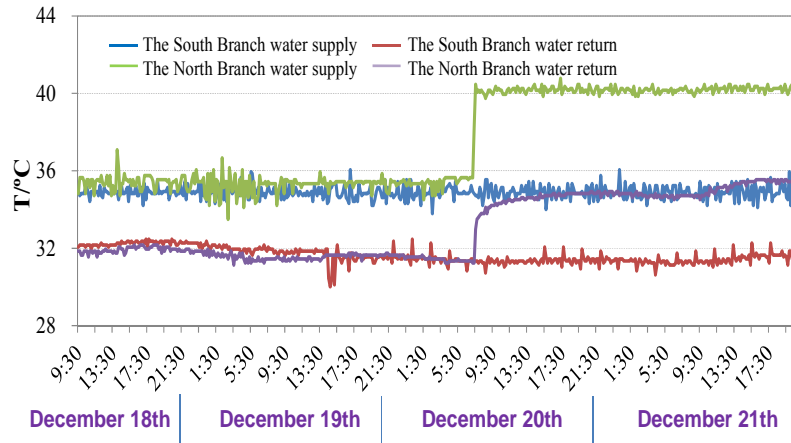


Fig. 4-18 Supply and return water temperatures of the radiant floors.

Then Fig. 4-19(a) shows the variances of the surface temperatures with different distances from the gate of the check-in hall. As the supply water temperature was about 35°C, the surface temperatures were among 26~29°C. When the supply water temperature was increasing to about 40°C, the surface temperature was then about 27~30°C, which was a bit higher than those with a lower supply water temperature. As indicated by this figure and Fig. 4-17(a), the surface temperature of the radiant floor was about 5~8°C higher than indoor air temperature. Heating capacities of the radiant floors with different distances from the gate are given as Fig. 4-19(b): as the supply water temperature was about 35°C, the heating capacities were within 30~50 W/m²; as the supply water temperature was increased to around 40°C, heating capacities were increasing to about 40~70W/m².

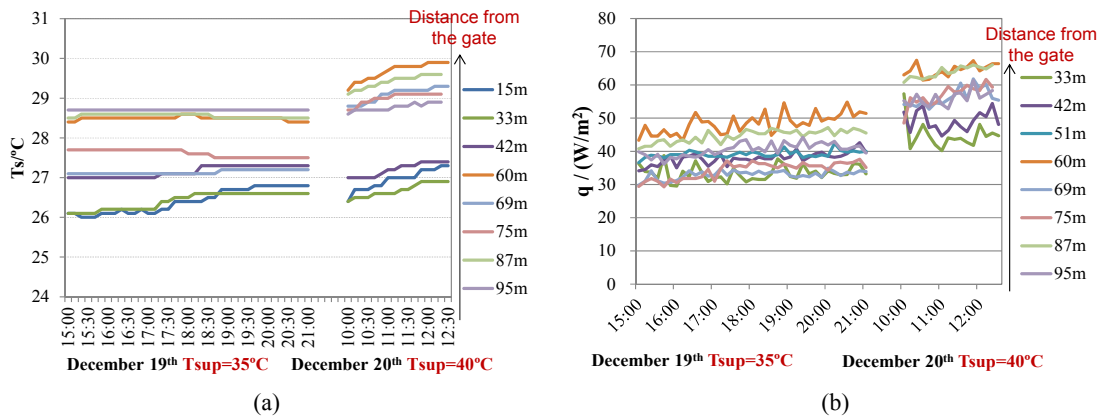


Fig. 4-19 Operating performance of the radiant floor for heating: (a) surface temperature; (b) heating capacity.

3) Performance comparison between different heating terminal devices

As indicated by the tested indoor air temperatures and performances of the radiant floors shown above, the THIC system adopting radiant floor for heating in Terminal 3 could provide a comfortable indoor thermal environment. Fig. 4-20(a) and Fig. 4-20(b) illustrate the vertical temperature distributions of the arrival hall (using radiant floor as the terminal device for

temperature control) and the check-in hall with different measuring points, respectively. It shows that the temperature gradient for both the arrival hall and the check-in hall is relative low and the vertical temperature distributions are almost uniform. However, as the arrival hall is in the first floor just under the check-in hall as shown in Fig. 4-6, the cold air infiltration influences the indoor thermal environment, leading to a lower indoor temperature (about 17°C as shown in Fig. 4-20(a)) compared with that of the check-in hall (about 22°C as shown in Fig. 4-20(b)).

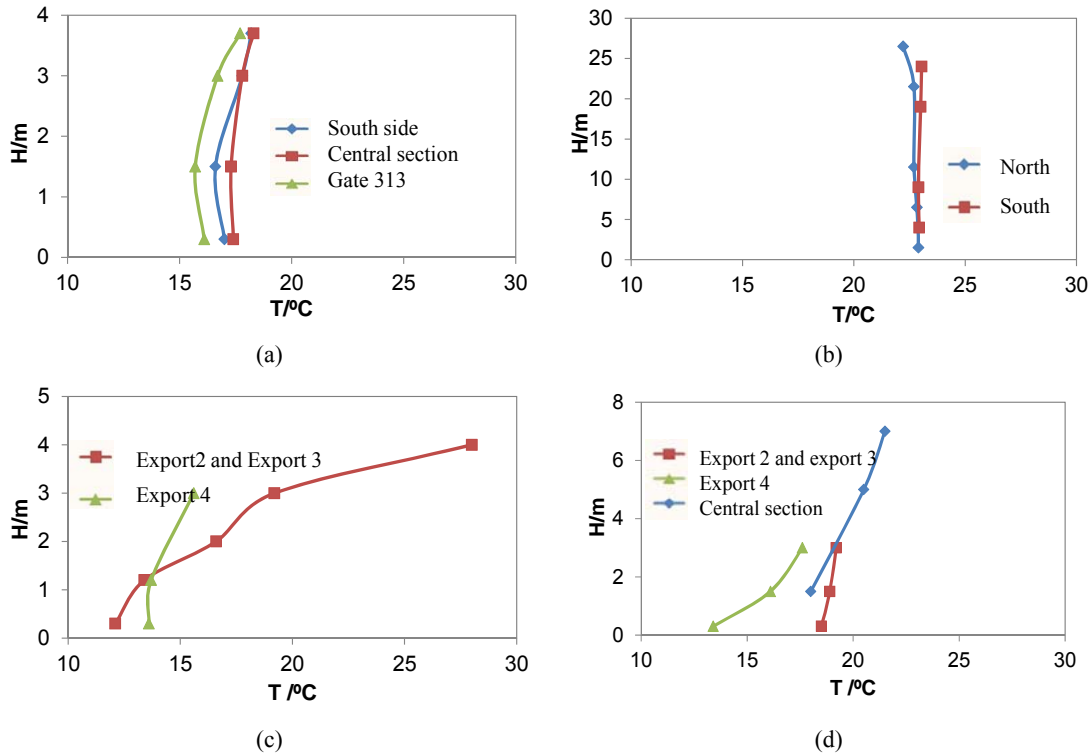


Fig. 4-20 Temperature distributions in the vertical direction: (a) arrival hall of Terminal 3; (b) check-in hall of Terminal 3; (c) arrival hall of Terminal 2; (d) check-in hall of Terminal 2.

Currently, all-air jet ventilation is the most common method adopted in large space buildings. One such system is used in Terminal 2 of the Xi'an Xianyang International Airport (shown in Fig. 4-21). Fig. 4-20(c) shows the tested temperature distribution in the vertical direction. It indicates that for the area with a height lower than 2m where occupants always stay, the measured results show that the temperature is lower than 15°C, indicating a temperature gradient higher than 10°C. As to the check-in hall of Terminal 2 using the conventional nozzle air supply system, the vertical temperature distributions are given in Fig. 4-20(d). Compared with Fig. 4-20(b), there is also a significant temperature gradient for the check-in hall of Terminal 2: temperature for the space with a height of about 6m is about 22°C; for the space with a height lower than 2m, the temperature is about 15~19°C. Thus, as indicated by the temperature distributions in the vertical direction listed in Fig. 4-20(a)~ Fig.

4-20(d), there would be a more uniform vertical temperature distribution using the radiant floor for heating compared with the conventional diffuser or the nozzle air supply system.

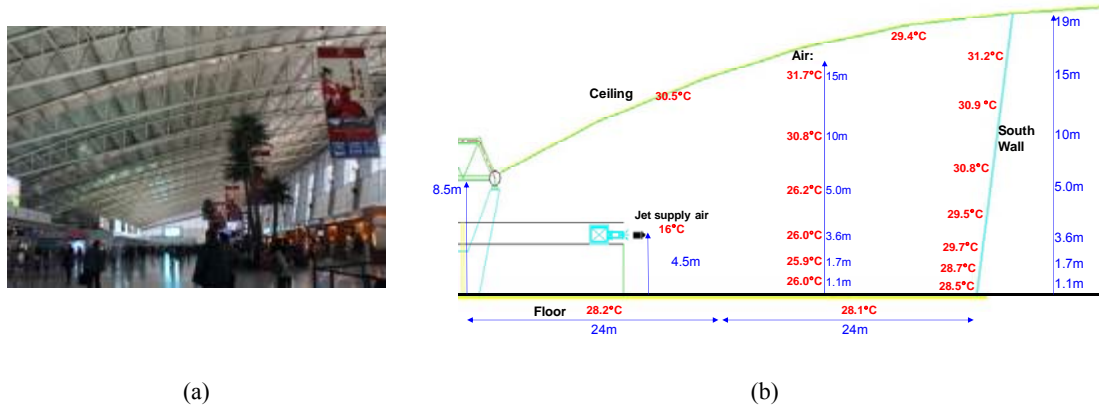


Fig. 4-21 Terminal 2 of Xi'an Xianyang International Airport (check-in hall): (a) Photo; and (b) Indoor temperature distribution at 15:30 on July 8, 2013.

4.1.4. Energy performance of the total air-conditioning system

This new terminal (Terminal 3) has been put into use since May, 2012 and the THIC system was adopted for regulating the indoor thermal environment of the large space. For terminal 2 (operated for 10 years), conventional jet ventilation system is adopted. The cold source (chilled water) for the HVAC systems of Terminal 3 and Terminal 2 are provided by two cooling plants respectively, while the heat is taken from the residual heat of a power plant. Fig. 4-22 gives the monthly HVAC energy consumption of the cooling plant and the terminal devices for Terminals 2 and 3 from the May to the December of 2012, including the cooling season, the transition season and the heating season. However, as the hot water was supplied by the district heating network in winter, the energy consumption in winter only took the power consumptions of the terminal devices, i.e. the fans and water pumps into account.

As indicated by this figure, power consumption for unit area of Terminal 3 is significantly lower than that of Terminal 2. Thus the new system adopting the THIC air-conditioning idea in Terminal 3 shows a better energy performance than the conventional system in Terminal 2. The total HVAC energy consumption of Terminal 3 from May to December is 49.9kWh/m², which is 36.4% lower than that of Terminal 2 (78.5kWh/m²): power consumption of the terminal devices in Terminal 3 is about 47.2% lower than that in Terminal 2; power consumption of the cooling plant in Terminal 3 is about 30.6% lower than that in Terminal 2. The initial cost of the HVAC system in Terminal 3 showed no significant increase compared with Terminal 2, as the price and installation charge of radiant floor is not more expensive than those of nozzles and air ducts.

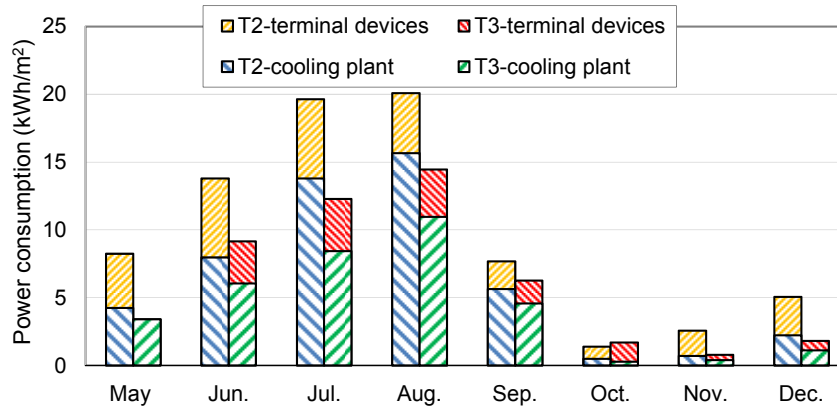


Fig. 4-22 Comparison of HVAC energy consumptions between Terminals 2 and 3.

4.1.X Thermal resistance analysis of the convective and radiant cooling systems

The cooling systems employed in Terminal 2 and Terminal 3 can be summarized as in Fig. 4-23.

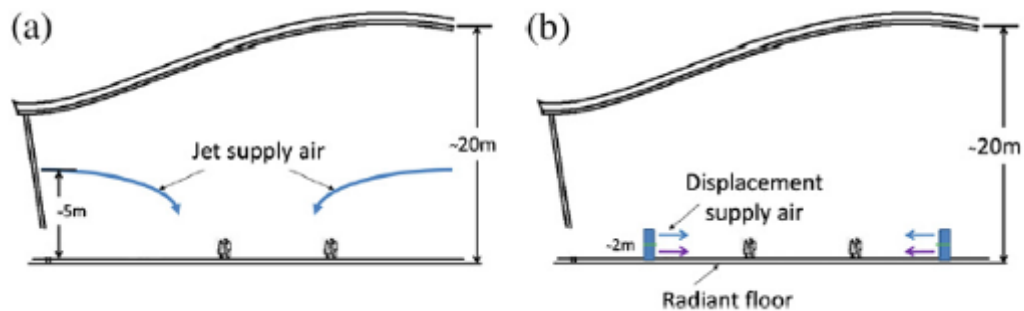


Fig. 4-23. Employed cooling strategies in Terminal 2 (a) jet ventilation, and in Terminal 3 (b) radiant floor cooling and displacement ventilation [REF: Zhang et al. 2013, Application of entransy analysis in the analysis of HVAC systems in buildings, Energy, 53, pp. 332-342]

In order to obtain the thermal indoor environments depicted in Fig. 4-23, different flow rates, working temperature levels and different capacities on the cooling system are needed. Fig. 4-24 shows the cooling systems used for Terminals 2 and 3.

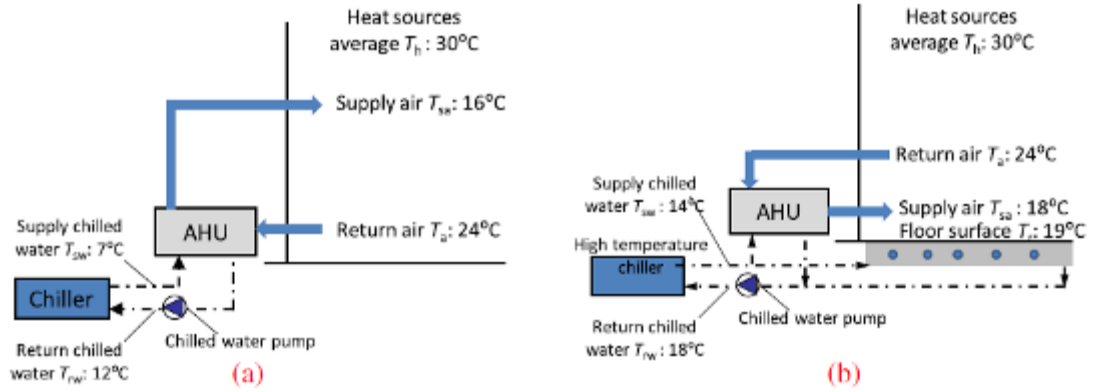


Fig. 4-24. Schematic drawings of the cooling systems used, (a) Jet ventilation, (b) Radiant floor cooling and displacement ventilation [REF: Zhang et al. 2013, Application of entransy analysis in the analysis of HVAC systems in buildings, Energy, 53, pp. 332-342]

After the cooling principles are determined, it is possible to show the cooling processes in T-Q diagrams and to calculate the entransy dissipation. Fig. 4-25 shows the cooling processes in T-Q diagram, and Fig. 4-26 shows the respective entransy dissipations of the two cooling systems.

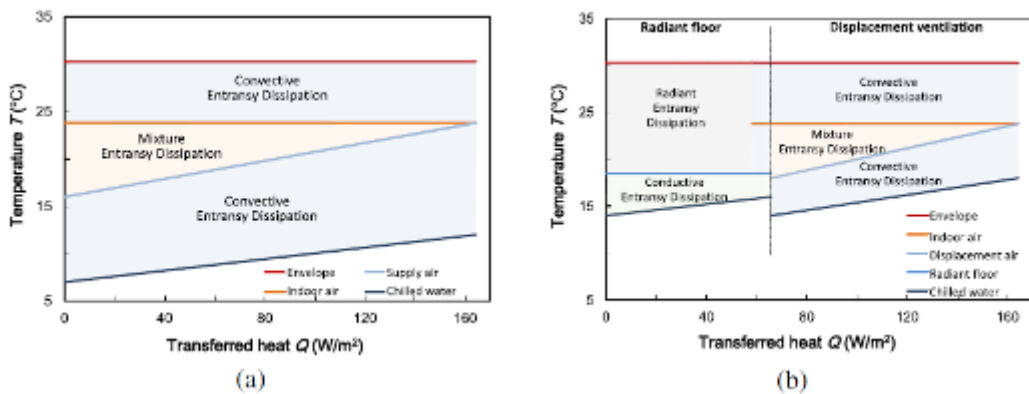


Fig. 4-25. T-Q diagrams of the cooling systems (a) Jet ventilation, (b) Radiant floor cooling and displacement ventilation [REF: Zhang et al. 2013, Application of entransy analysis in the analysis of HVAC systems in buildings, Energy, 53, pp. 332-342]

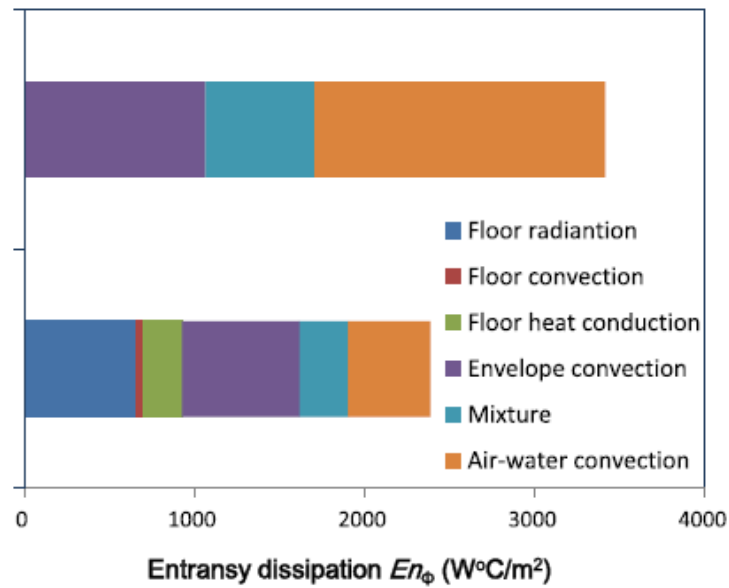


Fig. 4-26. Entransy dissipations of the two cooling systems, jet ventilation (top), radiant floor cooling and displacement ventilation (bottom) [REF: Zhang et al. 2013, Application of entransy analysis in the analysis of HVAC systems in buildings, Energy, 53, pp. 332-342]

The results show that cooling of a large space building with radiant floor cooling is a more beneficial approach than cooling the same space through an air-based, jet ventilation system. Significant energy savings are obtained during the months when the cooling loads are high.

The two different cooling systems were also analyzed with the entransy analysis, and the results show that entransy dissipation is significantly reduced in the radiant floor cooling case compared to the jet ventilation case. This is mainly due to the decreased thermal resistance between the heat sources (internal building surfaces, screens, etc.) and the heat sink (radiant floor), decreased mixing entransy dissipation in the indoor space, and the possibility of using high temperature chilled water for cooling purposes in the radiant floor and in the air handling unit used for displacement ventilation.

According to the analyses carried out in this chapter and as explained in 1.1.1, the internal heat sources have a mostly radiative nature and only a small part of the heat gains is convective. The results show that, due to the nature of heat sources, it is more effective to remove the internal heat gains with radiant cooling systems instead of convective systems. This enables reducing the mixing entransy dissipation and to remove the heat from the heat sources before they get mixed with the indoor air and turn into convective loads which then makes it possible to use high chilled water temperatures.

4.1.5. Conclusion

The air-conditioning system in Terminal 3 in Xi'an Xianyang International Airport has been in use since May 2012, and an advanced THIC system utilizing radiant floors has been adopted there. In this section, the operating principle of the system is introduced, and its performances both in summer and in winter are investigated. The main conclusions can be summarized as follows:

1) In the large spaces of the airport terminal, a THIC air-conditioning system was adopted instead of a system based on the common nozzle air supply method, and the indoor environment in these areas was shown to be comfortable for occupants. The performances of the terminal devices in this THIC system were measured: the liquid desiccant processor was able to dry the outdoor air sufficiently for humidity control, and the two kinds of radiant floors used for temperature control had measured cooling capacities of about 30~40 W/m² in a cloudy day.

2) In winter, hot water with a temperature of about 35~40°C is supplied to the radiant floor to achieve a “low temperature heating” process. The surface temperature of the radiant floor is about 25~30°C while the heating capacity varies from about 30W/m² to about 70W/m², sufficient to satisfy the indoor heating requirement. In contrast to the conventional diffuser or nozzle air supply system, vertical temperature distributions of the area adopting radiant floor for heating are more uniform, with a much lower temperature gradient for different heights; the indoor thermal environment adopting radiant floor is more comfortable.

3) Compared with the conventional air-conditioning system adopted in Terminal 2, power consumption of the new system in Terminal 3 is significantly lower. Based on the statistical data of power consumptions in these two terminals from May to December, the energy saving ratio of the new HVAC system for Terminal 3 is as high as 36.4%.

4.2. *Novel terminal units for HTC<H systems*

In a previous chapter, Chapter 2, operation characteristics, possibilities, and limitations of most commonly used terminal units were given. Recent developments in the HVAC industry have been aiming at addressing the limitations of these systems and combining the advantages of each system.

The following novel systems achieve provide comfortable thermal indoor environments and a high energy performance by combining the benefits of different systems.

The first system (hybrid system combining radiation and convection), combines the effects of radiation and convection to achieve cooling without creating draught and noise indoors. The incorporated latent heat storage material enables a stable cooling performance

while balancing the changes in the supply air temperature.

The second system (high temperature cooling and low temperature heating AC System) takes advantage of low temperature heating and high temperature cooling through an induction air beam, with incorporated heat storage radiation panel. The operation characteristic of this induction air beam enables energy efficiency through increased heating/cooling plant performance, and increased temperature differences.

The third system (dehumidifying chilled radiators) uses radiation and natural convection to achieve low temperature heating and high temperature cooling. One significant advantage of this terminal unit is to perform dehumidification, which under normal conditions is something to be avoided in radiant systems, and this feature makes it applicable in hot and humid climates without requiring a separate system to dehumidify the air. The surface temperature of the terminal unit is very close to the average water temperature.

Basic operation principles, working temperature levels on water- and air-sides together with examples from actual operation performances are given in the following subchapters.

4.2.1. Hybrid system combining radiation and convection

Fig. 4-23 shows the structure of the ceiling radiative panel, which combines radiant heating/cooling and convective heating/cooling together. The chamber box contains latent heat storage material that moderates the temperature fluctuation of the supply air. This system offers a gently heated or cooled and quiet indoor environment that cannot be offered by a traditional system. Conditioned air is sent through a duct to the metal ceiling radiation panel mounted in the ceiling and supplied to the room quietly from very small holes in the panel. A metal ceiling panel is heated or cooled by conditioned air, and the radiative effect in the panel surface is obtained.

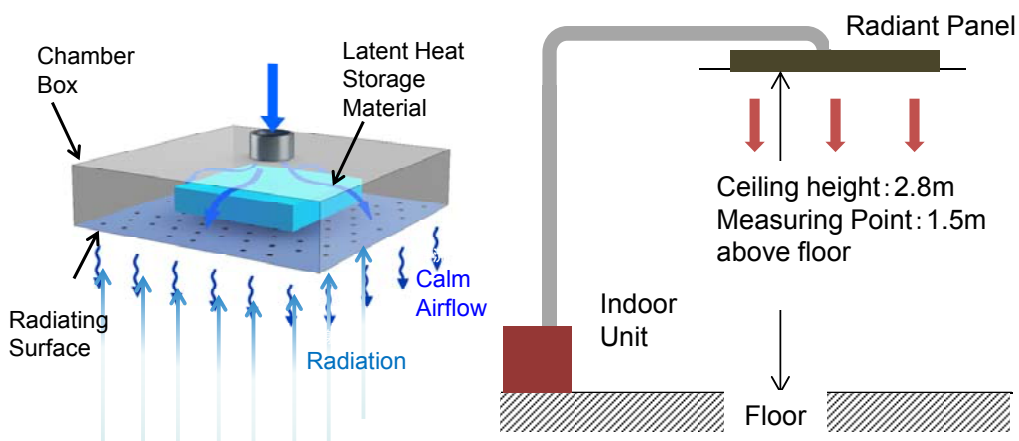


Fig. 4-23 Structure of ceiling radiative panel

Following are the features of the system.

- Occupant friendly air-conditioning that does not create draught
- Almost no temperature gradient in the room
- Quiet indoor environment with no noise from an air-conditioner
- Air-conditioner body is not exposed to indoor, and the design of the room and decoration stand out
- Even a moderate temperature setting is effective enough, and a certain energy conservation effect is obtained.

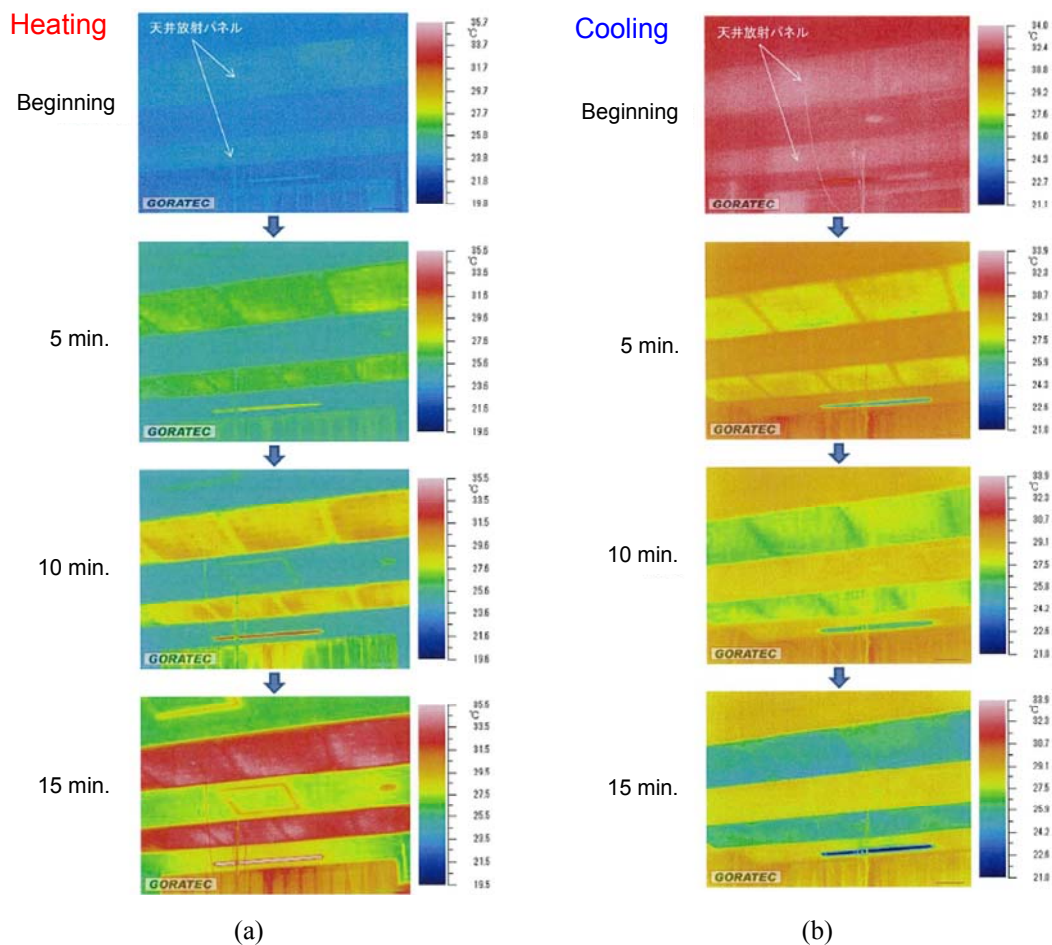


Fig. 4-24 Start-up characteristics: (a) heating; and (b) cooling.

Fig. 4-24 shows the thermography of the start-up stage; the start-up time is less than 15 min. Thus, this type of hybrid system combining radiation and convection is sufficient for indoor radiant heating or cooling in time.

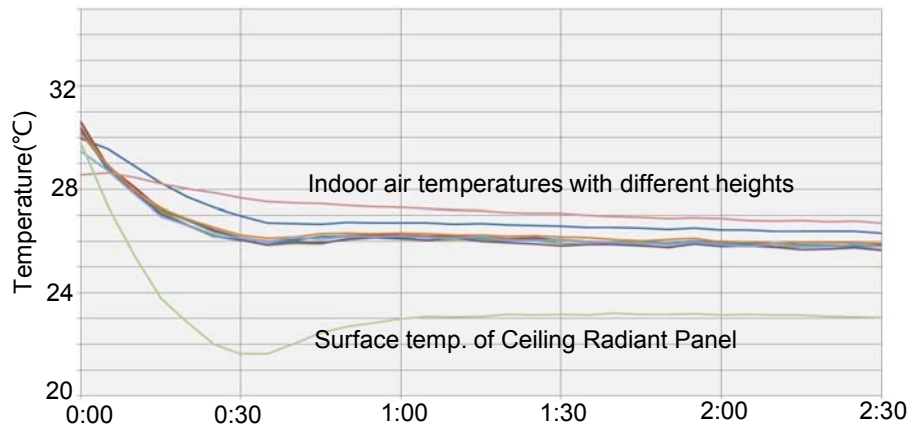


Fig. 4-25 Tested indoor air temperature and surface temperature

Fig. 4-25 shows the test results of indoor air temperature and surface temperature of the radiant panel. As indicated by this figure, this novel terminal combining radiant cooling and convective cooling is effective in controlling indoor temperature.

4.2.2. High temperature cooling and low temperature heating AC System

Fig. 4-26 shows the concept of the system. This system offers a gently heated or cooled and quiet indoor environment by using an induction chilled beam system that controls the indoor thermal environment by a combination of convection and radiation. The system uses high-temperature chilled water and low-temperature hot water. This results in a high COP of the heat source equipment.

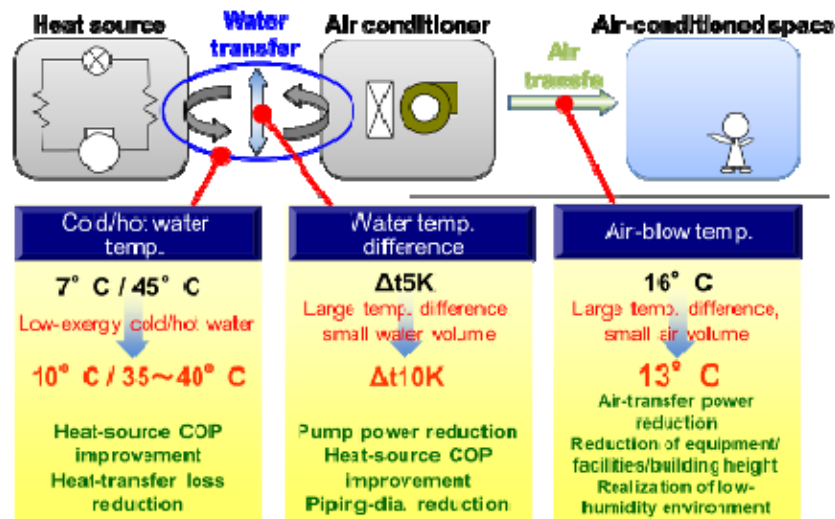


Fig. 4-26 Concept of the novel system

Fig. 4-27 shows the mixing chamber and humidity control outdoor air treatment air-conditioner. The mixing chamber allows outdoor air treatment with a humidity control air-conditioner and can be installed in a compact machine room.

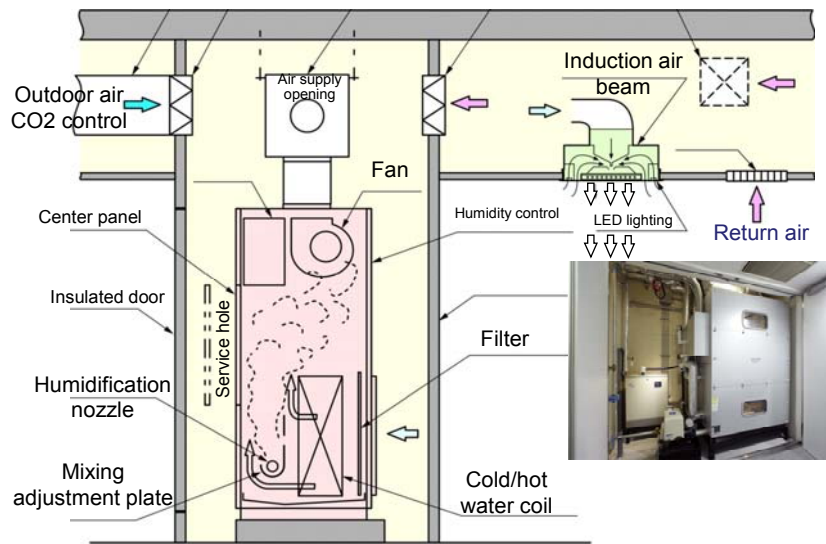


Fig. 4-27 Mixing chamber and humidity control outdoor air treatment air conditioner

This air-conditioning system has the following features: CO₂ control and adjustable control of outdoor air/return air volume at the chamber room are carried out by the automatic proportional control of the outdoor-air damper and the return-air damper. In winter, outdoor air can be used for outdoor-air cooling by mixing it with return air.

An example structural diagram of the all air supplied radiant and laminar flow unit (hereinafter called “Induction air beam”) is shown in Fig. 4-28. An induced and mixed air supply cools or heats the heat storage radiation plate and the radiant and laminar flow panel. Afterwards, from the panel opening, heat is radiated and a laminar flow is realized. The radiation directly acts on objects and surfaces. The laminar flow has a speed of 0.2 to 0.8 m/s. Therefore, no draft is felt in the occupied zone. The air outlet, to which 16°C air-blow had inevitably been applied for preventing dew condensation, was changed to an inducing structure to mix air with indoor air to keep the blowing temperature higher than the dew point, and this low-temperature blowing is realized with a large temperature difference.



Fig. 4-28 Diagram of the all air supplied radiant and laminar flow unit (Induction air beam)

The novel system greatly improves the efficiency of the air-cooled chiller of the heat source unit. Table 4-5 shows a comparison of the novel system and conventional system under different load factors. Compared with the COP in the conventional specification, the COP in the novel system is improved from 3.3 to 4.0 in the 100% load factor condition, with an increasing ratio of approximately 21.5%.

Table 4-5 Comparison of novel and conventional systems

	Novel system			Conventional spec.
Outdoor air (°C)	35		20	35
Load factor (%)	100	59	50	100
Inlet water temp. (°C)	10			7
Outlet water temp. (°C)	20			12
Water temp. difference (K)	10			5
Air supply temp.	13°C low temp. of air-blow			16°C air-blow
COP	4.01	5.15	8.67	3.30

Considering a typical office building as an example, the energy use of a novel high-temperature cooling/low-temperature heating system adopting radiant cooling is measured. Regarding actual measurement, the results obtained from July 2011 to June 2012 were compared with the calculation values of the conventional system in Fig. 4-29.

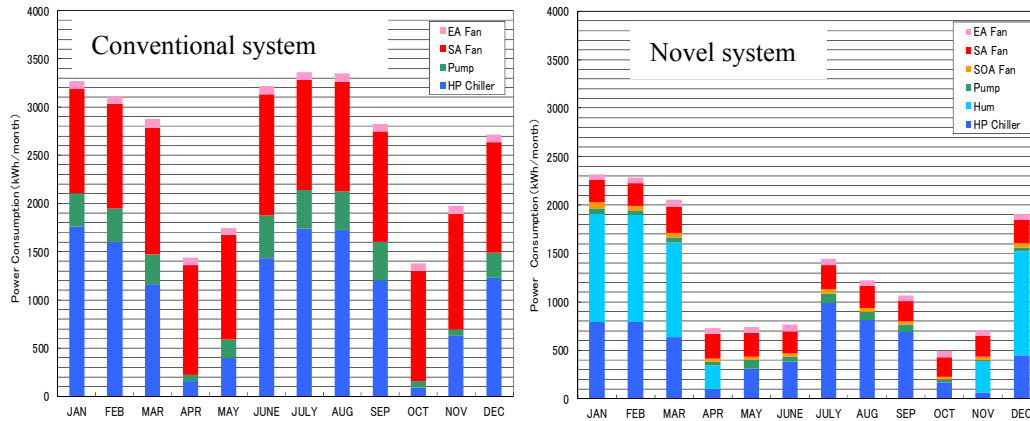


Fig. 4-29 Energy consumptions of different systems

The result showed that the actual measurement value of power consumption in each month for the novel system was significantly less. A large proportion of the increased actual measurement values are the power consumption of humidification in winter. This is because an electrode-type steam humidifier was employed in order to stably maintain an indoor relative humidity of 45% or more. The trial calculation of the conventional system includes a vaporizing humidifier, which is generally used and included in the HP chiller. As for the *COP*, it is easily inferred to be less than the actual value of the electrode-type steam humidifier. For the annual energy use, the novel system used 15730 kWh, while the conventional system used 31300 kWh; therefore, there was a reduction of about 49.7%. The high-temperature cooling and the low-temperature heating system helps reduce energy consumption of air-conditioning systems significantly.

4.2.3. Dehumidifying chilled radiators

Fig. 4-30 shows the operating schematic of dehumidifying chilled radiators. High-temperature chilled water and low-temperature hot water (15–20°C in summer and 30–40°C in winter) are adopted as heating and cooling sources. Surface temperature is similar to the water temperature. Cooling and heating takes place by natural convection and radiation. Moreover, an important feature of the system is that it allows condensation to take place on the surface of the radiation panel. During the humid summer months, the moisture present in air condenses on the radiator surface, and it is collected at the bottom and drained, thus reducing the moisture content of air.



Fig. 4-30 Example of dehumidifying chilled radiators

A typical building is chosen as an example to investigate the performance of this novel radiator system by considering an outdoor temperature of 33°C, indoor air temperature of 28°C, and relative humidity of 50%. Fig. 4-31 shows the real application of the novel chilled radiators, and the surface temperature of the cooling radiator is around 20°C. The novel cooling radiator with high-temperature chilled water creates a comfortable radiant cooling environment without draught and noise from fans.

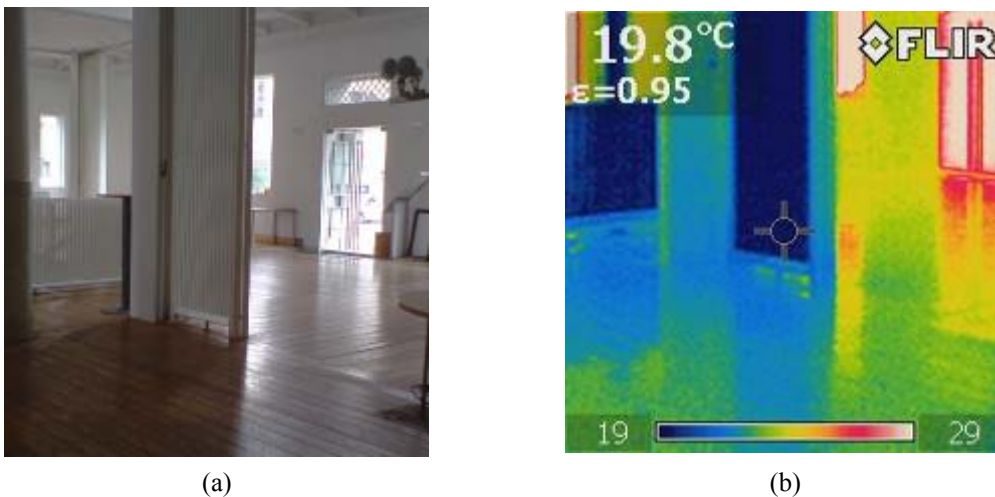


Fig. 4-31 Novel chilled radiators: (a) application; and (b) surface temperature.

Fig. 4-32 shows the seasonal operation of the novel cooling radiator from January to December. As indicated by the figure, the indoor temperature is almost stable and varies between 20–25°C. The supply water temperature in winter is about 30°C while in summer it is about 15–20°C. Thus, the novel cooling/heating radiator provides high-temperature cooling and low-temperature heating for an indoor space. Compared to conventional air based system, the novel radiator system achieves a 30% reduction in energy use in the building considered.

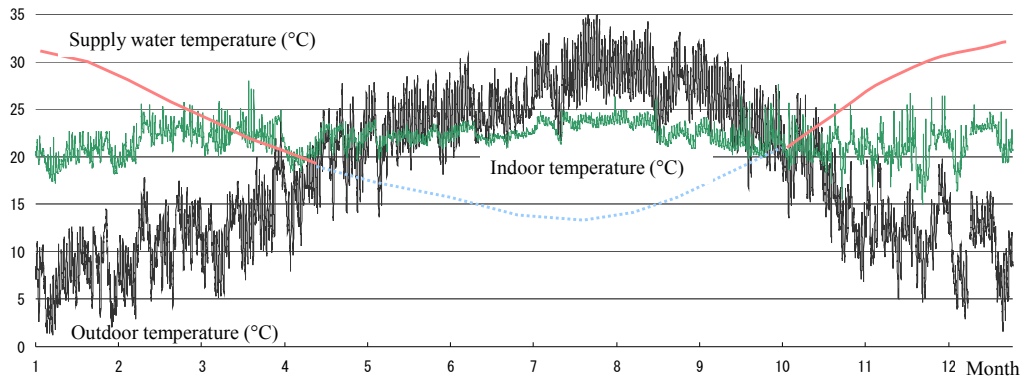


Fig. 4-32 Annual supply water temperature and indoor temperature

The novel cooling radiator cools and warms the entire room by radiation. When the entire room is cooled or warmed once, the comfort limits can be maintained with reasonable energy use. Cooling or heating a large space with a high ceiling is time and cost-extensive. The system can realize efficient cooling and heating for large spaces. This system creates a quiet environment without draught and noise. Therefore, this system is suitable for spaces occupied for long durations and for spaces where sedentary activity is the main activity type. This novel terminal unit improves the perception of thermal comfort and allows higher air temperature settings for cooling (lower temperature for heating) because of the effect of radiation. It also allows using smaller heat pumps.

5. Conclusions

Subtask B is responsible for the indoor temperature and humidity fields and indoor terminal units. Indoor terminal units are active building components that emit or remove heat and moisture from indoor spaces. The indoor heat and moisture sources are clearly identified. On basis of the investigation on the temperature levels of heat sources, optimization objectives for indoor heat collection or indoor terminals are obtained. According to the entransy dissipation analysis, there are two aspects to be considered in removing indoor heat. The first is to reduce the heat to be removed by the terminal units (for example to reduce heat transfer through a building envelope in summer), and the second is to improve the required temperature of the cooling source for cooling (lower the heating temperature of the source for heating). Thus, the high-temperature cooling and low-temperature heating system is effective in achieving an optimized terminal process with a lower entransy dissipation.

Indoor terminal units are building elements that use different heat transfer mechanisms and media to emit and remove heat or moisture from indoor spaces. Currently, existing literature and data were used to gather information about the indoor terminal units. These

indoor terminals mainly rely on convection (natural or forced), radiation, or both. Then, the characteristics of the terminal units are studied with the help of the entransy dissipation analysis method and the $T-Q$ figure. As indicated by the dissipation analysis of different terminal processes, it was found that significant dissipation exists in a conventional air-conditioning system owing to the coupled handling solutions of sensible heat and moisture. To prevent this type of dissipation, temperature- and humidity-independent control is regarded as an energy efficient solution. In constructing an indoor terminal process or choosing indoor terminal units, the other guiding principle is to reduce indoor mixing entransy dissipation. A radiant terminal is supposed to be superior to a convective terminal that could remove heat for cooling (supply heat for heating) through radiation and help reduce heat transfer links.

In this subtask, a radiant terminal is regarded as an important approach to construct an HTC<H system. The characteristics of radiant terminals are investigated, including their variant dynamic behaviors during intermittent operation as well the impact of transient solar radiation. Dynamic equivalent heat resistance is defined to reflect the thermal behavior of a radiant floor. At the same time, the influence of material emissivity on longwave radiant heat exchange between the radiant floor surface and the indoor wall surfaces is estimated. The detailed analysis on dynamic performance and cooling capacity prediction of a radiant terminal (with the aim of clarifying the radiant terminal's characteristics) is useful for real applications.

Case studies and the novel terminal system applications were obtained with the help of project participants. In addition to the indoor thermal environment analysis, energy performance analyses of these systems were used to evaluate the chosen terminal units and heating, ventilation and air-conditioning (HVAC) systems in order to identify the possibility of improving the existing terminal units and systems. Analyses carried out in this report show that the low-temperature heating and high-temperature cooling systems are superior to conventional solutions in terms of energy performance and, in many cases, also in terms of occupant thermal comfort.

Appendix A: Terminal units and corresponding characteristics

Table A1. The chosen terminal units and their corresponding possibilities, limitations and operational characteristics (Y: Yes, N: No, NC: Not Common) ****

Name of terminal	Type	Possibilities				Method of heat emission or removal				Capacity (W/m ²)		Medium of energy distribution		
		Heating	Cooling	Ventilation (fresh air)	Humidification + Dehumidification	Convection	Mainly convection	Radiation	Mainly radiation	Heating	Cooling	Air	Water	Electricity
Radiant systems	Floor*	Y	Y	N	N	Y	N	Y	Y	99	42	Y	Y	Y
	Wall	Y	Y	N	N	Y	N	Y	Y	160	72	N	Y	Y
	Ceiling	Y	Y	N	N	Y	N	Y	Y	42	99	Y	Y	Y
Air systems**	Mixing ventilation	Y	Y	Y	Y	N	Y	N	N	34°C	14°C	Y	N	N
	Displacement ventilation	Y/N	Y	Y	Y	N	Y	N	N	NC	18°C	Y	N	N
	Personalized ventilation	Y/N	Y	Y	Y	N	Y	N	N	NC	20°C	Y	N	N
Beams	Passive	Y	Y	N	N	N	Y	N	N	NC	80	N	Y	N
	Active	Y	Y	Y	Y***	N	Y	N	N	50	120	Y	Y	N

*: Floor in the occupied zone.

** : For air systems, typical maximum and minimum supply air temperatures are provided. The heating and cooling capacity will depend on the ventilation rate.

***: Humidification and dehumidification is possible with the primary air and it should be done by the air-handling unit. Beams operate in dry, non-condensing conditions.

****: The given values are only intended to provide guidance. The indicated capacities could vary depending on the application.

Appendix B: Numerical model of radiant floor

1) Concrete core radiant floors (Type I)

In the concrete core radiant floor, water pipes are encased in a concrete core, and a floor covering (marble, tiling, parquet floor, etc.) is laid above it, as shown in Fig. B-1. This concrete slab is therefore included in the heat transport mechanism and acts as a heat accumulator. This type of radiant floor can be referred to as a “heavy floor” due to the large thermal capacity of the concrete slab.

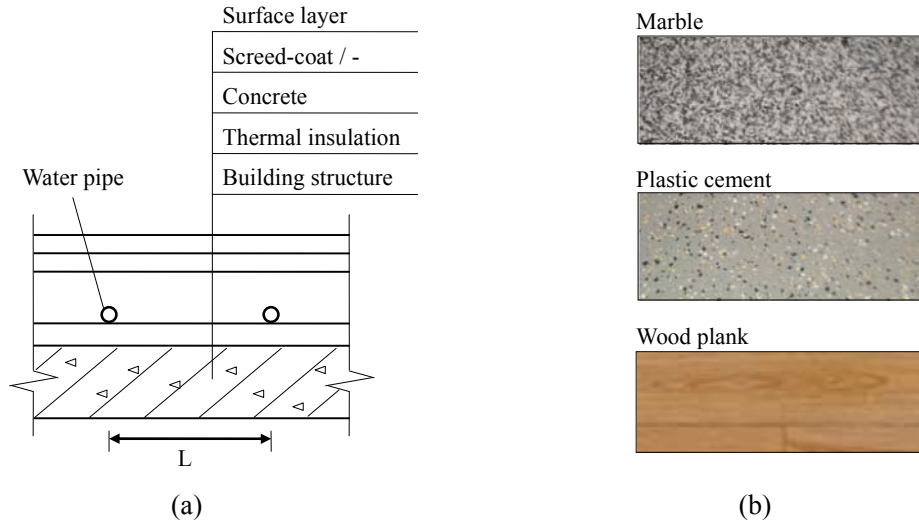


Fig. B-1 Typical types of “heavy floors”: (a) Structure; and (b) Surface layers

Several typical configurations of concrete core radiant floors from the literature are listed in Table B-1. In many ways, I(a) and I(b) are similar in terms of construction, with identical pipes installed at 150-mm intervals in a 70-mm-thick concrete layer. However, the materials of their surface layers are different: the surface layer of I(a) is marble, and that of I(b) is plastic cement. In contrast to both I(a) and I(b), the construction of I(c) features 300-mm pipe spacing and a surface layer of wood plank. The heat transfer properties of these radiant floors vary according to their pipe spacing, thickness, and surface layer material.

For radiant floors with a variety of structure parameters, in order to characterize the internal bi-dimensional heat conduction processes among multiple layers in steady state, equivalent heat resistance R , which is kept constant in the heating/cooling condition, is proposed:

$$R = \frac{T_s - \bar{T}_w}{q} \quad (\text{B-1})$$

where T_s is the mean temperature of the radiant floor surface, \bar{T}_w is the mean temperature of the supply and return water in the pipes, and q is the heat flux transferred from the floor

surface to the chilled water in steady state.

According to previous experimental results (Wei, 2010; Liu, 2004), the equivalent heat resistances of radiant floors I(a), I(b), and I(c) shown in Table B-1 are 0.09, 0.21, and 0.25 ($\text{m}^2\cdot\text{K}/\text{W}$), respectively. Among the three radiant floors, radiant floor I(a) has the best heat conduction performance, followed by I(b) and I(c), due to the low thermal conductivity of plastic cement and the increased pipe spacing.

2) Light floors (Type II)

In this type of radiant floor, pipes transporting hot or cold water are embedded in wood planks or insulation panels, and aluminum chips are adopted to draw the heat flow upwards to the floor covering, as shown in Fig. B-2. The structure and material parameters of two types of light floors are listed in Table B-2. The pipe diameter and spacing of II(a) are 20 mm and 150 mm, respectively, which are identical to those of common concrete core radiant floors I(a) and I(b). The total thickness of II(a) is only about 25 mm, making it much thinner than the concrete core radiant floors. The structure of radiant floor II(b) is even more compact, with pipes with an outer diameter of 7 mm installed in 12-mm-thick insulation board at 75 mm intervals.

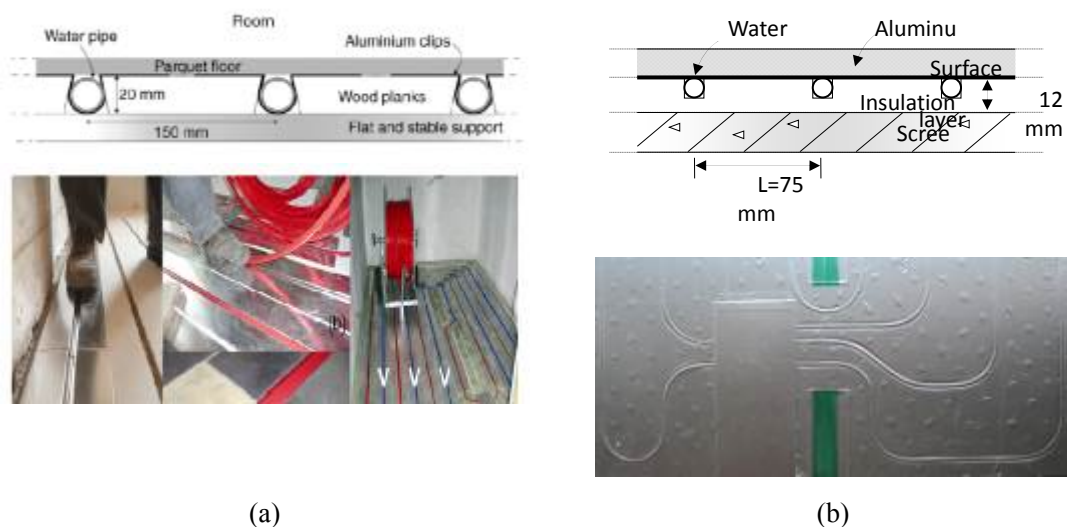


Fig. B-2 Typical types of “light floors”: (a) II(a) (Thomas, 2011); and (b) II(b)

According to experimental results from the literature (Thomas, 2011; Liu, 2013), the equivalent heat resistances of radiant floors II(a) and II(b) are 0.12 and 0.20 ($\text{m}^2\cdot\text{K}/\text{W}$), respectively, as shown in Table B-2.

Table B-1 Structure and heat resistance of concrete core radiant floor (Type I)

	I(a) / I(b) (Wei, 2010)				I(c) (Liu, 2004)			
	Density ρ (kg/m ³)	Thermal conductivity k (W/(m·K))	Specific heat c_p (kJ/(kg·K))	Thickness H (mm)	Density ρ (kg/m ³)	Thermal conductivity k (W/(m·K))	Specific heat c_p (kJ/(kg·K))	Thickness H (mm)
Surface layer	2600 /1380	3.84 / 0.04	750 /900	25 /5	900	0.15	1880	10
Cement mortar	1800	0.93	840	25	1800	0.93	840	20
Concrete layer	2344	1.84	800	70	2300	1.3	920	70
Water pipe	1200	0.38	1400	2	1200	0.24	1400	2
Pipe diameter δ and spacing L	$\delta=20$ mm, $L=150$ mm				$\delta=20$ mm, $L=300$ mm			
Heat resistance R ((m ² ·K)/W)	0.09~0.10 / 0.20~0.22				0.24~0.25			

Table B-2 Structure and heat resistance of light radiant floor (Type II)

	II(a) (Thomas, 2011)				II(b) (Liu, 2013)			
	Density ρ (kg/m ³)	Thermal conductivity k (W/(m·K))	Specific heat c_p (kJ/(kg·K))	Thickness H (mm)	Density ρ (kg/m ³)	Thermal conductivity k (W/(m·K))	Specific heat c_p (kJ/(kg·K))	Thickness H (mm)
Surface layer	900	0.143	1880	5	900	0.12	1880	10
Aluminum foil	2700	222	950	0.3	2702	237	903	0.12
Supporting layer	700	0.18	1880	20	50	0.029	2100	12
Water pipe	1200	0.38	1400	2	1200	0.38	1400	1
Pipe diameter δ and spacing L	$\delta=20$ mm, $L=150$ mm				$\delta=7$ mm, $L=75$ mm			
Heat resistance R ((m ² ·K)/W)	0.11~0.13				0.18~0.22			

3) Numerical model and validation

To analyze the dynamic performance of the radiant floors, a numerical model was built using the finite difference method. In order to simplify the model of heat transfer, a representative domain is selected (shown in Fig. B-3), and a 2-D model is used to handle the thermal behavior of the radiant floors when the following assumptions are applied:

- i. The materials of each layer are homogeneous and the property parameters remain constant;
- ii. The pipes have a symmetrical layout, which allows for temperature symmetry on both sides of the vertical axes located in the center of the pipes;
- iii. The mean temperature of the chilled water along the pipes is uniform, so that the heat conduction along the pipe axes is ignored and the heat conduction inside the radiant floors is two-dimensional;
- iv. The bottom surface of the insulating layer is adiabatic.

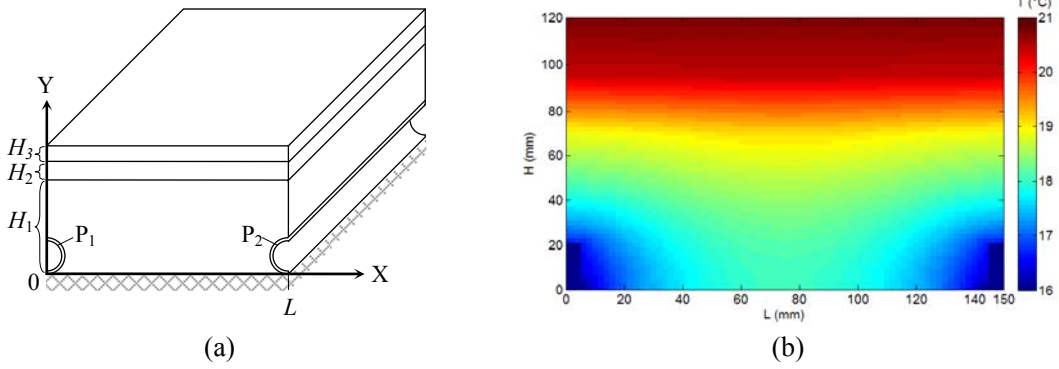


Fig. B-3 Representative domain of radiant floor: (a) Physical model; and (b) Temperature distribution

The governing equation for the radiant floor is

$$\frac{\partial T}{\partial \tau} = a \left(\frac{\partial^2 T}{\partial x^2} + \frac{\partial^2 T}{\partial y^2} \right) \quad (\text{B-2})$$

The boundary conditions of the governing equation are

$$\left. \frac{\partial T}{\partial x} \right|_{x=0} = \left. \frac{\partial T}{\partial x} \right|_{x=L} = 0 \quad (\text{B-3})$$

$$k \left. \frac{\partial T}{\partial y} \right|_{y=H} = h_z (T_z - T) + q_{sr} \quad (\text{B-4})$$

$$\left. \frac{\partial T}{\partial y} \right|_{y=0} = 0 \quad (\text{B-5})$$

$$T = \begin{cases} T_{w,s} & \text{(at pipe internal surface } P_1 \text{)} \\ T_{w,r} & \text{(at pipe internal surface } P_2 \text{)} \end{cases} \quad (\text{B-6})$$

The equations are discretized by the finite difference method, and the temperature distribution can be seen in Fig. B-3(b). The different regions of the model are carefully treated in the meshing process to ensure that the meshes are sufficiently refined and the results are independent of the number of nodes.

Table B-3 Validation of numerical model in steady state

	I(a)	I(b)	I(c)
Experiment result	0.092~0.100 (Wei, 2010)	0.204~0.221 (Wei, 2010)	0.243~0.249 (Liu, 2004)
Numerical calculation	0.094	0.219	0.264
Error	+2.1% ~ -6.0%	+7.4% ~ -0.9%	+8.6%~+6.0%
	II(a)	II(b)	
Experiment result	0.114~0.126 (Thomas, 2011)	0.183~0.220 (Liu, 2013)	
Numerical calculation	0.119	0.200	
Error	+4.4% ~ -5.6%	+9.3% ~ -9.1%	

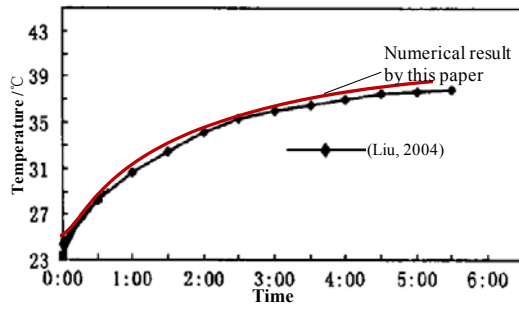
The floor surface average temperature (T_s) is calculated according to Eq. (B-7). The indoor heat/cold absorbed by the radiant floor surface (q_s) and the heat/cold extracted by the chilled/heated water (q_w) are calculated according to Eqs. (B-8) and (B-9), respectively. In the steady state, the value of q_s is equal to q_w .

$$T_s(\tau) = \frac{1}{L} \int_0^L T(x, y = H) dx \quad (\text{B-7})$$

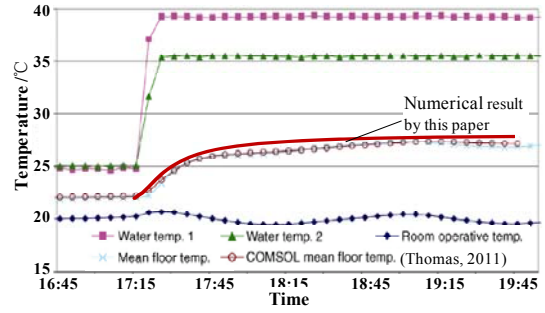
$$q_s(\tau) = h_z (T_z - T_s(\tau)) + q_{sr} \quad (\text{B-8})$$

$$q_w(\tau) = \frac{1}{L} \int_{P_1+P_2} k \left(\left| \frac{\partial T}{\partial x} \right| dy + \left| \frac{\partial T}{\partial y} \right| dx \right) \quad (\text{B-9})$$

Validation of the model is conducted by comparing the steady-state results and dynamic performances reported in the literature with those of the numerical model. Table B-3 shows the comparison of different steady-state values of equivalent heat resistance R defined by Eq. (B-1). The error between the numerical calculations and the experimental results is within 10%, and the calculation results during the intermittent period are also consistent with the experimental results, as shown in Fig. B-4. Hence, the numerical model can be used for further research on the dynamic performance of the radiant floors.



(a)



(b)

Fig. B-4 Validation results during intermittent period: (a) Concrete layer with embedded water pipes (Liu, 2004); and (b) Radiant floor II(a) (Thomas, 2011)

Appendix C: Experimental analysis of different terminal units

The system is composed of:

- Production loop: a reversible 10kW air to water heat pump + a 1000l storage tank for the heating or a 500l storage tank for the cooling.
- Distribution loop and emission: OPAL pipes + a light radiant floor heating or cooling (Fig. C-7).
- Air loop: A variable rate pulsing air-handling unit (100 to 800m³/h) including galvanized steel ducts, a heating/cooling coil (heating power: 2.4kW/sensible cooling power: 1.3kW/total cooling power: 3.6kW), a wall grill or a displacement air diffuser.

All the measurements were performed in the climatic chamber of the laboratory located in Arlon in the south of Belgium (Fig. C-1). Terminals used in this study case are: a displacement diffuser (Fig. C-2, Table C-1) compared with 2 mixing ventilation diffusers (Figs. C-3~C-4 and Tables C-2~C-3) combined with a light radiant floor (Fig. C-7). In cooling mode, we can expect an efficiency gain by using the displacement ventilation combined with the radiant floor because of the reduction of mixture losses due to ventilation and mixing ventilation.

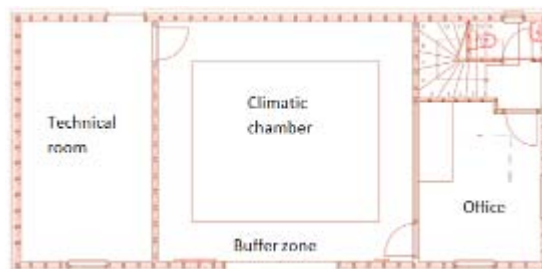


Fig. C-1 First floor of the laboratory. Tests were performed in the climatic chamber in the center of the building. But offices were also air-conditioned in order to increase the cooling or heating load.

Ventilation diffusers

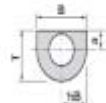
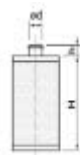


Fig. C-2 Wall displacement diffuser QL – WH – R0.

Table C-1 Specifications of the wall displacement diffuser QL – WH – R0

Specification	Value	Unit
Air diffusion		
Air flow	200	m ³ /h
Supply air velocity	0.4	m/s
Zone NS ($\Delta T=3^{\circ}\text{C}$)	1.3	m
Zone NS ($\Delta T=6^{\circ}\text{C}$)	2.1	m
Total pressure drop	70	Pa
Sound power level	54	dB(A)
Dimensions		
B*H*T	320*600*190	mm
Ød	125	mm
H	60	mm
Material		
The internal distribution of the sheet of the diffuser	Galvanized steel	
Nozzles	Plastic	
Weight	8	kg

where: ΔT = Temperature difference between supply air and ambient air at 1 m above ground; Zone NS: unoccupied area with air velocity > 0.2 m/s

Table C-2 Specifications of the wall mixing diffuser TMM-160

Specification	Value	Unit
Air diffusion		
Air flow	200	m ³ /h
Supply air velocity	2.8	m/s
L _{t0.25}	8.5	m
Total pressure drop	6	Pa
Sound power level	26	dB(A)
Dimensions		
A*B*C	251*190*22	mm
Ød	155	mm
Free area	110	cm ²
Material		
Diffuser	White aluminium	
Weight	0.735	kg

where: L_{t0.25} is the throw length while air velocity > 0.25m/s out of the occupation zone for an isothermal jet.

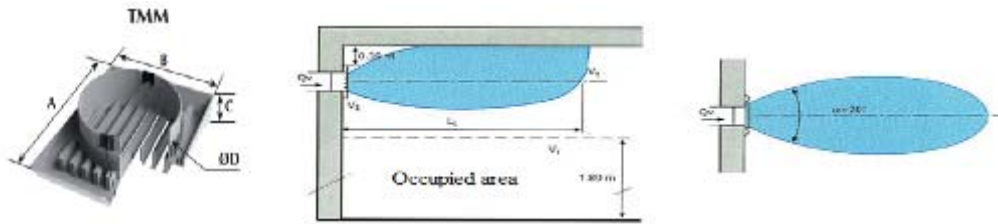


Fig. C-3 Wall mixing diffuser TMM-160 and air diffusion characteristics.

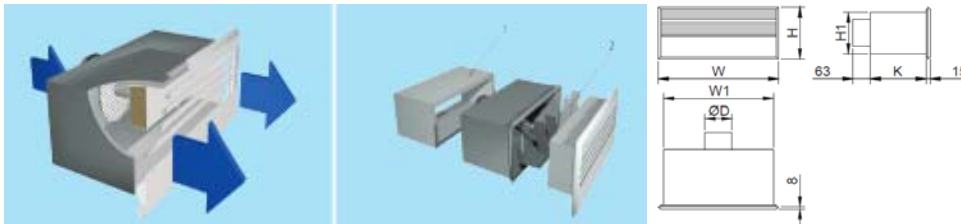


Fig. C-4 Wall mixing diffuser TLB-160.

Table C-3 Specifications of the wall mixing diffuser TLB-160

Specification	Value	Unit
Air diffusion		
Air flow	200	m ³ /h
Supply air velocity	Has to be measured	m/s
L _{t0.2}	5.5	m
Total pressure drop	20	Pa
Sound power level	23	dB(A)
Dimensions		
W*H*K	541*241*241	mm
W1	503	mm
H1	203	mm
Ød	159	mm
Material		
Diffuser face	Steel	
Sound absorbing material	Mineral wool	
Plenum	Galvanized steel	
Connection	Galvanized steel	
Deflection panel	Galvanized steel	
Covering sleeve	Galvanized steel	

where: L_{t0.2} is the throw length while air velocity > 0.2m/s out of the occupation zone when the ambient temperature=24°C and the supply temperature=16°C.

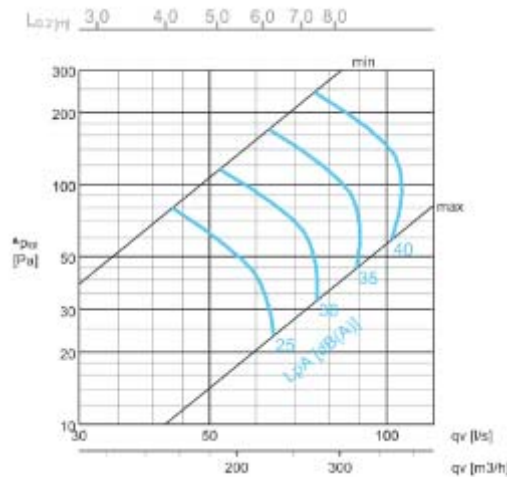


Fig. C-5 Wall mixing diffuser TLB-160, air diffusion characteristics.

Light radiant heating/cooling floor (opal system)

The light heating floor compared to the traditional heavy one reduces the thermal resistance between the water and the ambient air. The thermal inertia is also reduced and the reactivity of the system increased which could improve the control of the system for maintaining thermal comfort because response time to perturbations will be reduced. The Fig. C-6 (results from simulations) compares the reactivity of both terminals. Time for implementation is also reduced so this can kind of terminal is adapted for building renovations.

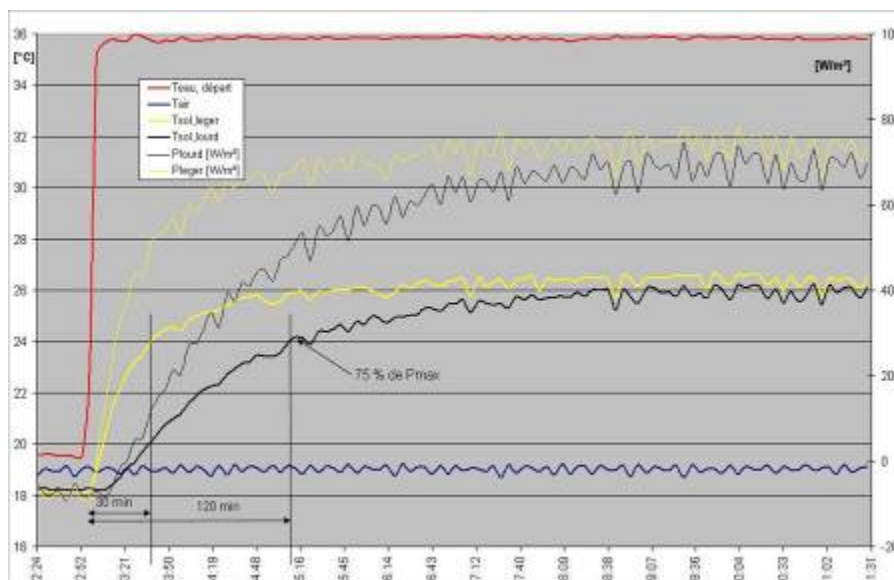


Fig. C-6 Comparison of the reactivity for light and heavy radiant floor. The light radiant heating floor reaches 75% of the maximum heating power emission in 30min while the heavy one takes 120min. In yellow the surface temperatures for both terminals.

In order to reduce the distance between pipes and the emitter the following design had been adopted by the designer (Fig. C-7).

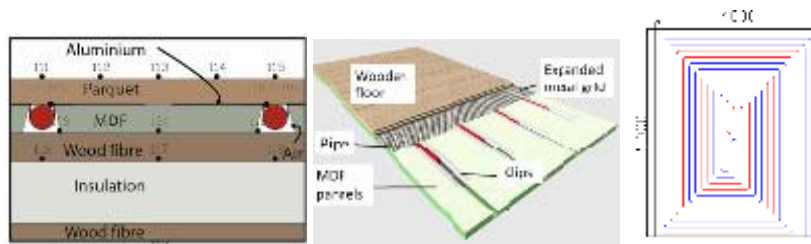


Fig. C-7 The light radiant heating/cooling floor (OPAL-system) and OPAL-system pipes in the climatic chamber. There are 2 pipes. The distance between 2 pipes is 15cm and the distance between an edge pipe and the nearby wall is 7.5cm. One pipe is 65.5m length, the other one is 65.2m. The area covered by pipes is 19.8m².

Results from experimental monitoring

Experimentation 1

This test was performed in cooling mode to cool the climatic chamber using the light radiant floor and the mixing ventilation with the diffuser TMM-160. We also cooled the offices in order to increase the cooling demand and have the chiller reach a good COP. We maintained the buffer zone at 30°C using a resistor controlled by a PID controller. Inside the climatic chamber 2 electrical carpets (240W) and 2 computers were used to represent the presence of two people working in an office. A third electrical carpet was used to emulate solar gains (300W). The experimentation was performed for steady state for 7h30. The operative temperature in the chamber is maintained at 24°C and the temperature in the storage tank is fixed at 11°C. The control of the operative temperature in the chamber is performed by a 2 inlets and one outlet flow mixer. For this experimentation the flow rate in the radiant floor is maintained at 5.2l/min. Comfort parameters inside the chamber are measured: resultant and air temperatures at 16 locations, surface temperatures at 10 locations and air velocity at 2 locations near the people emulators heads. Fig. C-8 represents the configuration inside the chamber and sensors locations. Table C-5 summarizes test conditions. Temperatures, flow rates and electric consumptions are measured at production and distribution loops of the system.

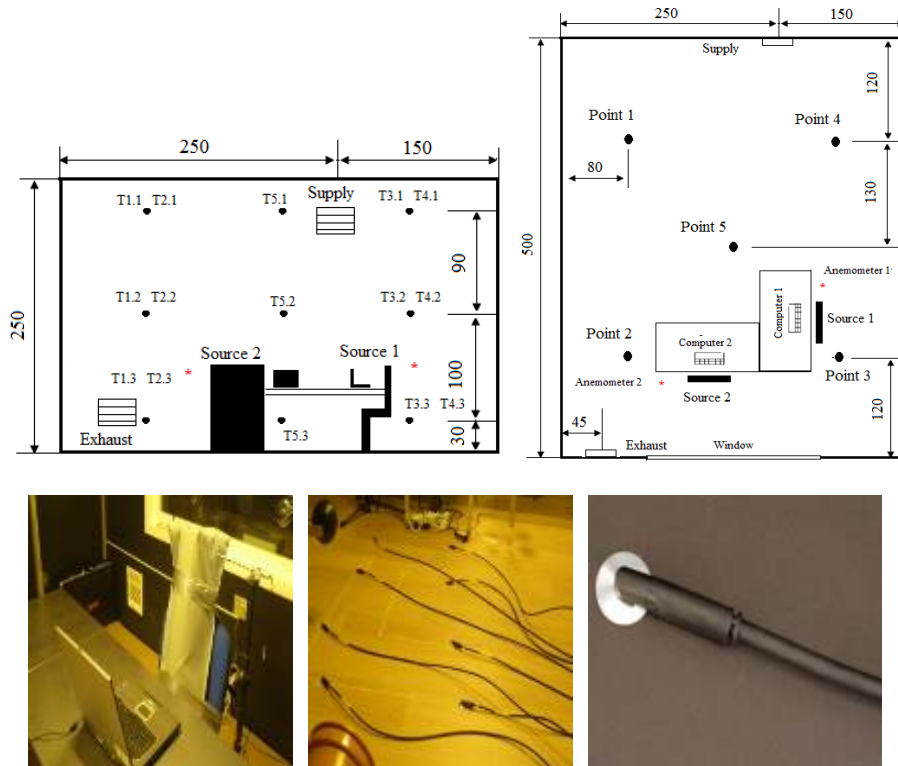


Fig. C-8 Position of the probes inside the climatic chamber, thermal sources and ventilation terminals. The two last photos show the surface temperature sensors.

The chamber is also cooled by AHU where the air is recirculated and cooled to 21°C through a cooling coil fed by cold water coming from the tank. Air temperature is also measured at exhaust and supply. The air flow rate is maintained at 200m³/h. Surface temperatures are measured using a thermistor designed for measuring the back of PV module temperature because it is the same range of temperature as the radiant floor and PV are covered by a polymer which thermal conductivity is close to this of a wooden floor: 0.18W/m. The aluminum disk promotes heat transfer from surfaces and the link between the sensor and the surface is strong. The maker guarantees a precision of +/- 0.2°C.

Table C-4 Measurements. Refer to Figs. C-1 and C-7 to see probes locations.

Measurement	Unit	Probe accuracy
Th. measurements		
Operative temperatures	[°C]	+/-0.2[°C]
Air temperatures	[°C]	+/-0.2[°C]
Surface temperatures	[°C]	+/-0.2[°C]
Water temperatures	[°C]	+/-0.2[°C]
Elec. measurements		
Compressor cons.	[W]	1.6%
Chiller fan consumption	[W]	2%

Chiller pump consumption	[W]	0.6%
Radiant floor pump consumption	[W]	
Offices pump consumption	[W]	
AHU fan consumption	[W]	
Flow rates		
Water flow rates	[l/min]	
Air flow rate in AHU	[m ³ /h]	

Table C-5 Setpoints for chamber indoor environment and average temperatures measured

Measurement	Setpoint	Measured	Probe accuracy
Indoor operative temperature	24°C	24°C	+/-0.2[°C]
Supply air temperature	21°C	20.4°C	+/-0.2[°C]
Buffer air temperature	30°C	30.2°C	+/-0.2[°C]
Storage tank cold water temperature	11°C	11.4°C	+/-0.2[°C]
Supply water temperature	—	12.5°C	+/-0.2[°C]
Return water temperature	—	14.5°C	+/-0.2[°C]
Mean surface temperature	—	18.7°C	

For this first experimentation the water flow rate in the cooling floor is 5.2l/min and supply air flow rate is 200m³/h (4V-1 which means category I of the standards EN15251).

Results

Energy analysis

Table C-6 Energy balance for the complete system and average electric power for components

Measurement	Value	Unit
Energy balance for the complete system		
Average thermal power produced	2058	[W]
Average Electric power consumed	824	[W]
Average electric power consumed by components		
Chiller	702 (85%)	[W]
Compressor	555 (68%)	[W]
Pump	35 (4%)	[W]
Fan	112 (14%)	[W]
Pump offices	20 (2.4%)	[W]
Pump chamber	22 (2.7%)	[W]
Pump AHU	48 (5.8%)	[W]
Fan AHU	32 (3.9%)	[W]
COP for chiller	2.93	—

Table C-7 Energy balance for the climatic chamber and components transferring energy to it

Measurement	Value	Unit
Energy produced or used for cooling the chamber		
Average thermal power	1359	[W]
Average Electric power consumed	662	[W]
Cooling load from radiant floor	37	[W/m ²]
Average electric power consumed by components for cooling chamber		
Chiller	560	[W]
Compressor	442	[W]
Pump	28	[W]
Fan	89	[W]
Pump chamber	22	[W]
Pump AHU	48	[W]
Fan AHU	32	[W]

17.7%

15.4%

Thermal comfort analysis

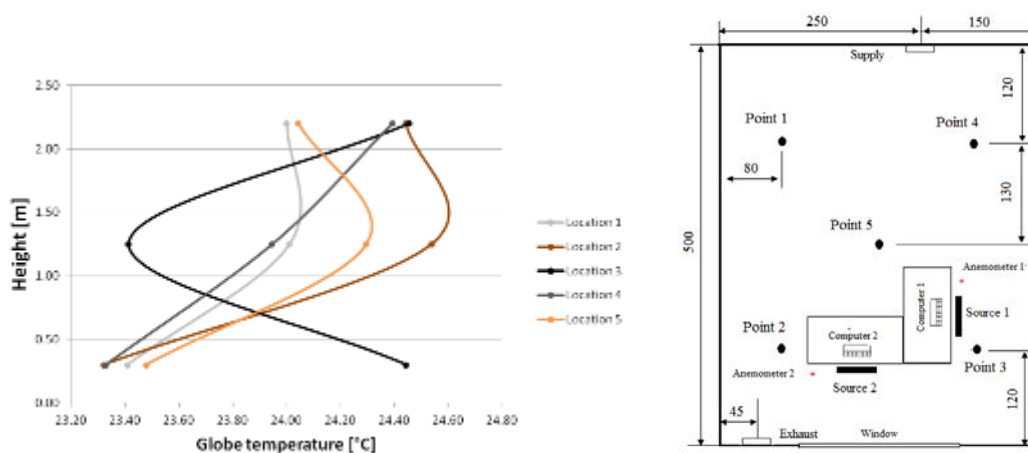


Fig. C-9 Globe temperatures in the climatic chamber. The lowest value measured is 23.3°C and the highest one does not exceed 24.6°C. Except location 3 temperatures increases with height until 1.25m, due to the cooling radiant floor effect. Temperatures measured at 2.2m decreases because of the air jet.

Both air velocities do not exceed 0.1m/s.

Entransy analysis

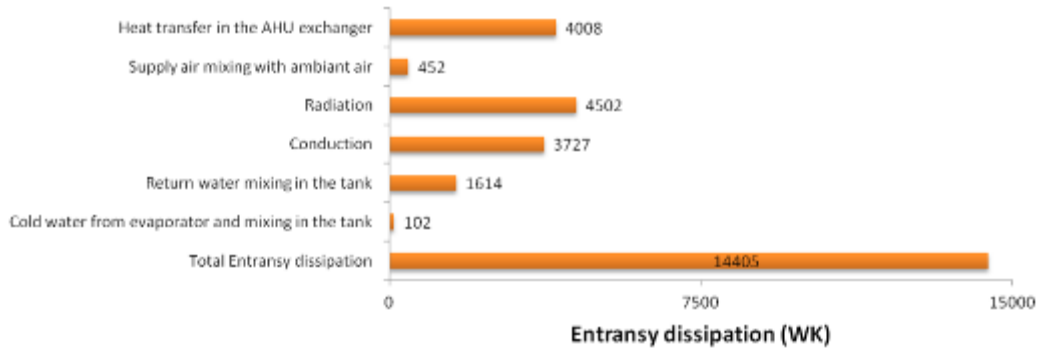


Fig. C-10 Entransy dissipation analysis.

Auxiliaries' consumption represents a quite important part of the total consumption about 15%. This consumption can be “detected” by the entransy dissipation. In fact difference of temperatures contributes to increase entransy dissipation but also flow rates that are correlated with pump and fan consumption. This can be used as a tool to choose between several alternative HVAC systems.

Experimentations 2

We performed the same tests but we modified some of the experimental conditions. In these tests we vary the water flow in the cooling floor and the water temperature of the tank. We test the light radiant floor combined with mixing ventilation, the light radiant floor combined with displacement ventilation, the mixing ventilation, the displacement ventilation. We maintained the buffer zone at 26°C. Inside the climatic chamber 2 electrical carpets (240W) and 2 computers were used to represent the presence of two people working in an office. Three other electrical carpets were used to emulate solar gains (100W+100W+150W). The experimentation was performed for steady state. The operative temperature set point in the chamber is 26°C. The chamber is also cooled by AHU where the air is recirculated and cooled to 23°C through a cooling coil fed by cold water coming from the tank for all tests except the tests 6 and 7 where the air is cooled to 15.8°C and 15.1°C in order to meet the thermal comfort conditions. The air flow rate is maintained at 200m³/h (category 1 in terms of indoor air quality according to standards EN 15251) for all the tests. Table C-8 summarizes test conditions.

Table C-8 Configuration, measured average temperatures and water flow rate in the cooling floor

Test	Configuration	Water flow rate	Storage tank cold water temperature	Supply air temperature	Mean floor surface temperature	Measured indoor operative temperature	Cooling load of the light radiant

							floor
1	Light radiant floor /displacement ventilation	4.9l/min	13.9°C	23°C	21.3°C	25.5°C	29.4W/m ²
2	Light radiant floor /displacement ventilation	3.2l/min	14.5°C	23°C	22.2°C	26.3°C	28.7W/m ²
3	Light radiant floor /displacement ventilation	3.2l/min	12.5°C	23°C	21.1°C	25.7°C	32.2W/m ²
4	Light radiant floor / mixing ventilation	3.2l/min	14.6°C	23°C	22.4°C	27.1°C	32.9W/m ²
5	Light radiant floor / mixing ventilation	1.6l/min	12.8°C	23°C	21.8°C	27.5°C	39.9W/m ²
6	Displacement ventilation	---	11.6°C	15.8°C	---	27°C	
7	Mixing ventilation	---	10.8°C	15.1°C	---	27°C	

Thermal comfort analysis

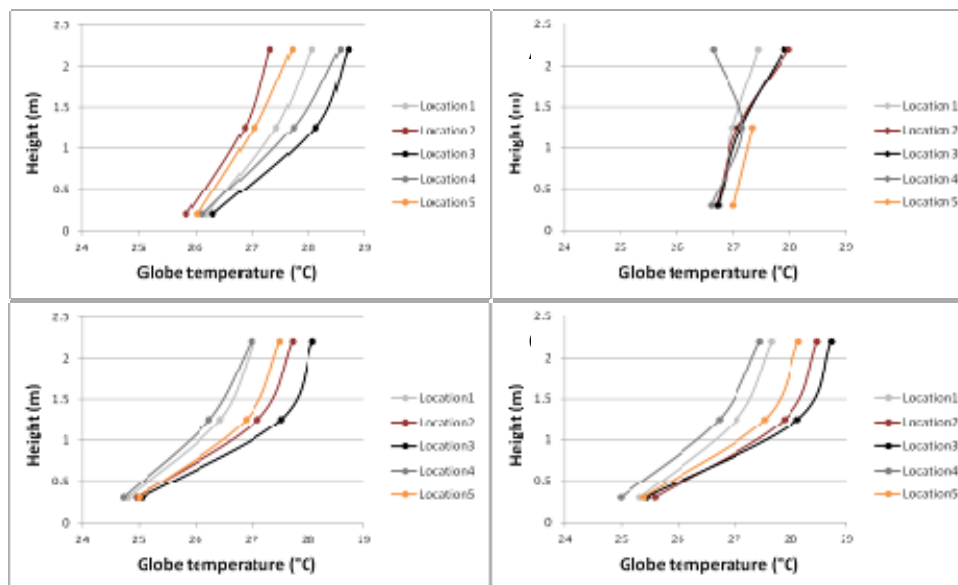


Fig. C-11 Temperature stratification within the climatic chamber. A) Radiant floor 3.2l/min + mixing ventilation (test 4). B) Mixing ventilation (test 7). C) Radiant floor 3.2l/min + displacement ventilation (test 2). D) Displacement ventilation (test 6).

If the chamber is cooled by only using mixing ventilation then the vertical air temperature difference does not exceed 1°C. If the mixing ventilation is combined with the low inertia radiant floor then the vertical air temperature difference can reach 2.2°C at location 3 above the plume created by occupants. It means that PD (percentage of dissatisfied)

less than 10% according to standards ISO7730-2005. Now if the chamber is cooled by using displacement ventilation or displacement ventilation combined with the radiant floor then the stratification is a little bit more important: the vertical air temperature difference can reach 3°C above the plume created by occupants. It means that to PD<10% and it corresponds to category A according to standards ISO7730-2005.

In the Table C-8 operative temperatures are measured 1m above the floor because in an office people are most of the time are sitting. In this case we note that mixing and displacement ventilations never meet thermal comfort conditions even if the tank water temperature is low and supply temperature decreases to about 15°C since the air flow rate is maintained to hygienic flow rate and corresponds to the first category according to standards EN 15251. It is the same when the mixing ventilation is combined with the radiant floor. This is because in these combinations the whole volume of the chamber is cooled. These results are confirmed by the entransy analysis.

Entransy analysis

The diagram T-Q is the same as that of Fig. C-10. Results are summarized by the 3 entransy diagrams of Figs. C-12~C-15. The fourth diagram is just a synthesis of the three first diagrams. Fig. C-12 shows the comparison of displacement ventilation combined with radiant floor, with mixing ventilation combined with radiant floor. If these both systems run with the same tank water temperature (about 14.5°) and the same water flow rate (3.2l/min) then the thermal comfort provided by the displacement ventilation (category 1 according to EN 15251) combined with radiant floor is better than that provided by mixing ventilation combined with radiant floor. If the chamber is only cooled by the ventilation entransy dissipation is much more important and tank water temperature is lower.

Fig. C-13 shows the displacement ventilation combined with radiant floor. If we increase the water flow rate in the radiant floor then tank water temperature increases by 1.4°C from 12.5°C to 13.9°C while thermal comfort is maintained. Tank water temperature is well correlated with entransy dissipation. This figure also shows that ventilation when combined with radiant floor is better than ventilation alone in terms of entransy dissipation and thermal comfort.

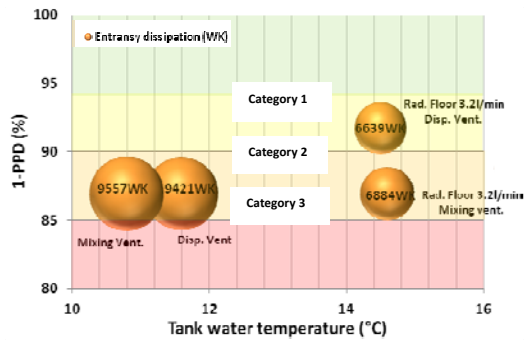


Fig. C-12 Comparison of displacement ventilation combined with radiant floor, with mixing ventilation combined with radiant floor.

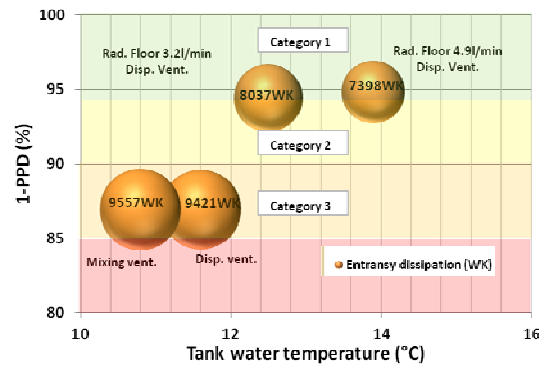


Fig. C-13 Displacement ventilation combined with radiant floor.

Fig. C-14 shows the mixing ventilation combined with radiant floor. If the water flow rate increases from 1.6l/min to 3.2l/min then tank water temperature increases from by 1.8°C from 12.8°C to 14.6°C and thermal comfort is better. Low water flow rate cannot be able to provide a thermal comfort respecting the standards even if the tank water temperature is lower. Entransy dissipation reflects the efficiency of the system and the compromise between thermal comfort and tank water temperature (energy consumption) if we suppose that pump consumption does not vary a lot. But this assumption will depend on the efficiency of the water pump and in general of the size of the system.

Fig. C-15 shows that displacement ventilation combined with floor radiant floor seems to be the best system in terms of entransy dissipation and thermal comfort. If we consider this combination then the best compromise between thermal comfort and energy consumption is the couple [3.2l/min; 14.5°C] because it provides a comfort equivalent to that of category 2 according to EN 15251 but less energy from production (tank water temperature) and pump electricity consumption (water flow rate) is consumed than using other parameters.

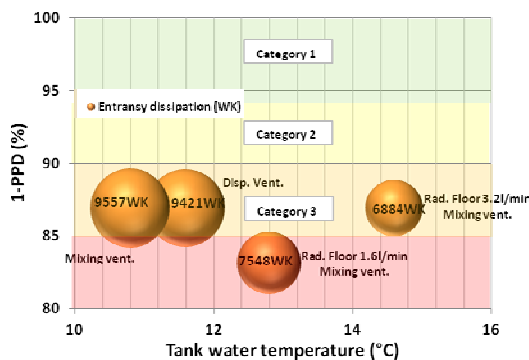


Fig. C-14 Mixing ventilation combined with

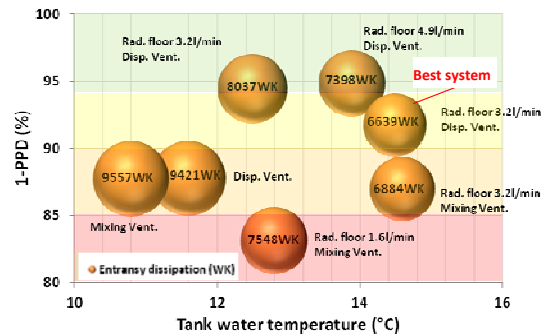


Fig. C-15 Comparison of different systems.

radiant floor.

In conclusion we can affirm that the entransy concept is an interesting tool for the choice of the best terminal units in a HVAC system and the choice of the parameters like water flow rates and level of temperatures. Entransy dissipation is clearly correlated with tank water temperature i.e. the energy efficiency of the production system. Thermal comfort analysis and entransy analysis show that the best system is the combination of radiant floor with displacement ventilation. A good compromise is to run the system with a medium water flow rate and a high water temperature. Using only ventilation to cool the chamber is less efficient than using the combination of radiant floor with ventilation. A very low water flow rate cannot be able to meet a good thermal comfort.

References

- [1] International Energy Agency, 22 February 2015. [Online]. Available: <http://www.iea-ebc.org/>.
- [2] IEA EBC Annex 59, 22 February 2015. [Online]. Available: <http://www.annex59.com/>.
- [3] J. D. Spitler, Load Calculation Applications Manual, Second Edition, Atlanta: American Society of Heating, Refrigerating and Air-Conditioning Engineers, 2014.
- [4] ASHRAE, ASHRAE Handbook - Fundamentals, Atlanta: American Society of Heating, Refrigerating and Air-Conditioning Engineers, 2013.
- [5] ISO 8996, "Ergonomics of the thermal environment - Determination of metabolic heat production," International Organization for Standardization, Geneva, 2004.
- [6] C. K. Wilkins and M. H. Hosni, "Plug load design factors," ASHRAE Journal, pp. 30-34, 2011.
- [7] EN 15251, "Indoor environmental input parameters for design and assessment of energy performance of buildings addressing indoor air quality, thermal environment, lighting and acoustics," European Committee for Standardization, Brussels, 2007.
- [8] J. Babiak, B. W. Olesen and D. Petráš, Low temperature heating and high temperature cooling, Brussels: REHVA - Federation of European Heating, Ventilation and Air Conditioning Associations, 2009.
- [9] B. W. Olesen, "Using Building Mass To Heat and Cool," ASHRAE Journal, pp. 44-52, 2012.
- [10] B. W. Olesen, E. Michel, F. Bonnefoi and M. De Carli, "Heat Exchange Coefficient Between Floor Surface and Space by Floor Cooling - Theory or a Question of Definition," ASHRAE Transactions, vol. Part I, pp. 684-694, 2000.
- [11] X. Liu, Y. Jiang and T. Zhang, Temperature and Humidity Independent Control (THIC) of Air-conditioning System, Springer-Verlag Berlin Heidelberg, 2013.
- [12] B. W. Olesen, "Possibilities and Limitations of Radiant Floor Cooling," ASHRAE Transactions, pp. 42-48, 1997.
- [13] P. Simmonds, S. Holst, S. Reuss and W. Gaw, "Using Radiant Cooled Floors to Condition Large Spaces and Maintain Comfort Conditions," ASHRAE Transactions, pp. 695-701, 2000.
- [14] ISO 18566, "Building environment design — Design, test methods, control and operation of radiant heating and cooling panel systems," International Organization for Standardization, Geneva, 2013.
- [15] ISO 11855, "Building environment design - Design, dimensioning, installation and control of embedded radiant heating and cooling systems," International Organization for Standardization, Geneva, 2012.
- [16] B. W. Olesen, "Cooling and heating of buildings by activating the thermal mass with embedded hydronic pipe systems," in Proceedings of CIBSE/ASHRAE joint conference,

Dublin, 2000.

- [17] G. Cao, H. Awbi, R. Yao, Y. Fan, K. Sirén, R. Kosonen and J. Zhang, "A review of the performance of different ventilation and airflow distribution systems in buildings," *Building and Environment*, no. 73, pp. 171-186, 2014.
- [18] D. Müller (Ed.), C. Kandzia, R. Kosonen, A. K. Melikov and P. V. Nielsen, *Mixing Ventilation - Guide on mixing air distribution design*, Brussels: REHVA - Federation of European Heating, Ventilation and Air Conditioning Associations, 2013, p. 114.
- [19] DS 469, 2nd edition, "Heating- and cooling systems in buildings," Danish Standards, Charlottenlund, 2013.
- [20] H. Recknagel, E. Sprenger and E.-R. Schramek, *Taschenbuch für Heizung und Klimatechnik*, München: Oldenbourg Industrieverlag, 2011.
- [21] H. Awbi, *Ventilation of Buildings*, 2nd ed., London: Spon Press, 2003.
- [22] H. Skistad, E. Mundt, P. V. Nielsen, K. Hagström and J. Railio, *Displacement ventilation in non-industrial premises*, Brussels: REHVA - Federation of European Heating, Ventilation and Air Conditioning Associations, 2004.
- [23] A. K. Melikov, "Personalized ventilation," *Indoor Air*, no. 14 (Suppl 7), pp. 157-167, 2004.
- [24] A. K. Melikov, M. A. Skwarczynski, J. Kaczmarczyk and J. Zabecky, "Use of personalized ventilation for improving health, comfort, and performance at high room temperature humidity," *Indoor Air*, no. 23, pp. 250-263, 2013.
- [25] L. Fang, G. Clausen and P. O. Fanger, "Impact of temperature and humidity on the perception of indoor air quality," *Indoor Air*, vol. 8, no. 2, pp. 80-90, 1998.
- [26] L. Fang, D. P. Wyon, G. Clausen and P. O. Fanger, "Impact of indoor air temperature and humidity in an office on perceived air quality, SBS symptoms and performance," *Indoor Air*, vol. 14, no. Suppl. 7, pp. 74-81, 2004.
- [27] B. W. Olesen, "Revision of EN 15251: Indoor Environmental Criteria," *REHVA Journal*, pp. 6-12, 2012.
- [28] CR 1752, "Ventilation for buildings - Design criteria for the indoor environment," European Committee for Standardization, Brussels, 1998.
- [29] American Society of Heating, Refrigerating and Air-Conditioning Engineers, "ASHRAE Standard 62.1, Ventilation for Acceptable Indoor Air Quality," ASHRAE, Atlanta, 2013.
- [30] A. K. Melikov, *Indeklima og Aktiv Ventilation*, Kgs. Lyngby: International Centre for Indoor Environment and Energy, 2010.
- [31] J. Woollett and J. Rimmer, Eds., *Active and Passive Beam Application Design Guide*, Brussels: REHVA - Federation of European Heating, Ventilation and Air Conditioning Associations, 2014.

-
- [32] M. Virta, D. Butler, J. Gräslund, J. Hogeling, E. L. Kristiansen, M. Reinikainen and G. Svensson, Chilled Beam Application Guidebook, Brussels: REHVA - Federation of European Heating, Ventilation and Air Conditioning Associations, 2007.
- [33] EN 14518, "Ventilation for buildings - Chilled beams - Testing and rating of passive chilled beams," European Committee for Standardization, Brussels, 2005.
- [34] EN 15116, "Ventilation in buildings - Chilled beams - Testing and rating of active chilled beams," European Committee for Standardization, Brussels, 2008.
- [35] ASHRAE, ASHRAE Handbook - HVAC Systems and Equipment, Atlanta: American Society of Heating, Refrigerating and Air-Conditioning Engineers, 2012.
- [36] EN ISO 7730, "Ergonomics of the thermal environment - Analytical determination and interpretation of thermal comfort using calculation of the PMV and PPD indices and local thermal comfort criteria (ISO 7730:2005)," European Committee for Standardization, Brussels, 2005.
- [37] American Society of Heating, Refrigerating and Air-Conditioning Engineers, "ASHRAE Standard 55, Thermal Environmental Conditions for Human Occupancy," ASHRAE, Atlanta, 2010.
- [38] O. B. Kazanci and B. W. Olesen, "IEA EBC Annex 59 - Possibilities, limitations and capacities of indoor terminal units," Energy Procedia - 6th International Building Physics Conference, IBPC 2015, 2015.
- [39] Larsen, S.F., Filippín, C., Lesino G., 2010. Transient simulation of a storage floor with a heating/cooling parallel pipe system. *Building Simulation* 3(2), 105–115.
- [40] Liu, X.H., Jiang, Y., Zhang, T., 2013. Temperature and humidity independent control of air-conditioning systems. China Architecture & Building Press, Beijing (in Chinese).
- [41] Liu, Y.F., 2004. Study on basic theory of designing and running control of imbed pipe floor heating. Xi'an: Xi'an University of Architecture and Technology. (in Chinese)
- [42] Olesen, B.W., 2002. Radiant floor heating in theory and practice. *ASHRAE Journal* 44(7), 19–24.
- [43] Thomas, S., Franck, P.Y., André, P., 2011. Model validation of a dynamic embedded water base surface heat emitting system for buildings. *Building Simulation* 4(1), 41–48.
- [44] Wei, L.F., Dai, L.S., Yang, Q., et al., 2010. Research on cooling capacity based on radiant floor. In: Proceedings of the Chinese conference on HVAC&R 2010, Hangzhou (in Chinese).
- [45] Zhao, K., Liu, X.H., Jiang, Y., 2013. Application of radiant floor cooling in a large open space building with high-intensity solar radiation. *Energy and Buildings* 66(9), 246–257.
- [46] Zhang, L., Liu, X., & Jiang, Y. (2013). Application of entransy in the analysis of HVAC systems in buildings. *Energy*, 332-342.